Prepared for submission to JHEP DESY 16-089

On Asymptotics and Resurgent Structures of Enumerative Gromov–Witten Invariants

Ricardo Couso-Santamaría,[a] **Ricardo Schiappa,**[a,b] **Ricardo Vaz**[a,c]

[a] *CAMGSD, Departamento de Matemática, Instituto Superior Técnico, Universidade de Lisboa, Av. Rovisco Pais 1, 1049-001 Lisboa, Portugal*

[b] *Département de Physique Théorique & Section de Mathématiques, Université de Genève, Genève, CH-1211 Switzerland*

[c] *DESY Theory Group, DESY Hamburg, Notkestrasse 85, D-22603 Hamburg, Germany*

E-mail: santamaria@math.tecnico.ulisboa.pt, schiappa@math.tecnico.ulisboa.pt, ricardo.carmo.vaz@tecnico.ulisboa.pt

Abstract: Making use of large-order techniques in asymptotics and resurgent analysis, this work addresses the growth of enumerative Gromov–Witten invariants—in their dependence upon genus and degree of the embedded curve—for several different threefold Calabi–Yau toric-varieties. In particular, while the leading asymptotics of these invariants at large genus or at large degree is exponential, at combined large genus *and* degree it turns out to be factorial. This factorial growth has a resurgent nature, originating via mirror symmetry from the resurgent-transseries description of the B-model free energy. This implies the existence of nonperturbative sectors controlling the asymptotics of the Gromov–Witten invariants, which could themselves have an enumerative-geometry interpretation. The examples addressed include: the resolved conifold; the local surfaces local $\mathbb{P}^2$ and local $\mathbb{P}^1 \times \mathbb{P}^1$; the local curves and Hurwitz theory; and the compact quintic. All examples suggest very rich interplays between resurgent asymptotics and enumerative problems in algebraic geometry.

Keywords: Asymptotics, Resurgent Analysis, Enumerative Geometry, Algebraic Geometry, Topological Strings, Gromov–Witten Invariants, Gopakumar–Vafa Invariants

Contents

1 Introduction

Geometrical-counting problems, albeit many times rather natural and simple to formulate, may lead to remarkably rich and interesting structures. Among these, enumerative invariants play an important classification role within algebraic geometry. For example, counting pseudo-holomorphic curves inside symplectic manifolds gives rise to the famous Gromov–Witten (GW) invariants. These are invariants associated to the symplectic manifold $\mathcal{X}$, which are rational numbers (implying a "virtual" counting) depending on both genus, g, and degree, d, of the embedded curve. We shall denote them by $N_{g,d}$. The computation of GW invariants is generically hard, becoming simpler when the manifold is Calabi–Yau (CY) where they are generated by the A-model topological-string free energy. This is a long story which goes back to the discovery of mirror symmetry; see, *e.g.*, [1–10] for early references, and, *e.g*, [11–15] for reviews.

Consider the A-model on a CY $\mathcal{X}$, in the large-radius phase (valid when the Kähler parameter t is large). The A-model free energy is then given by an asymptotic, genus expansion

$$F(\mathcal{X}) \simeq \sum_{g=0}^{+\infty} g_{\text{s}}^{2g-2} F_g(t), \tag{1.1}$$

where the genus-g contributions to the free energy may be decomposed as [6]

$$F_g(t) = \sum_{d>0} N_{g,d}\, Q^d. \tag{1.2}$$

The sum over degree d corresponds to a sum over topological sectors as classified by worldsheet instantons (where $Q = \text{e}^{-t}$ in units where $\alpha' = 2\pi$). While this explicitly shows how the topological-string free energy is a generating function for the genus g, degree d, enumerative GW invariants of $\mathcal{X}$, $N_{g,d}$, the two expansions above have rather different properties: while the fixed-genus (1.2) is a *convergent* series, with a non-zero radius of convergence, *e.g.*, [16], (1.1) is instead a *divergent* asymptotic series, with zero radius of convergence, *e.g.*, [17]. The reason for this is the factorial growth of the genus-g contributions with genus, as $F_g \sim (2g)!$.

From the standpoint of defining the string free energy, the asymptotic nature of the perturbative expansion (1.1) implies that $F(\mathcal{X})$ cannot be properly defined by perturbation theory alone. One way to move forward is to use the theory of resurgence [18]. In this context, the perturbative expansion gets enlarged into a transseries, an object which fully captures all information concerning the observable that it represents, including both perturbative/analytic components (in powers of the string coupling g_{s}) and nonperturbative/non-analytic components (in powers of the "instanton" factor $\text{e}^{-1/g_{\text{s}}}$). The asymptotic and resurgent nature of the perturbative sequence implies the existence of these instanton-type terms, of which there can be many distinct types and with different strengths. Remarkably, all these seemingly independent perturbative and nonperturbative sectors in the transseries turn out to be related to each other via a tight web of asymptotic resurgence relations. In particular, the leading factorial growth of perturbation theory is a consequence of these asymptotic relations, as is any other subleading growth correcting that factorial term. As a result, one may in fact extract, or decode, nonperturbative information from perturbation theory alone and vice-versa. Moreover, these interrelations have somewhat universal forms, and should be expected to hold across a wide range of different problems.

In recent years resurgence has been applied within[1] topological string theory [20–34] and its double-scaled limits at special points in moduli space [21, 35, 36, 23, 37, 27, 28]. In particular,

[1] For an introduction to the main ideas of resurgent asymptotics, and a very complete list of references concerning many other recent applications of resurgence, we refer the reader to [19].

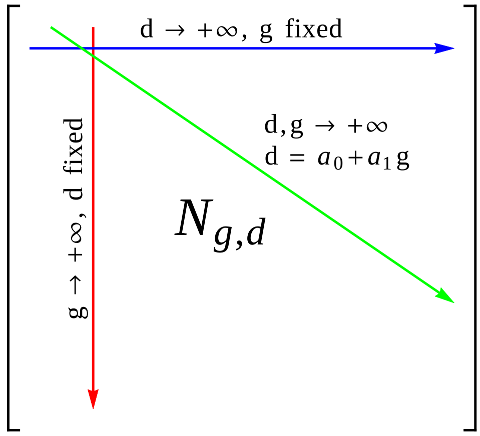

Figure 1: Schematic display of the GW invariants $N_{g,d}$ as a two-dimensional array, with genus and degree representing row and column, respectively. The three arrows are the types of growth that we shall address in this paper: large degree with fixed genus (blue), large genus with fixed degree (red), and combined large degree and genus, with $d = a_0 + a_1 g$ (green).

nonperturbative transseries-solutions to the holomorphic-anomaly equations of the B-model were constructed in [29, 31, 34]. These references further focused on the example of local $\mathbb{P}^2$, a non-compact CY threefold, where a very rich nonperturbative structure was uncovered, with diverse instanton actions vying for dominance on the Borel plane as the moduli changed. In our present paper we wish to turn our attention to the A-model instead, and in particular to the enumerative invariants it generates.

From the standpoint of computing enumerative invariants, the convergence properties of their generating functions might not seem terribly important at first sight. It is nonetheless the case that these convergence properties will dictate the asymptotic behavior of these invariants, in genus and in degree, and this is one of the main question we address in the present work. Furthermore, within the A-model the GW invariants are the internal ingredients constructing the string free energies, and it seems reasonable to transfer resurgence questions and properties from the free energies to the invariants themselves. In particular, one natural question is to ask exactly how the GW invariants are responsible for the (known) factorial growth of the free energies they build. For example, the convergence of (1.2) roughly implies that, at fixed genus, the large-degree asymptotics of the GW invariants[2] $N_{\boldsymbol{g},d}$ corresponds at most to a leading exponential growth. On the other hand, the asymptotic nature of (1.1) might seem to imply that, at fixed degree, the large-genus asymptotics of the GW invariants $N_{g,\boldsymbol{d}}$ corresponds instead to a leading factorial growth, giving rise to the factorial growth inside the free energy. But this will turn out *not* to be the case. The fixed degree, large-genus asymptotics of the GW invariants is *not* factorial, and we shall see how the factorial growth of the free energy is more subtly encoded at the level of GW invariants.

Note that there are some important differences between addressing resurgent transseries for the B-model free energy, and investigating resurgent asymptotics of A-model enumerative invariants. In the former case, one deals with an asymptotic *series*, which subsequently gets completed into a transseries by the addition of new, nonperturbative sectors. In the latter case,

[2]We shall use the notation where the boldface character specifies which index (if any) remains fixed.

one deals instead with a two-dimensional array of (rational) *numbers*, labeled by both genus and degree (which is represented schematically in figure 1). The GW invariants in this array are not directly the coefficients of any series, so the concept of their transseries extension is not well-defined. However, any asymptotic resurgence relations explaining the different growths of the $N_{g,d}$, in particular along directions with factorial growth, should themselves be dictated by nonperturbative content in the free-energy transseries—possibly also with an enumerative-geometry interpretation. This opens the door to the existence of nonperturbative analogues of the GW invariants. With this idea in mind, we wish to make precise the asymptotic growth of GW invariants along particular directions on this array, as depicted in figure 1:

- $\rightarrow$ **Fixed-genus**, large-degree. Possibly the most "classical" direction previously addressed in the literature, giving rise to leading exponential growth.
- $\downarrow$ Large-genus, **fixed-degree**. Less studied, also giving rise to leading exponential growth.
- $\searrow$ Large-genus, large-degree. Not previously addressed in the literature, finally giving rise to the factorial growth characteristic of the free energy.

Asymptotics of GW invariants[3], with focus on the fixed-genus and large-degree regime, have been previously addressed in [6, 40–44], where leading exponential[4] growth was found. To the best of our knowledge, the "enumerative source" of the free-energy factorial growth has never been addressed previously in the literature, and we start filling such gap with our present work. We shall investigate these different asymptotics in several examples, including both compact and non-compact CY threefolds. In particular, our analysis of the exponential growth along horizontal and vertical directions both recovers and generalizes some of the aforementioned previously-known results. The factorial growth is new, and relates to the B-model transseries with its plethora of nonperturbative sectors. Along certain diagonal directions we uncover an universal behavior which is common to geometries in different topological-string universality classes, and which is controlled by the large-radius instanton action. Asymptotic resurgence-like formulae may be written for the "diagonal" growth of GW invariants, with their growth dictated by nonperturbative information encoded in the free-energy transseries. In this sense, one should not wonder about transseries completions of GW invariants, but rather about decoding possibly new "nonperturbative" enumerative invariants, hidden inside the nonperturbative completions to the B-model topological-string transseries [29, 31, 34].

2 Setting the Stage and Main Ideas

Let us formalize the ideas spelled out in our introduction, before addressing an exactly-solvable model (the resolved conifold) in section 3, and then computationally addressing many different examples in section 4, including the cases of local $\mathbb{P}^2$, a diagonal slice of local $\mathbb{P}^1 \times \mathbb{P}^1$, some local curves, Hurwitz theory, and the quintic compact CY threefold. We begin with general expectations and what sort of structures we wish to unveil, to later materialize in our examples.

[3] Asymptotics of related enumerative invariants, such as Donaldson–Thomas or Gopakumar–Vafa invariants, and their relevance towards the computation of M-theoretic black hole entropies, have been addressed in [38, 39].

[4] References [45, 43, 44] address the asymptotics of Weil–Petersson volumes of moduli spaces of algebraic curves, with genus g and n marked punctures (which in some sense corresponds to addressing enumerative invariants of a point). Note that they find some (extra) factorial growth $\sim n!$, but which is associated to the (extra) number of punctures, n. In our context this number is $n = 0$, as GW invariants arise from the free energy.

Going back to the topological-string asymptotic-series for the free energy (1.1), let us describe it in the B-model as $F^{(0)}(g_{\rm s}; z, \bar{z})$. Here, the string coupling $g_{\rm s}$ is also the resurgent variable, and the (0) superscript specifies perturbative. The pair $(z, \bar{z})$ may be regarded as just external parameters, or interpreted as complex-structure moduli of the underlying CY threefold. The free energy is asymptotic, of Gevrey-1 type (see, *e.g.*, [46]),

$$F^{(0)} \simeq \sum_{g=0}^{+\infty} g_{\rm s}^{2g-2} F_g^{(0)}, \qquad F_g^{(0)} \sim \Gamma(2g-1) \text{ as } g \to +\infty, \tag{2.1}$$

for generic values of $(z, \bar{z})$. Understanding the resurgent properties of $F^{(0)}$ and the role played by the moduli $(z, \bar{z})$ was the main purpose of [29, 31]. There, it was shown how to look for a transseries completion to the topological-string free energy of the form

$$F = \sum_{n=0}^{+\infty} \sigma^n \, {\rm e}^{-nA(z)/g_{\rm s}} \, F^{(n)}(g_{\rm s}; z, \bar{z}), \tag{2.2}$$

where the (multi) instanton sectors $F^{(n)}(g_{\rm s})$ are also given by asymptotic series. In particular, it was found—both generically and in examples—that (2.2) has several nonperturbative sectors, with associated actions A_α, all of them holomorphic and determined by the CY geometry.

The transseries (2.2) was constructed by combining a nonperturbative interpretation of the holomorphic anomaly equations of [6] with the resurgence relations that transseries generically satisfy, such as, for example,

$$F_g^{(0)}(z, \bar{z}) \sim \frac{\Gamma(2g-1)}{A(z)^{2g-1}} \, F_0^{(1)}(z, \bar{z}), \qquad \text{as } g \to +\infty. \tag{2.3}$$

Here $F_0^{(1)}$ is the first coefficient of the one-instanton series $F^{(1)}(g_{\rm s})$ and $A(z)$ is one of the instanton actions (the smallest one in absolute value, for the particular value of z). Subleading corrections to (2.3) lead to further multi-loop coefficients, $F_h^{(1)}$ with $h = 1, 2, \ldots$. Generalizations of (2.3), now addressing the large-order behavior of the $F_g^{(n)}$ sequences, provide new constraints and relations between higher instanton coefficients.

This route towards the construction of (2.2), further developed in [34], draws a rather complete picture of what a transseries for $F(g_{\rm s})$ should look like. In principle, such a transseries should contain all nonperturbative information concerning the B-model, but also, via mirror symmetry [10], all A-model nonperturbative information. It is within this context that we shall set our attention upon structures of interest in algebraic and enumerative geometry, arising from the A-model set-up, in particular the case of enumerative GW invariants.

Let us spell out our strategy. The B-model construction (2.2) depends upon $(z, \bar{z})$, the complex-structure moduli. From the standpoint of resurgence, these moduli may be regarded as external parameters, without any resurgent properties by themselves. But upon mirror symmetry, they relate the B-model CY threefold $\widetilde{\mathcal{X}}$, with complex structure z, to the A-model mirror-CY threefold $\mathcal{X}$, with Kähler structure t. A functional relation $t = t(z)$ is then provided by the mirror map. This means that one may in fact compute the *mirror transseries* to (2.2), where its $F_g^{(0)}(t)$ components are nothing but the GW generating functions as in (1.2). Let us next focus on these enumerative invariants in greater detail, with the goal of uncovering which resurgent properties they carry, either intrinsic or merely inherited from the free energy.

2.1 Enumerative Gromov–Witten Invariants

GW invariants count embeddings of Riemann surfaces of a given genus into a CY threefold $\mathcal{X}$, attending to the homology class of the image of this map. Thus, GW invariants are labelled by $g \in \mathbb{N}$, like the topological-string free energies, and $\beta \in H_2(\mathcal{X}, \mathbb{Z})$,

$$N_{g,\beta} \in \mathbb{Q}. \tag{2.4}$$

Akin to (1.2), they show up in the A-model perturbative free-energies through the expansion

$$F_g^{(0)} = \sum_{\beta \in H_2(\mathcal{X},\mathbb{Z})} N_{g,\beta}\, Q^\beta. \tag{2.5}$$

Here we have used the mirror map to translate from complex structure moduli, z_i, to Kähler moduli, $t_i =: -\log Q_i$ (roughly, the mirror map is $Q_i = \mathcal{O}(z_i)$). More precisely, if ω is the (complexified) Kähler form in $\mathcal{X}$ and $[S_i]$, with $i = 1, 2, \ldots, b_2(\mathcal{X})$, is a basis of $H_2(\mathcal{X}, \mathbb{Z})$, then one finds $\beta = \sum_i n_i [S_i]$ and $t_i := \int_{[S_i]} \omega$, in which case we may denote $Q^\beta = \prod_i Q_i^{n_i} = \exp(-\sum_i n_i\, t_i)$. In order to simplify things in the following, we shall restrict to examples where $b_2(\mathcal{X}) = 1$, in which case the sum over homology classes simplifies to

$$F_g^{(0)}(t) = \sum_{d=1}^{+\infty} N_{g,d}\, Q^d. \tag{2.6}$$

The index d is called the degree of the embedding. See, *e.g.*, [14] for more details on the relation between the enumerative GW invariants and their A-model generating functions.

Now (2.6) is a convergent series in Q, which, in particular, implies that it is *not* resurgent. Its non-vanishing radius of convergence is generically finite, due to a nearby singularity located at the so-called conifold locus [8]. This convergence may already suggest that the factorial growth of the free energies $F_g^{(0)}$ in genus must somehow arise from a combined contribution of several different degrees. We shall next try to understand how this might come about.

2.2 Growth of Enumerative Invariants in Degree and in Genus

As we introduce most of our main ideas, let us illustrate them with (partial) results from upcoming diverse examples. The simplest such example is naturally attached to the resolved conifold, for which the free energies can be computed exactly (see, *e.g.*, [47] for a review)

$$F_g^{(0),\text{coni}}(t) = (-1)^{g-1} \frac{B_{2g}}{2g\,(2g-2)!} \operatorname{Li}_{3-2g}\left(\mathrm{e}^{-t}\right), \qquad g \geq 2, \tag{2.7}$$

where $\operatorname{Li}_p(x)$ is the polylogarithm function. This immediately yields all GW invariants as

$$N_{g,d}^{\text{coni}} = f_g^{\text{CS}}\, d^{2g-3}, \qquad f_g^{\text{CS}} := (-1)^{g-1} \frac{B_{2g}}{2g\,(2g-2)!}. \tag{2.8}$$

More interesting geometries we shall later address include the (non-compact) local $\mathbb{P}^2$ and the (compact) quintic CY threefolds, for which there are no such closed-form expressions. Enumerative invariants may, nonetheless, be generated on the computer to see in more detail how they grow in degree and genus. An example of the sort of numbers we have to work with is show in figure 2, in the instance of local $\mathbb{P}^2$ (to be addressed in section 4.1).

$\log\lvert N_{g,d}\rvert$	20	21	22	23	24	25	26	27	28	29	30	31	32	33	34	35	36	37	38	39	40
20	111.4	117.1	122.6	128.0	133.2	138.3	143.4	148.3	153.2	157.9	162.6	167.3	171.8	176.3	180.8	185.2	189.5	193.9	198.1	202.3	206.5
21	113.7	119.6	125.3	130.8	136.2	141.4	146.6	151.6	156.6	161.5	166.3	171.0	175.7	180.3	184.8	189.3	193.7	198.1	202.5	206.8	211.1
22	116.0	122.0	127.9	133.5	139.1	144.5	149.7	154.9	160.0	165.0	169.9	174.7	179.5	184.2	188.8	193.4	197.9	202.4	206.8	211.2	215.5
23	118.2	124.4	130.4	136.2	141.9	147.4	152.8	158.1	163.3	168.4	173.4	178.4	183.2	188.0	192.8	197.4	202.0	206.6	211.1	215.6	220.0
24	120.4	126.7	132.9	138.9	144.7	150.3	155.9	161.3	166.6	171.8	177.0	182.0	187.0	191.8	196.7	201.4	206.1	210.7	215.3	219.9	224.4
25	122.5	129.0	135.3	141.5	147.4	153.2	158.9	164.4	169.9	175.2	180.4	185.6	190.6	195.6	200.5	205.4	210.1	214.9	219.5	224.2	228.7
26	124.5	131.2	137.7	144.0	150.1	156.0	161.8	167.5	173.1	178.5	183.9	189.1	194.3	199.3	204.3	209.3	214.1	219.0	223.7	228.4	233.0
27	126.5	133.4	140.0	146.5	152.7	158.8	164.8	170.6	176.2	181.8	187.2	192.6	197.8	203.0	208.1	213.1	218.1	223.0	227.8	232.6	237.3
28	128.5	135.5	142.3	148.9	155.3	161.5	167.6	173.5	179.3	185.0	190.6	196.0	201.4	206.7	211.9	217.0	222.0	227.0	231.9	236.8	241.6
29	130.4	137.6	144.6	151.3	157.9	164.2	170.4	176.5	182.4	188.2	193.9	199.4	204.9	210.3	215.6	220.8	225.9	231.0	236.0	240.9	245.8
30	132.2	139.6	146.7	153.7	160.4	166.9	173.2	179.4	185.4	191.3	197.1	202.8	208.4	213.8	219.2	224.5	229.7	234.9	240.0	245.0	249.9
31	134.0	141.6	148.9	155.9	162.8	169.5	175.9	182.2	188.4	194.4	200.3	206.1	211.8	217.4	222.9	228.2	233.6	238.8	244.0	249.1	254.1
32	135.7	143.5	151.0	158.2	165.2	172.0	178.6	185.1	191.4	197.5	203.5	209.4	215.2	220.9	226.4	231.9	237.3	242.7	247.9	253.1	258.2
33	137.4	145.4	153.0	160.4	167.6	174.5	181.3	187.8	194.3	200.5	206.6	212.7	218.5	224.3	230.0	235.6	241.1	246.5	251.8	257.1	262.3
34	139.0	147.2	155.0	162.6	169.9	177.0	183.9	190.6	197.1	203.5	209.7	215.9	221.9	227.7	233.5	239.2	244.8	250.3	255.7	261.0	266.3
35	140.6	149.0	157.0	164.7	172.2	179.4	186.4	193.3	199.9	206.4	212.8	219.0	225.1	231.1	237.0	242.8	248.4	254.0	259.5	265.0	270.3
36	142.2	150.7	158.9	166.8	174.4	181.8	188.9	195.9	202.7	209.3	215.8	222.2	228.4	234.5	240.4	246.3	252.1	257.7	263.3	268.8	274.3
37	143.7	152.4	160.7	168.8	176.6	184.1	191.4	198.5	205.5	212.2	218.8	225.3	231.6	237.8	243.8	249.8	255.7	261.4	267.1	272.7	278.2
38	145.1	154.0	162.6	170.8	178.7	186.4	193.9	201.1	208.2	215.0	221.8	228.3	234.7	241.0	247.2	253.3	259.2	265.1	270.9	276.5	282.1
39	146.6	155.6	164.3	172.7	180.8	188.7	196.3	203.7	210.8	217.8	224.7	231.4	237.9	244.3	250.6	256.7	262.8	268.7	274.6	280.3	286.0
40	147.9	157.2	166.1	174.6	182.9	190.9	198.6	206.2	213.5	220.6	227.6	234.3	241.0	247.5	253.9	260.1	266.3	272.3	278.3	284.1	289.9

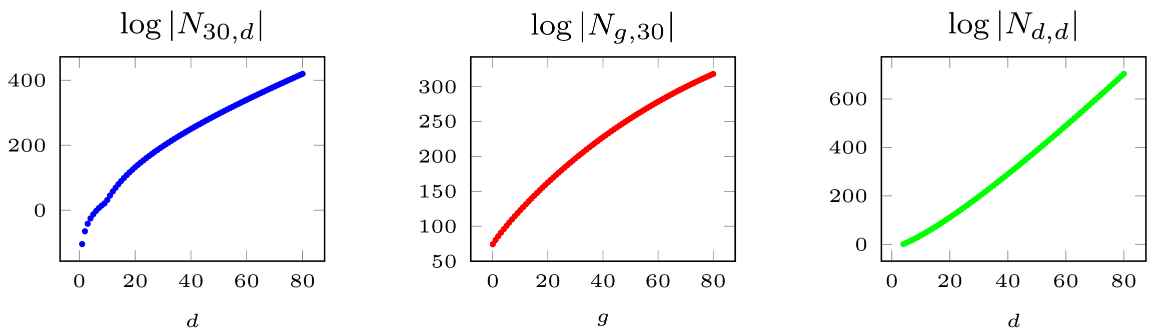

Figure 2: Sample of GW invariants for the local $\mathbb{P}^2$ CY threefold, alongside a visual representation of their growth with respect to degree d (in blue), genus g (in red), and a linear combination of the two (in green). Only in this latter case shall we find a factorial growth.

Growth in Degree

Let us first consider the growth in degree at fixed genus. For the resolved conifold the answer is immediate from (2.8): it is given by the degree d, raised to a linear function of the genus g, namely $2g-3$. For other, more intricate geometries the growth is similar but includes further parameters, such as a critical exponent γ which captures distinct topological-string universality classes, *i.e.*, distinct critical behaviors at the phase-transition point (see, *e.g.*, [42] for a discussion). In general one finds[5] [4, 6, 40]

$$N_{\boldsymbol{g},d} \sim d^{(\gamma-2)(1-\boldsymbol{g})-1}\, \mathrm{e}^{dt_{\mathrm{c}}} \left(\log d\right)^{\alpha+\beta\boldsymbol{g}}\,, \qquad \text{as } d \to +\infty \tag{2.9}$$

(further including a possibly g-dependent pre-factor). In this expression, $\mathrm{e}^{-t_{\mathrm{c}}} = Q_{\mathrm{c}}$ marks the radius of convergence of $F_g^{(0)}$ on the Q-plane. Expression (2.9) implies that the resolved conifold has $\gamma = 0$, being in the same universality class as, *e.g.*, the local $\mathbb{P}^2$ or the quintic CY threefolds. For example, for the quintic we have [4, 6]

$$N_{\boldsymbol{g},d}^{\text{quint}} \sim d^{2\boldsymbol{g}-3}\, \mathrm{e}^{dt_{\mathrm{c}}} \left(\log d\right)^{2\boldsymbol{g}-2}, \tag{2.10}$$

where $t_{\mathrm{c}} = 7.58995\ldots$. For local $\mathbb{P}^2$ this growth is illustrated in the leftmost plot of figure 2, at fixed genus $g = 30$. For very large degree d, the plotted curve must tend to a straight line of slope $|t_{\mathrm{c}}|$. On the other hand, for the family of local curves $X_p = \mathcal{O}(p-2) \oplus \mathcal{O}(-p) \to \mathbb{P}^1$ $(p \geq 3)$

[5] Recall the notation where the boldface character specifies which index (if any) is the fixed one.

the critical exponent is instead $\gamma = -1/2$ [42], implying a distinct universality class and we shall discuss this example later in section 4.3.

As mentioned earlier, the radius of convergence Q_c signals a singularity of the (free energy) generating function. This is the conifold point [8], the point in moduli space where the A-model geometric interpretation breaks down, with a phase transition taking place from the large-radius (geometric) phase to a non-geometric phase. Near this singularity,

$$F_g^{(0)} \sim c_g \left(Q_\mathrm{c} - Q\right)^{(1-g)(2-\gamma)}, \qquad g \geq 2. \tag{2.11}$$

Nearby Q_c all geometries within the same universality class will resemble each other, which implies that the coefficients c_g are universal. For example, for $\gamma = 0$ there is a double-scaling limit

$$g_s \to 0, \quad Q \to Q_c, \qquad \text{with} \quad \kappa := g_\mathrm{s} \left(Q_\mathrm{c} - Q\right)^{-1} \quad \text{fixed}, \tag{2.12}$$

such that

$$F^{(0)}(g_\mathrm{s}; t) \to F_{\mathrm{ds}}^{(0)}(\kappa) \simeq \sum_{g=2}^{+\infty} \frac{B_{2g}}{2g\,(2g-2)}\, \kappa^{2g-2}, \tag{2.13}$$

which matches the $c = 1$ string at self-dual radius [8]. For other values of γ the coefficients c_g may be more complicated, being solutions to a nonlinear ODE such as Painlevé I, for example.

Growth in Genus

As we turn towards understanding the dependence of GW invariants on genus, at fixed degree, $N_{g,\boldsymbol{d}}$, it becomes useful to introduce the Gopakumar–Vafa (GV) invariants. These invariants are integer numbers, roughly counting the number of BPS states inside a CY threefold $\mathcal{X}$, and resulting from a reorganization of the A-model free energy as introduced in [48, 49]. The complete result involves a Schwinger-type computation which rewrites the free energy as an index that counts string-theoretic BPS states via an M-theory uplift, and which finally yields

$$\sum_{g=0}^{+\infty} g_\mathrm{s}^{2g-2} F_g^{(0)}(Q) = g_\mathrm{s}^2\, c(t_i) + \ell(t_i) + \sum_{r=0}^{+\infty} \sum_{\beta} n_r^{(\beta)} \sum_{m=1}^{+\infty} \frac{1}{m} \left(2 \sin \frac{m g_\mathrm{s}}{2}\right)^{2r-2} Q^{\beta m}. \tag{2.14}$$

Here, the $n_r^{(\beta)} \in \mathbb{Z}$ are the GV invariants, labeled by the Kähler class β and a spin index r. The polynomials $c(t_i)$ and $\ell(t_i)$ will play no role in the following.

It is straightforward to check that, generically, the GW invariants may be written explicitly in terms of the GV invariants as

$$N_{g,d} = \sum_{r=0}^{g} c_{r,g} \sum_{\beta | d} n_r^{(\beta)} \left(\frac{d}{\beta}\right)^{2g-3}, \qquad \text{using} \quad \left(2 \sin \frac{x}{2}\right)^{2r-2} =: \sum_{h=r}^{+\infty} c_{r,h}\, x^{2h-2}. \tag{2.15}$$

In here we already find the d^{2g-3} dependence which is characteristic of the resolved conifold. Now, an important property of the GV invariants, which will be useful in the following, is that for each degree d there is a specific genus, $G(d)$, after which all these invariants vanish, *i.e.*, $n_r^{(d)} = 0$ for $r > G(d)$ [49]. This function $G(d)$ is a polynomial in d, and this will simplify the dependence on g in (2.15) by replacing the upper limit in the r-sum,

$$N_{g,d} = \sum_{r=0}^{G(d)} c_{r,g} \sum_{\beta | d} n_r^{(\beta)} \left(\frac{d}{\beta}\right)^{2g-3}. \tag{2.16}$$

In this expression the only remaining dependence upon the genus, g, lies in the coefficients $c_{r,g}$ and in the power of d/β. Since the coefficients $c_{r,g}$ are *independent* of the CY geometry, we should expect a generic formula to hold for the large growth of $N_{g,\boldsymbol{d}}$ in genus. For example, as we shall discuss later on, for the quintic threefold and degree $d=4$ we find

$$N^{\text{quint}}_{g,d=4} \sim (-1)^{g-1} \frac{B_{2g}}{2g\,(2g-2)!}\, 4^{2g-3} \left(3 - \frac{6}{2^{2g-3}} - \frac{192}{4^{2g-3}}\right) + \frac{(-1)^{g-1}}{(2g-2)!} \frac{2^{2g-2}}{4} \left(120 + \frac{336}{2^{2g-2}}\right), \tag{2.17}$$

This formula, involving Bernoulli numbers and factorials, is actually *exact* for $g \geq 2$, not just a large-g approximation. The first numbers $(3, -6, -192)$ can be recognized as the GV invariants $n_0^{(1)}$, $n_0^{(2)}$, and $n_0^{(3)}$ for the quintic threefold, whereas the other $(120, 336)$ are more complicated combinations involving higher-genera invariants. As such, in general, we can expect the following formula to hold (see appendix A for a proof)

$$N_{g,d} = f_g^{\text{CS}} \left\{ \sum_{n|d} a_n \left(\frac{d}{n}\right)^{2g-3} + \frac{2g}{B_{2g}} \frac{1}{d} \left(c_d\, \delta_{g,1} + \sum_{n=1}^{G(d)-1} b_{d,n}\, n^{2g-2} \right) \right\}. \tag{2.18}$$

where $a_d \equiv n_0^{(d)}$ and $b_{d,n}, c_d \in \mathbb{Z}$. In this expression the dependence on the genus g is explicit—one could even plug-in non-integer values of the genus after analytically continuing the Bernoulli numbers. If we fix the degree, as in $N_{g,\boldsymbol{d}}$, it is then simple to see that the leading growth in genus is exponential, $\boldsymbol{d}^{2g-3}$, with further subleading exponential and inverse-of-factorial corrections in g. The second plot in figure 2 illustrates this genus dependence, at fixed degree $d=30$, for local $\mathbb{P}^2$. The plotted curve is asymptotic to a straight line of slope $2\log \boldsymbol{d}$.

Expression (2.18) shows how the contribution of GW invariants, $N_{g,\boldsymbol{d}}$, to the free energies at a fixed single degree, $\boldsymbol{d}$, again cannot be responsible for the factorial growth we need to find. In this way, the only option we have left to find the $\sim (2g)!$ factorial growth of the free energies, encoded in the GW invariants, is to address the *combined* growth in genus and degree.

Combined Growth in Genus and Degree

Upon a second look at the (already familiar) characteristic behavior of GW invariants in d^{2g-3}, it should be straightforward to deduce that when d and g are linearly related, then the factorial growth is immediately realized. The link is the classical Stirling approximation,

$$n^n \sim \frac{n!\, \mathrm{e}^n}{\sqrt{2\pi n}}. \tag{2.19}$$

Consider one more time the example of the resolved conifold in (2.8), and assume the dependence $d = a_0 + a_1 g$ for some values of a_0 and a_1. Then, to leading order in g, one finds

$$N^{\text{coni}}_{g,d=a_0+a_1 g} \sim \frac{\Gamma\left(2g - \frac{3}{2}\right)}{\left(\frac{4\pi}{\mathrm{e}\, a_1}\right)^{2g-\frac{3}{2}}} \frac{\left(\frac{2\,\mathrm{e}}{a_1}\right)^{\frac{3}{2}} \mathrm{e}^{2\frac{a_0}{a_1}}}{2\pi^2}. \tag{2.20}$$

The factorial in g is now explicit and it comes from the term d^{2g-3} when $d = a_0 + a_1 g$. On the other hand, recall that the leading growth of the free energy $F_g^{(0),\text{coni}}$ in this case is [23]

$$F_g^{(0),\text{coni}}(Q) \sim \frac{\Gamma(2g-1)}{(2\pi t)^{2g-1}} \frac{t}{\pi}, \tag{2.21}$$

with instanton action $A = 2\pi t$. To connect this resurgence relation to the one in (2.20), one has to recall the definition of GW invariants (2.6)

$$F_g^{(0),\text{coni}} = \sum_{d=1}^{+\infty} N_{g,d}^{\text{coni}}\, Q^d, \tag{2.22}$$

and then notice that the largest contribution to this sum, for a fixed value of Q on the right-hand side, comes from

$$\frac{\partial}{\partial d}\left(N_{g,d}^{\text{coni}} Q^d\right) = 0 \qquad \Rightarrow \qquad d = \frac{2g-3}{t}. \tag{2.23}$$

So we should expect that taking $a_1 = 2/t$ and $a_0 = -3/t$ in (2.20) will reproduce something resembling (2.21). Indeed, one can easily check that we obtain the same instanton action as $\frac{4\pi}{a_1} = 2\pi t$ (where we ignore the exponential factor, e, since it belongs within Q^d).

This strategy of selecting the leading contribution from the Q-expansion inside $F_g^{(0)}(Q)$ can be pushed further. One way to do so is to approximate the sum over the degree by an integration, and then perform a saddle-point approximation—and this will be a main theme throughout our analyses. Consider the following saddle-point approximation around $x = x_0$ (where $V'(x_0) = 0$),

$$\Phi(\lambda) = \int_0^{+\infty} \mathrm{d}x\, \mathrm{e}^{\lambda V(x)} \sim \mathrm{e}^{\lambda V(x_0)} \sqrt{-\frac{2\pi}{\lambda V''(x_0)}} \left(1 + \mathcal{O}\left(\frac{1}{\lambda}\right)\right). \tag{2.24}$$

To apply this generic formula to our problem one just has to identify

$$\Phi(\lambda) \leftrightarrow F_g^{(0)}(Q), \qquad \mathrm{e}^{\lambda V(x)} \leftrightarrow N_{g,x}\, Q^x, \qquad x \leftrightarrow d, \qquad \lambda \propto g. \tag{2.25}$$

The only subtlety in this identification is that the saddle-point x_0 is also proportional to the coupling λ, as we saw for the resolved conifold (2.23). In any case, our goal is to solve for $\mathrm{e}^{\lambda V(x_0)}$ in (2.24). Then, the only obstacle we have in order to do so is knowing the value of $V''(x_0)$. For the resolved conifold we had an explicit formula and, as such, we knew that it was $-t/(a_0+a_1 g)^2$ where $x_0 = a_0 + a_1 g$ and λ chosen the same; but in general there are no such explicit formulae. Nonetheless, let us postulate a completely similar dependence in g, namely

$$V''(x_0) \equiv -\frac{a_2(Q)}{\lambda^2} + \mathcal{O}\left(\frac{1}{\lambda^3}\right), \tag{2.26}$$

where we have chosen the explicit relation $\lambda = a_0 + a_1 g$, and introduced the function $a_2(Q)$. If one makes further use of the leading large-order growth of the free energies [29],

$$\Phi(\lambda) = F_g^{(0)}(Q) \sim \frac{\Gamma\left(2g-\beta\right)}{A^{2g-\beta}}\, F_0^{(1)}, \tag{2.27}$$

we finally obtain

$$N_{g,x_0}\, Q^{x_0}\big|_{x_0=a_0+a_1 g} \sim \frac{\Gamma\left(2g-\beta-\frac{1}{2}\right)}{A^{2g-\beta-\frac{1}{2}}} \left(\frac{a_2}{\pi a_1 A}\right)^{\frac{1}{2}} F_0^{(1)}. \tag{2.28}$$

Note that this large-order relation depends on a_1 and a_2, functions of Q which define the position and shape of the saddle. For the resolved conifold, and even for other geometries with actions proportional to a Kähler parameter, we find that $a_1 = 2/t$ and $a_2 = t$. But for general geometries

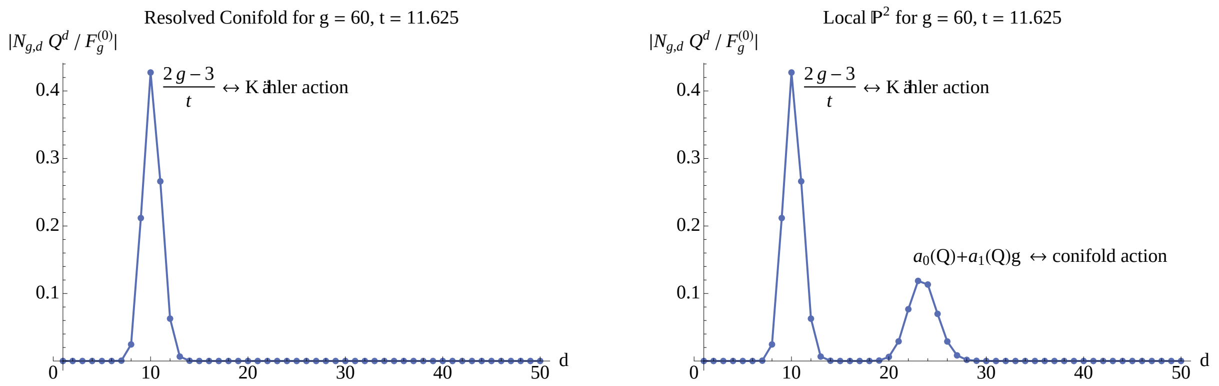

Figure 3: Graphical representation of which GW invariants contribute the most to a free energy $F_g^{(0)}(Q)$, for fixed values of g and $Q = \mathrm{e}^{-t}$. This contribution is estimated by comparing the value of $N_{g,d}\, Q^d$, at different values of the degree d, against the total value of the genus-g perturbative free energy $F_g^{(0)}$. The resolved conifold, portrayed on the left, has a single saddle-point corresponding to the action $A = 2\pi t$; whereas for local $\mathbb{P}^2$, portrayed on the right, an extra saddle-point attached to the conifold action is also present. These saddles may exchange dominance depending on the value of Q, but the set of leading degrees will always be in correspondence with the set of leading instanton actions.

we do not know what these functions are or should be, and one has to run computational experiments in order to judiciously try to fix them. Note that once one approximates the sum over the degree by an integration, then different saddles will correspond to different leading actions, which may depend on the value of Q. For the resolved conifold there is only one leading action and one saddle. But for general geometries we can expect several of them—albeit one is always proportional to the Kähler parameter t. This is illustrated in figure 3, where we have plotted saddles for the resolved conifold and local $\mathbb{P}^2$ (we shall discuss these plots in greater detail later on). The saddles are identified by numerically selecting, at fixed values of g and t but varying d, the GW invariants which contribute the most to the perturbative free energy. Both models clearly show a saddle associated to a Kähler action, with $A = 2\pi t$. For local $\mathbb{P}^2$ there is one further saddle, related to a conifold action, to be discussed in section 4.1.

The Main Question

Let us finally address the main question motivating this paper. Are there nonperturbative extensions of the enumerative GW invariants—denote them by "$N_{g,d}^{(n)}$", with n an "instanton label"—just like there are nonperturbative extensions $F_g^{(n)}$ of the perturbative free energy? And if so, what is their enumerative interpretation, *i.e.*, which counting problem is associated to these new numbers? An argument in favor of an affirmative answer arises from considering the A-model mirror to the B-model resurgent analysis of the free energy, and its associated transseries constructions [29, 31]. But while the perturbative $F_g(Q)$ collect the GW invariants as a Q-expansion, the higher instanton sectors $F_g^{(n)}(t)$ are not regular at $Q = 0$ and a naive Q-expansion is now not an option. Then how do we extract the nonperturbative counterparts?

Schematically, we want to make sense of the following diagram

$$
\begin{array}{ccc}
F_g^{(0)} & \xrightarrow{\text{resurgence}} & F_g^{(n)} \\
{\scriptstyle Q\text{-expansion}}\big\downarrow & & \big\downarrow{\scriptstyle \text{expansion?}} \\
N_{g,d} & \underset{\text{resurgence + interpretation?}}{\dashrightarrow} & \text{“}N_{g,d}^{(n)}\text{”?}
\end{array}
\tag{2.29}
$$

The left and upper arrows are well understood. The left arrow is just the A-model definition of GW invariants, while the upper arrow was made precise within the B-model set-up in [29, 31]. In this paper we try to take the first (exploratory) steps towards the definition of lower and right arrows, but a complete answer can only come with a geometric/enumerative interpretation of these conjectured quantities “$N_{g,d}^{(n)}$”, which is beyond the scope of the present work.

Further note that, as GW invariants themselves have no transseries completions, we do not expect the lower arrow to be defined directly but rather as combination of left, upper, and right arrows (alongside the mirror map). In this way, one will have to extract the “$N_{g,d}^{(n)}$ invariants” directly out of the nonperturbative sectors $F_g^{(n)}$. Now, the Q-expansion of the perturbative sector arises from a worldsheet-instanton expansion and thus naturally relates to a counting problem. But the nonperturbative sectors lack such power-series expansions in Q, implying that any nonperturbative GW invariants hidden inside the nonperturbative free-energies might be difficult to extract and their enumerative interpretation harder to decode. Furthermore, even after performing an asymptotic resurgent analysis of $N_{g,d}$, we have to disentangle the dependence in t, coming from the parameters a_0 and a_1, in the linear dependence between degree and genus. At the end of the day, this leaves the right arrow to be defined. What one has to do is to understand, via mirror symmetry, how to relate nonperturbative multi-loop multi-instanton coefficients in the B-model transseries, to the nonperturbative sectors appearing in the asymptotic resurgence relations for the combined genus/degree growth of GW invariants.

Our goal in this paper is to initiate this line of research, computationally exploring diverse CY examples. We try to identify the structure of these new invariants, as they are encoded in the nonperturbative content of the A-model free energy, but shall leave open their subsequent enumerative interpretation for future research.

3 An Exactly-Solvable Model: The Resolved Conifold

This section addresses our first example, concerning an exactly solvable model: the resolved conifold. This toric variety is a non-compact CY threefold which is the total space of the bundle $\mathcal{O}(-1)\oplus\mathcal{O}(-1)\to\mathbb{P}^1$. The perturbative free-energy for the resolved conifold can be computed exactly to all orders in the genus expansion (see, *e.g.*, [47] and references therein). This of course translates to the fact that one may obtain analytical expressions for all its (infinite) GW invariants [50]. For any genus g, the results are

$$F_0^{(0)} = \frac{t^3}{12} - \frac{\pi^2 t}{6} + \zeta(3) - \mathrm{Li}_3\left(\mathrm{e}^{-t}\right), \tag{3.1}$$

$$F_1^{(0)} = -\frac{t}{24} + \zeta'(-1) + \frac{1}{12}\,\mathrm{Li}_1\left(\mathrm{e}^{-t}\right), \tag{3.2}$$

$$F_g^{(0)} = \frac{B_{2g} B_{2g-2}}{2g\,(2g-2)\,(2g-2)!} + (-1)^{g-1} \frac{B_{2g}}{2g\,(2g-2)!} \mathrm{Li}_{3-2g}\left(\mathrm{e}^{-t}\right), \qquad g \geq 2, \tag{3.3}$$

where $\mathrm{Li}_p(z)$ is the polylogarithm of index p. In the following we will drop the contribution from the constant map [51, 50] and mostly focus on the large-order contributions $g \geq 2$.

Due to the polylogarithm these free energies grow factorially in the genus and lead to an asymptotic, Gevrey-1 perturbative free-energy [46]. The resurgent properties of this series have been studied in detail in [23, 32], with the result

$$F_g^{(0)} \sim \sum_{n=1}^{+\infty} \sum_{m\in\mathbb{Z}} \left\{ \frac{\Gamma\left(2g-1\right)}{\left(nA_m\right)^{2g-1}} \frac{A_m}{2\pi^2 n} + \frac{\Gamma\left(2g-2\right)}{\left(nA_m\right)^{2g-2}} \frac{1}{2\pi^2 n^2} \right\}, \tag{3.4}$$

where $A_m(t) = 2\pi\left(t + 2\pi \mathrm{i} m\right)$ are the instanton actions. For our purposes, we shall focus on the *leading* contribution, whose action is $A = 2\pi t$, in which case

$$F_g^{(0)} \sim \frac{\Gamma\left(2g-1\right)}{A^{2g-1}} \frac{A}{2\pi^2}. \tag{3.5}$$

Let us next translate these resurgent properties to the level of GW invariants.

The GW invariants for the resolved conifold can be immediately read from the free energies, by simply expanding the polylogarithm in power series. One finds

$$N_{g,d}^{\text{coni}} = f_g^{\text{CS}}\, d^{2g-3}, \tag{3.6}$$

where f_g^{CS} includes the Bernoulli dependence and is defined in (2.8). These invariants have such a simple form, given that they are actually generated by a single non-vanishing GV invariant

$$n_0^{(1)} = 1. \tag{3.7}$$

Likewise, the *abc*-coefficients we introduced in (2.18) vanish except for the one which equals the GV invariant, $a_1 = n_0^{(1)} = 1$. This makes this geometry considerably simpler than the ones we shall explore later, allowing for an analytic treatment whose features will also show up later.

As we anticipated in some detail in the previous section, the factorial growth of the free energy arises from the term d^{2g-3} when d grows linearly with g. This is completely precise when the degree is a saddle point, in the sense explained earlier. This point, $d = (2g-3)/t$, was computed in equation (2.23) and graphically represented in figure 3 (left plot). One caveat about the saddle-point approximation is that generically the saddle-point lands on non-integer values of the degree. In order to be able to do numerical analyses with actual GW invariants, we look at nearby (integer) values of the degree. A practical computational choice, one that we will also use for other geometries, is to set

$$g = \frac{t}{2} d + q, \quad \text{with} \quad -\left\lfloor \frac{t}{4} - \frac{3}{2} \right\rfloor \leq q \leq \left\lfloor \frac{t}{4} + \frac{3}{2} \right\rfloor, \tag{3.8}$$

and set t to an even integer (and q must consequentially be an integer).

Since in this example there is an analytic expression for all GW invariants, we can use it to obtain the resurgence relation

$$f_g^{\text{CS}}\, d^{2g-3}\, Q^d \Big|_{g=\frac{t}{2}d+q} \sim \sum_{h=0}^{+\infty} \frac{\Gamma\left(2g-\frac{3}{2}-h\right)}{\left(2\pi t\right)^{2g-\frac{3}{2}-h}} \frac{t^{\frac{3}{2}-h}}{2^{2h+1}\,\pi^{h+2}}\, \mathcal{P}_h(q). \tag{3.9}$$

where the $\mathcal{P}_h(q)$ are polynomials in q of degree $2h$ with rational coefficients, the first of which are

$$\mathcal{P}_0(q) = 1, \tag{3.10}$$

$$\mathcal{P}_1(q) = -\frac{71}{12} + 12q - 4q^2, \tag{3.11}$$

$$\mathcal{P}_2(q) = \frac{11545}{288} - 131q + \frac{419q^2}{3} - \frac{176q^3}{3} + 8q^4, \tag{3.12}$$

$$\mathcal{P}_3(q) = -\frac{17534803}{51840} + \frac{33553q}{24} - \frac{157393q^2}{72} + \frac{15220q^3}{9} - \frac{2062q^4}{3} + \frac{416q^5}{3} - \frac{32q^6}{3}, \tag{3.13}$$

and in general they are such that they make the following asymptotic expansion hold for any q as $x \to +\infty$,

$$\sqrt{2\pi}\, e^{2q-x}\, (x-1)\, (x-2q)^{x-3} \sim \sum_{h=0}^{+\infty} \Gamma\left(x - \frac{3}{2} - h\right) 2^{-h}\, \mathcal{P}_h(q). \tag{3.14}$$

Note that expression (3.9) conforms to the usual resurgence relations, which, for some generic free-energy perturbative expansion, look like (see, *e.g.*, [19] for an introduction)

$$\begin{aligned} F_g^{(0)} &\sim \sum_{n=1}^{+\infty} \frac{\Gamma\left(2g-n\beta\right)}{(nA)^{2g-n\beta}} \frac{S_1^n}{2\pi \mathrm{i}} \sum_{h=0}^{+\infty} \frac{\Gamma\left(2g-n\beta-h\right)}{\Gamma\left(2g-n\beta\right)} F_h^{(n)} \left(nA\right)^h = \\ &= \frac{\Gamma\left(2g-\beta\right)}{A^{2g-\beta}} \frac{S_1}{2\pi \mathrm{i}} \left(F_0^{(1)} + \frac{A}{2g-\beta-1} F_1^{(1)} + \frac{A^2}{(2g-\beta-1)\,(2g-\beta-2)} F_2^{(1)} + \cdots \right) + \\ &+ \frac{\Gamma\left(2g-2\beta\right)}{(2A)^{2g-2\beta}} \frac{S_1^2}{2\pi \mathrm{i}} \left(F_0^{(2)} + \frac{2A}{2g-2\beta-1} F_1^{(2)} + \cdots \right) + \mathcal{O}(3^{-2g}). \end{aligned} \tag{3.15}$$

Indeed, in (3.9) one immediately identifies the $\sim (2g)!$ growth, alongside the instanton action $A = 2\pi t$ which is the *same* action that appears in the free energies. Of course (3.9) also has higher instanton corrections which improve the asymptotics further as in the above expression. These arise from including the (exponentially) subleading terms in $\zeta(2g) = \sum_{n=1}^{+\infty} n^{-2g}$ in the large-g expansion of the Bernoulli numbers, B_{2g}, in (2.8); and from computing the complete large-d transseries expansion of $d^{td+2q-3}$. The result is

$$f_g^{\text{CS}}\, d^{2g-3}\, Q^d \Big|_{g=\frac{t}{2}d+q} \sim \sum_{n=1}^{+\infty} \sum_{h=0}^{+\infty} \frac{\Gamma\left(2g-\frac{3}{2}-h\right)}{(nA)^{2g-\frac{3}{2}-h}} \frac{t^{\frac{3}{2}-h}}{2^{2h+1}\, \pi^{h+2}\, n^{\frac{3}{2}+h}} \mathcal{P}_h(q). \tag{3.16}$$

Some computational tests on the validity of (3.9) are shown in figures 4 and 5. Figure 4 presents a test of the instanton action. We plot the analytical $A_{\text{K}} = 2\pi t$ against numerical tests of this action via (three) Richardson transforms (similar to tests done in, *e.g.*, [21]). An illustration of these transforms for different values of t and q is shown in the inclosed figures. We do this for varying t (the horizontal axis) but also varying q, *i.e.*, each black dot is actually several overlapping black dots, each one the third Richardson transform of the numerical sequence for the instanton action, for that particular value of t and for a range of different values of q. Then figure 5 tests the validity of (3.10) through (3.13) (in fact up to $h = 5$), this time around for fixed q. Each inverted triangle in the plot is again the third Richardson transform of the tested sequence. All these plots very cleanly illustrate the validity of (3.9).

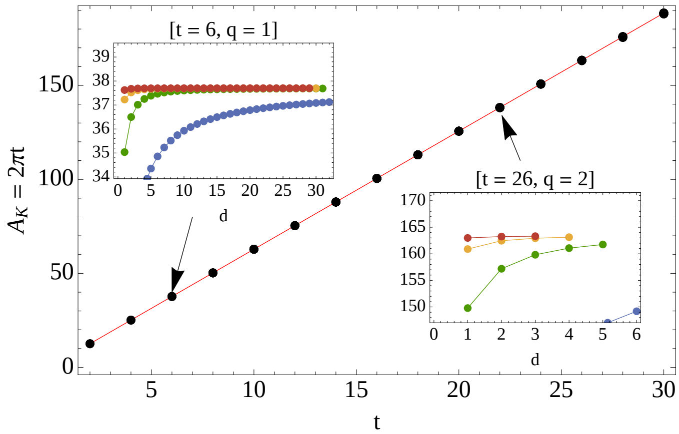

Figure 4: Test of the instanton action $A_{\rm K} = 2\pi t$, from the Kähler saddle-point, for the resolved conifold. The inclosed plots show the convergence for a couple of values of t and q.

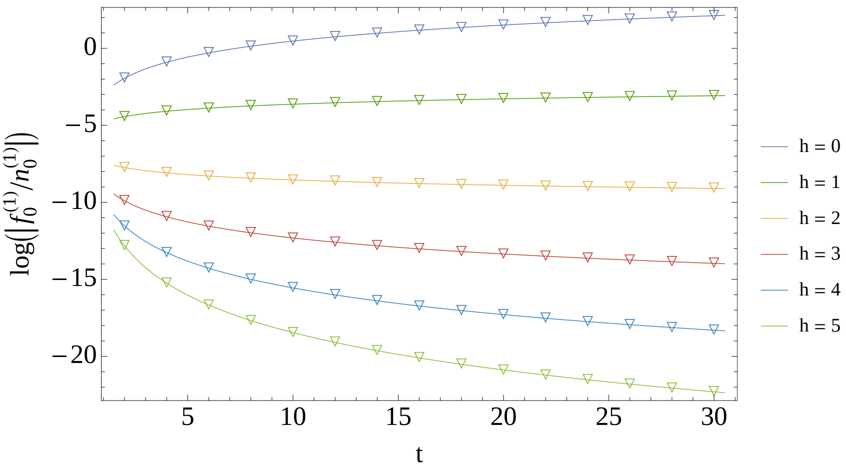

Figure 5: Numerical check of the loop-corrections $f_h^{(1)} := \frac{n_0^{(1)} t^{\frac{3}{2}-h}}{2^{2h+1}\pi^{h+2}}\, \mathcal{P}_h(q)$, for $h = 0, \ldots, 5$ and $q = 1$, for the resolved conifold. We plot the logarithm of the ratio $f_0^{(1)}/n_0^{(1)}$ so that all curves fit within the same graph (and where the GV invariant is $n_0^{(1)} = 1$).

In section 2 we showed how to relate GW asymptotics to free-energy instanton sectors, in particular relating the first term in the right-hand side of (3.9) with the one-loop one-instanton free energy $F_0^{(1)}$; see (2.28) and the discussion which follows. Ideally, one would now like to do the same for the multi-loop (eventually multi-instanton) one-instanton free energies and their relation to higher terms in (3.9). Unfortunately, already finding a direct relation at two-loops, between $F_1^{(1)}$ and any higher term in (3.9), turns out not to be possible using the saddle-point approximation from section 2. In fact, our saddle-point approach is non-standard, in the sense that the saddle-point itself grows with d (or g), which essentially obscures a clear-cut relation between free-energy asymptotics and GW asymptotics beyond the first term. For the present example of the resolved conifold we can bypass this problem, working directly with the explicit form of the GW invariants, but this will not be possible for more complicated examples.

Let us end our discussion of the resolved conifold by going back to our diagram (2.29). As we mentioned earlier, one cannot find nonperturbative GW invariants via a Q-expansion of the resurgent asymptotic expansion for the perturbative free energy $F_g^{(0)}$. This is already clear in equation (3.5), where, although the left-hand side does have a regular expansion around $Q = 0$ from which one reads the GW invariants, the same does not hold true for the right-hand side, where one finds a logarithmic singularity at that same point. In other words, the "resurgence rewriting" of the perturbative free energies, $F_g^{(0)}(Q)$, as an asymptotic series in $1/g$ does not respect, term by term, a regular Q-expansion. Only when we consider all corrections in $1/g$ and perform their resummation (yielding the polylogarithm, in this case of the resolved conifold) can we recover regularity at $Q = 0$. Looking directly at the resurgent GW expansion (3.9), one also sees how the right-hand side has a non-regular Q-dependence through $t = -\log Q$. Although the possibility remains that there might be a better variable than Q or t to establish the match against nonperturbative GW invariants, it may also be the case that there is no such variable and reading nonperturbative GW invariants (naturally formulated using a Q-expansion) from resurgence expressions (naturally written using the t variable) is in fact a nontrivial problem which might require some *a priori* enumerative interpretation to know what to look for. Perhaps the fact that the polynomials (3.10) through (3.13), appearing in the resurgence relation (3.9), have rational coefficients much like the GW invariants themselves, is a clue in that direction.

4 Computational Explorations in Calabi–Yau Threefolds

We shall now move on towards non-trivial geometries, for which there are no closed-form expressions for enumerative GW invariants. We shall instead resort to computational methods in order to explore their asymptotics and resurgent structures.

4.1 The Example of Local $\mathbb{P}^2$

Our first non-trivial example will be a local-surface toric-variety. We start with the non-compact CY threefold known as local $\mathbb{P}^2$, which is the total space of the line bundle $\mathcal{O}(-3) \to \mathbb{P}^2$. This example of local $\mathbb{P}^2$ has a single complex modulus z, and a mirror map of the schematic form $Q = \mathrm{e}^{-t} = \mathcal{O}(z)$, which eventually allows for a calculation of GW invariants [52, 40] (the resulting Kähler modulus being the size of the $\mathbb{P}^2$). In fact, the large-order data for the resurgence analysis first arises in the B-model and will thus require translation into A-model expressions. Specifically, the high genus GW invariants for local $\mathbb{P}^2$ will come out of B-model calculations, both perturbative [53] and nonperturbative [29, 31], followed by mirror symmetry [10].

Free Energies and Gromov–Witten Invariants

The perturbative free energies are best computed within the B-model using the holomorphic anomaly equations, which are recurrence relations in the genus [6, 54]. The GW invariants are then extracted using the mirror map back to the A-model, and removing the anti-holomorphic dependence (in $\bar{z}$) which is introduced by this computation. We shall not get into any details, which may be found in [53], but it is perhaps worth mentioning the Picard–Fuchs equation. Its solutions, the periods, are the source to the genus-zero free energy, the mirror map, and also the instanton actions [26]. For local $\mathbb{P}^2$, the Picard–Fuchs equation is

$$\left\{ (z\partial_z)^3 + 3z^2\, \partial_z \left(3z\partial_z + 1\right) \left(3z\partial_z + 2\right) \right\} f(z) = 0. \tag{4.1}$$

One of its three independent solutions is a constant. Another one, having a $\log z$ singularity, can be identified as the mirror map,

$$\log Q = -t = \log z - 6z + 45z^2 - 560z^3 + \cdots . \tag{4.2}$$

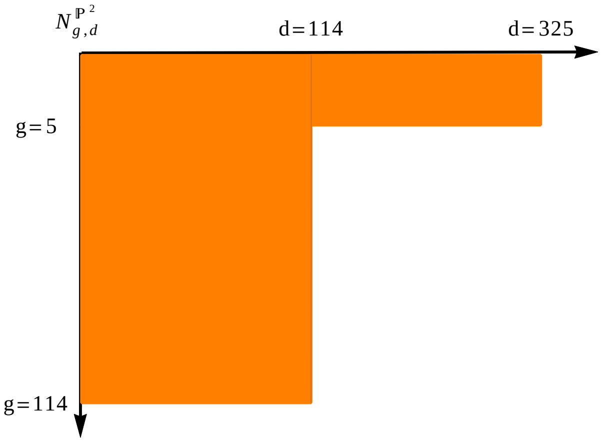

Figure 6: Maximum degree and genus of the GW invariants we computed for local $\mathbb{P}^2$.

The last solution, having a $\log^2 z$ singularity, can be associated to $\partial_t F_0^{(0)}$. Upon integration of this last solution, and use of the mirror map, one finds the genus-zero free energy as

$$F_0^{(0)} = c_3 t^3 + c_2 t^2 + c_1 t + 3Q - \frac{45}{8}Q^2 + \frac{244}{9}Q^3 + \cdots . \tag{4.3}$$

One can ignore the coefficients c_i and then read the GW invariants, $N_{0,d}$, from this Q-series.

Within the B-model, the higher-genus free energies[6], $F_g^{(0)}$, may be compactly written as polynomials in z and $S^{zz}(z,\bar{z})$, an auxiliary variable called the propagator [55]. To extract higher-genus GW invariants one has to use the holomorphic limit of the propagator S^{zz} (in the large-radius frame),

$$S^{zz}_{\text{hol},[\text{LR}]} = \frac{1}{2}Q^2 + 15Q^3 + 135Q^4 + \cdots . \tag{4.4}$$

Consider for example $F_2^{(0)}(z, S^{zz})$, which follows from the holomorphic anomaly equations as

$$F_2^{(0)} = \left(-\frac{1}{3z^3(1+27z)}\right)^2 \left(\frac{5}{24}(S^{zz})^3 - \frac{3z^2}{16}(S^{zz})^2 + \frac{z^4}{16}S^{zz} - \frac{(11-162z-729z^2)\,z^6}{1920}\right) - \frac{1}{1920}. \tag{4.5}$$

Taking the holomorphic limit and using the mirror map, $z = z(Q)$, one then obtains the A-model result

$$F_2^{(0)} = \frac{1}{80}Q + \frac{3}{20}Q^3 - \frac{514}{5}Q^4 + \cdots . \tag{4.6}$$

Here, the coefficients of the Q-expansion are the $N_{2,d}$ GW invariants. In this way, the holomorphic anomaly equations systematically compute $F_g^{(0)}$, out of $F_h^{(0)}$ with $h = 1, \ldots, g-1$, and from them one extracts the $N_{g,d}$ GW invariants as described above. An illustrative (*i.e.*, partial) table of GW invariants for local $\mathbb{P}^2$ may be found in appendix B.1. In figure 6 we schematically represent all the GW invariants we have computed and work with in the present paper.

[6] Note that the genus-one free energy is calculated separately (see [54] for details), and further has a direct relation to the propagator; namely $\partial_z F_0^{(1)} = \frac{1}{2}C_{zzz}S^{zz}$, where $C_{zzz} = \left(-3z^3(1+27z)\right)^{-1}$ is the Yukawa coupling computed out of the Picard–Fuchs equation.

As studied in great detail in [29, 31] the free energies for local $\mathbb{P}^2$, $F_g^{(0)}$, grow factorially fast and render the free-energy expansion asymptotic. The resurgent structure which was uncovered in those references may be summarized as follows. There are several instanton actions, labelled by A_1, A_2, A_3 and $A_{\rm K}$, which give rise to corresponding nonperturbative sectors within the total free-energy transseries. Out of these, two actions are leading at large-order, these are A_1 and $A_{\rm K}$, meaning that for some values of the complex-structure modulus z they are the actions controlling the leading growth of the $F_g^{(0)}$. Around the large-radius point in moduli space, $z = 0$, it is $A_{\rm K} = 2\pi t(z)$ which is leading, and elsewhere it is $A_1 = \frac{2\pi {\rm i}}{\sqrt{3}} T_{\rm c}(z)$, where $T_{\rm c}(z) = 12\sqrt{3}\pi^2 {\rm i}\, \partial_t F_0^{(0)}$ is the flat coordinate[7] around the conifold point $z = -1/27$. For obvious reasons, we name $A_{\rm K}$ as the Kähler action and A_1 as the conifold action (in fact also A_2 and A_3 are related to the conifold point, but they will not play any role in the present paper).

In this case, the large-order growth of the free energies may be either

$$F_g^{(0)} \sim \frac{\Gamma\left(2g-1\right)}{A_1^{2g-1}}\, F_0^{(1)[{\rm c}]} \qquad \text{or} \qquad F_g^{(0)} \sim \frac{\Gamma\left(2g-1\right)}{A_{\rm K}^{2g-1}}\, F_0^{(1)[{\rm K}]}, \tag{4.7}$$

depending on the value of Q. The one-loop one-instanton coefficients are computed from an extension of the holomorphic anomaly equations, alongside the above resurgent relations (which were needed in order to fix the holomorphic anomaly). One finds [31]

$$F_0^{(1)[{\rm c}]} = \frac{A_1}{2\pi}\, {\rm e}^{\frac{1}{2}(\partial_z A_1)^2 \left(S^{zz}_{{\rm hol},[{\rm LR}]} - S^{zz}_{{\rm hol},[{\rm c}]}\right)} \qquad \text{and} \qquad F_0^{(1)[{\rm K}]} = \frac{3A_{\rm K}}{2\pi^2}. \tag{4.8}$$

The left expression involves $S^{zz}_{{\rm hol},[{\rm LR}]}$, whose Q-expansion was written in (4.4), but it also involves the holomorphic limit of the propagator in the conifold frame, $S^{zz}_{{\rm hol},[{\rm c}]}$ (see [31]). It is interesting to note how the expression on the right of (4.8) is actually equivalent, up to a factor of $3 = n_0^{(1)}$, to the one we computed earlier for the resolved conifold. One may also write these expressions in the A-model, where their Q-expansions are explicitly non-regular

$$F_0^{(1)[{\rm c}]} = \frac{{\rm i}\,(-Q)^{\frac{3}{2}}}{4\pi} \left((\log(Q) - {\rm i}\pi)^2 - \pi^2 - 18Q + \frac{135}{2}Q^2 + \cdots \right) \left(1 - \frac{27}{2}Q + \frac{1539}{8}Q^2 + \cdots \right) \tag{4.9}$$

$$F_0^{(1)[{\rm K}]} = -\frac{3}{\pi}\log Q. \tag{4.10}$$

Analysis of Large-Degree Growth

At fixed genus, the GW invariants grow exponentially in the degree as

$$N_{\boldsymbol{g},d} \sim c_{\boldsymbol{g}}\, d^{2\boldsymbol{g}-3}\, {\rm e}^{d t_{\rm c}} \left(\log d\right)^{\delta}, \tag{4.11}$$

where $t_{\rm c} := t(z = -1/27) = 2.90759\ldots - {\rm i}\pi$ [56, 40]. Figure 7 shows a numerical verification of this value for $t_{\rm c}$. The exponent $2\boldsymbol{g} - 3$ of the degree d may be verified numerically from the following large-d sequence

$$f_d - 2 f_{d^2} \sim 2\boldsymbol{g} - 3, \qquad \text{where} \qquad f_d := d \left({\rm e}^{t_{\rm c}}\, \frac{N_{\boldsymbol{g},d+1}}{N_{\boldsymbol{g},d}} - 1 \right). \tag{4.12}$$

[7] References [29, 31] used the notation $t_{\rm c}$ for this flat coordinate. Herein we use $T_{\rm c}$ instead so as not to clash with our conifold critical point.

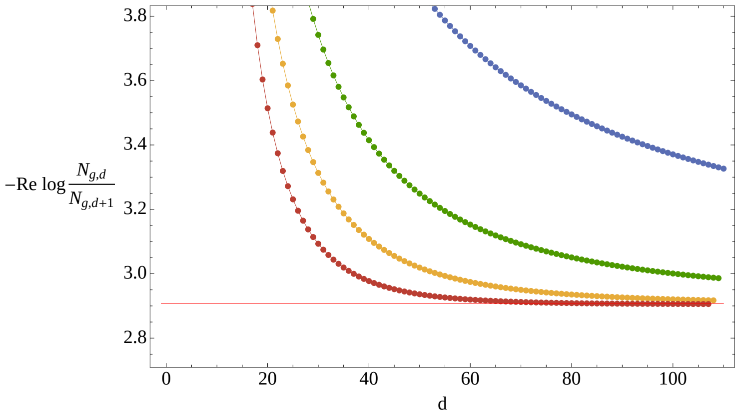

Figure 7: Local $\mathbb{P}^2$: The exponent t_c in the growth of $N_{\boldsymbol{g},d}$ is captured from the ratio of two consecutive GW invariants, when the degree is large. We plot that ratio alongside three Richardson extrapolations, which are clearly converging faster towards the expected result (up to a numerical relative error of about 0.06%).

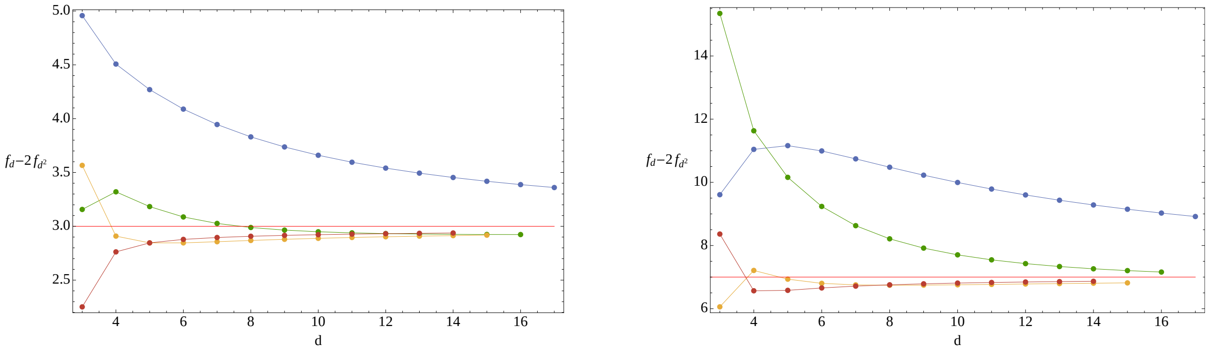

Figure 8: Local $\mathbb{P}^2$: The exponent $2\boldsymbol{g}-3$ is the leading large-order term in $f_d - 2f_{d^2}$. We have data up to $d = 325$ so that the horizontal axis can only reach $d = 17$. The plots illustrate the first few Richardson transforms for $g = 3$ (left) and $g = 5$ (right), converging faster towards the expected result (up to numerical relative errors of about 2% in both cases).

Due to the presence of the d^2 factor, and the limit upon available data, the results are not as good as those for t_c. Nonetheless, this exponent may also be cleanly verified numerically, as it is shown in figure 8. Finally, in similar fashion, we can determine the power of the logarithm $\log d$ from the sequence

$$2^\delta \sim \frac{\mathrm{e}^{d(d-1)t_c}}{d^{2\boldsymbol{g}-3}} \frac{N_{\boldsymbol{g},d^2}}{N_{\boldsymbol{g},d}}. \tag{4.13}$$

This is done in figure 9, where it is shown that this exponent may be well fitted to the expected $\delta = 2\boldsymbol{g} - 2$. Unfortunately, our available data does not allow us to numerically compute the genus-dependent pre-factor $c_{\boldsymbol{g}}$ with enough accuracy as to present it here.

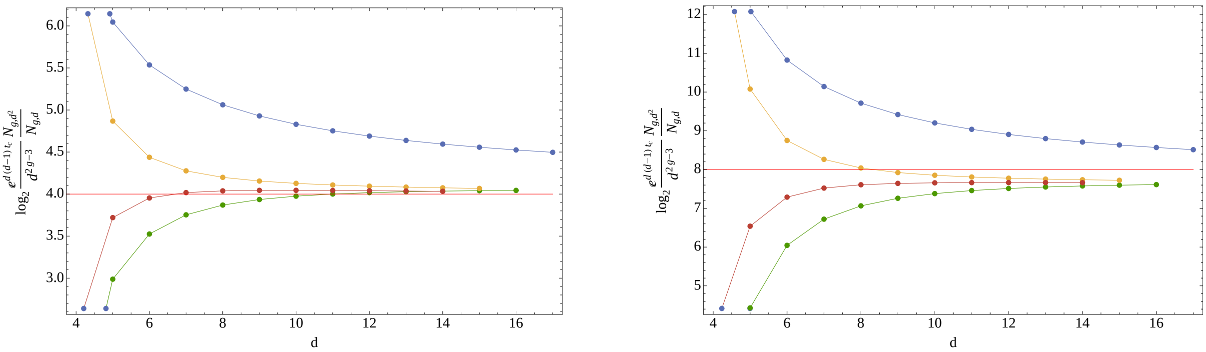

Figure 9: Local $\mathbb{P}^2$: The exponent δ of the logarithm $\log d$ is the leading term in the sequence (4.13). Having data up to $d = 325$ implies the horizontal axis only reaches $d = 17$. We plot the first few Richardson transforms for $g = 3$ (left) and $g = 5$ (right), converging faster towards the expected result (up to small numerical relative errors of about 3% and 4%, respectively).

Analysis of Large-Genus Growth

As explained in section 2, the large-genus expansion is best expressed in terms of the coefficients a_d, $b_{d,n}$, and c_d, as in (2.18), which we reproduce in here

$$N^{\mathbb{P}^2}_{g,\boldsymbol{d}} = f^{\mathrm{CS}}_g \left\{ \sum_{n|\boldsymbol{d}} a^{\mathbb{P}^2}_n \left(\frac{\boldsymbol{d}}{n}\right)^{2g-3} + \frac{2g}{B_{2g}} \frac{1}{\boldsymbol{d}} \left(c^{\mathbb{P}^2}_{\boldsymbol{d}}\, \delta_{g,1} + \sum_{n=1}^{G_{\mathbb{P}^2}(\boldsymbol{d})-1} b^{\mathbb{P}^2}_{\boldsymbol{d},n}\, n^{2g-2} \right) \right\}, \tag{4.14}$$

and where, for this example, one explicitly has $G_{\mathbb{P}^2}(d) = (d-1)(d-2)/2$. A table with these first few coefficients is shown in appendix B.1. Recall that these are just convenient integer numbers which essentially capture the very same information as either GW or GV invariants.

Some of these coefficients, $b_{d,n}$ with n close to $G_{\mathbb{P}^2}(d) - 1$, can be identified in closed form as

$$b^{\mathbb{P}^2}_{d,G_{\mathbb{P}^2}(d)-1-k} = p_{-3}(k)\,(-1)^d\, d\,((d+1)\,(d+2) - 2k)\,, \qquad 0 \le k \le d-2, \tag{4.15}$$

where the $p_{-3}(k)$ are given by the generating function

$$\sum_{k=0}^{+\infty} p_{-3}(k)\, q^k = \prod_{m=1}^{+\infty} \frac{1}{(1-q^m)^3}. \tag{4.16}$$

For larger values of k one can try to extend the above formula, at the cost of identifying similar coefficients to $p_{-3}(k)$. A conjectural partial formula for $b^{\mathbb{P}^2}_{d,n}$ is

$$b^{\mathbb{P}^2}_{d,G_{\mathbb{P}^2}(d)-1-k} \stackrel{?}{=} (-1)^d\, d \sum_{s=0}^{+\infty} \left(\alpha_{s,k-m_s d+n_s}\,(d+1-s)\,(d+2-s) - \beta_{s,k-m_s d+n_s}\right), \tag{4.17}$$

where

$$m_0 = 0, \quad n_0 = 0, \qquad \alpha_{0,n} = p_{-3}(n), \qquad \beta_{0,n} = 2n p_{-3}(n), \tag{4.18}$$

$$m_1 = 1, \quad n_1 = 1, \qquad \sum_{n=0}^{+\infty} \alpha_{1,n}\, q^n = -3\, \frac{1+q+q^2}{1-q} \prod_{m=1}^{+\infty} \frac{1}{(1-q^m)^3},$$

$$-\beta_{1,n} = 0, 18, 144, 684, 2484, 7578, 20628, 51390, 119736, 263970, 556308, 1127880, 2212704, ?, \tag{4.19}$$

$$m_2 = 2, \quad n_2 = 4, \qquad -\alpha_{2,n} = 6, 24, 72, 162, 315, ?, \qquad -\beta_{2,n} = 0, 36, 252, 1008, 3042, ?. \tag{4.20}$$

This is as far as we were able to reach with the data we have available for local $\mathbb{P}^2$.

Combined/Diagonal Large-Growth in Genus and Degree

As discussed earlier in section 2, and illustrated in figure 3, local $\mathbb{P}^2$ has two (different) growths of combined genus and degree. They are associated to the Kähler ($A_{\rm K} = 2\pi t$) and conifold ($A_{\rm c}$) instanton actions, and they are, respectively,

$$d = \frac{2g-3}{t} \qquad \text{and} \qquad d = a_0(Q) + a_1(Q)\, g. \tag{4.21}$$

Note that, as one varies t, the large-order growth of the free energies will be dominated by either $A_{\rm K}$ or $A_{\rm c}$, or a competition between both (see the analysis in [31]). The situation is slightly different with the GW large-order. Here, along *any* diagonal one will find a factorial growth. However, from a resurgence standpoint, perhaps the most interesting diagonals are the ones which connect back to the resurgent structure of the free energies [29, 31]. For any chosen diagonal, this connection will exist every time there is a value of t which realizes that chosen diagonal as one of the above (specific) slices. If such a value of t exists, then the large-order growth of the enumerative invariants will be dominated by either $A_{\rm K}$ or $A_{\rm c}$ and the connection to the free energies is rather clean. If not, one will instead be upon a "mixed" diagonal with both $A_{\rm K}$ and $A_{\rm c}$ vying for dominance. Below we shall focus only upon the leading diagonals.

The first leading degree above was explored and justified analytically for the resolved conifold, and the main features which were found in that example remain in the present one. The second leading degree above depends on t (or Q) through two *unknown* functions, $a_0(Q)$ and $a_1(Q)$. At this stage, these functions may only be accessed via *numerical* computations; and given limited data, with some significant limitations. In the following we shall summarize the resulting factorial growth of the GW invariants, along the leading diagonals of their (g,d)-table, and the relation of this growth with the resurgent structure of the topological-string free energy.

Kähler Leading Degree

In this case, the only difference with respect to the resolved conifold turns out to be a simple multiplying factor, the GV invariant $n_0^{(1)} = 3$ of local $\mathbb{P}^2$, in which case the analog of (3.9) is now

$$N^{\mathbb{P}^2}_{g,d}\, Q^d \Big|_{g=\frac{t}{2}d+q} \sim \sum_{h=0}^{+\infty} \frac{\Gamma\left(2g-\frac{3}{2}-h\right)}{A_{\rm K}^{2g-\frac{3}{2}-h}}\, \frac{n_0^{(1)}\, t^{\frac{3}{2}-h}}{2^{2h+1}\,\pi^{h+2}}\, \mathcal{P}_h(q). \tag{4.22}$$

The polynomials $\mathcal{P}_h(q)$ are precisely the *same* as in (3.14), and the integer q is introduced to make both g and d integer; see the discussion around equation (3.8).

Computational tests on the validity of (4.22) are shown in figures 10 and 11; with figure 10 testing the Kähler instanton action and figure 11 testing the (universal) validity of the polynomials $\mathcal{P}_h(q)$ for $h=0$ through 5. The precise nature of these computational tests is exactly the same as we did earlier for the resolved conifold, and we refer to that discussion for further details.

This formula (4.22), when restricted to the first approximation $h=0$, reproduces the prediction from the saddle-point approximation which was explained around equation (2.28) (and

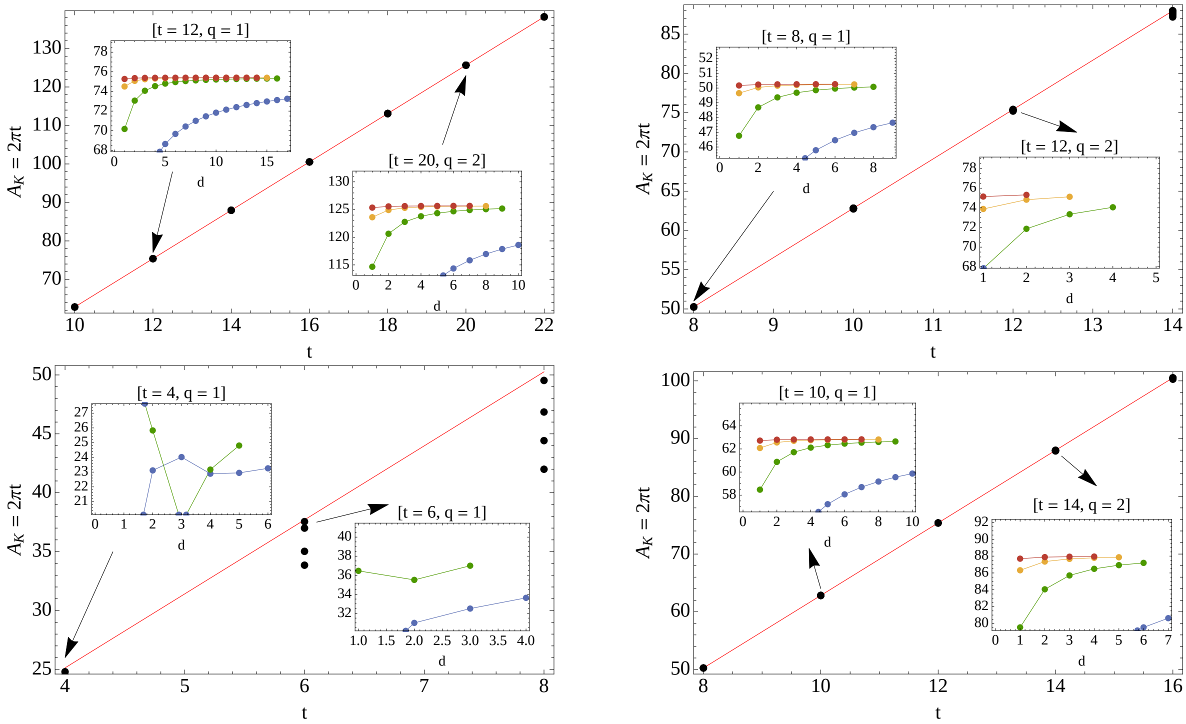

Figure 10: Tests of the instanton action $A_{\rm K} = 2\pi t$, from the Kähler saddle-point, for local $\mathbb{P}^2$, ABJM, the quintic, and the local curve X_3 (from left to right and top to bottom). The inclosed plots show the convergence for a couple of values of t and q. Note that for the quintic we do not have enough data to guarantee reaching a limit where all black dots overlap.

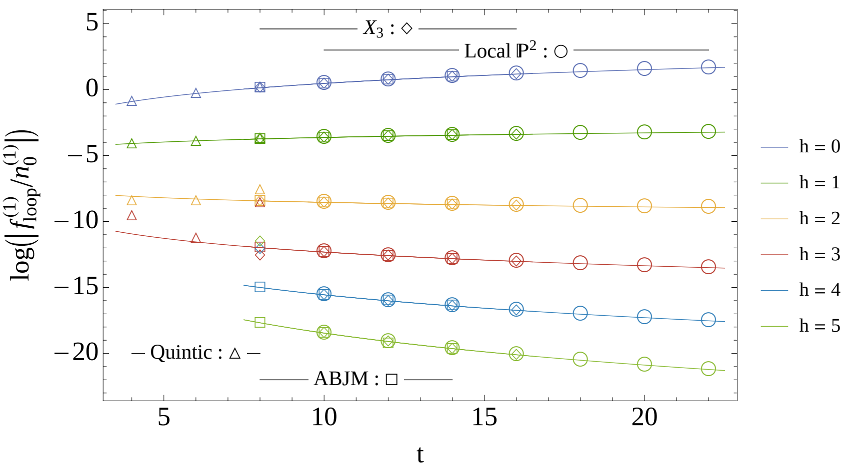

Figure 11: Numerical checks of the loop-corrections $f^{(1)}_h = \frac{n^{(1)}_0 t^{\frac{3}{2}-h}}{2^{2h+1}\pi^{h+2}} \mathcal{P}_h(q)$, for $h = 0, \ldots, 5$ and $q = 1$, for our several examples. We plot the logarithm of the ratio $f^{(1)}_0/n^{(1)}_0$ to have universal quantities which all fit within the same graph.

leading up to it). Indeed, for the case of Kähler leading degree, $a_0 = -3/t$, $a_1 = 2/t$, $a_2 = t$, and $F^{(1)}_0 = \frac{3A_{\rm K}}{2\pi^2}$. Using these values in equation (2.28) (with $\beta = 1$) we precisely reproduce (4.22)

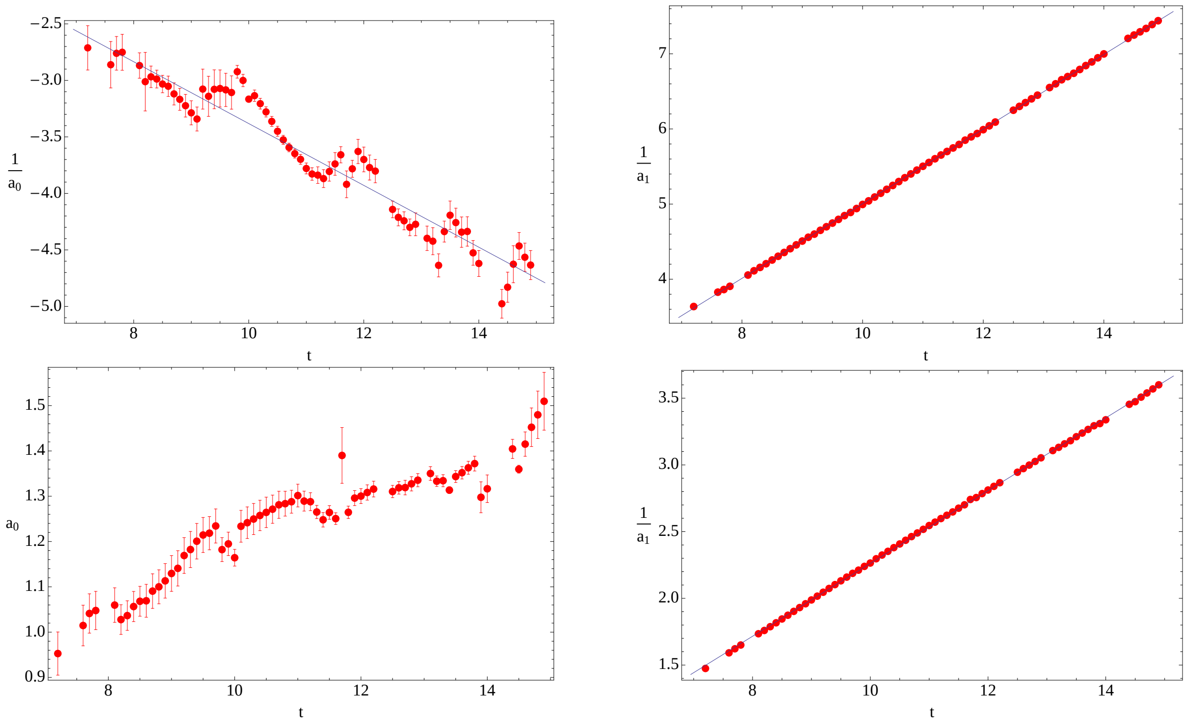

Figure 12: Local $\mathbb{P}^2$: Numerical calculation of $a_0(Q)$ and $a_1(Q)$ associated to the Kähler instanton action (the two upper plots) and to the conifold instanton action (the two lower plots). We are showing tests for their inverses whenever the dependence seems linear, although we were not able to confirm this analytically in the case of the conifold action.

truncated to $h = 0$. A numerical check of the values of a_0 and a_1 is shown in the upper plots of figure 12, for which we can nicely fit

$$a_0(Q)^{-1} = (-0.65 \pm 0.09) + (-0.274 \pm 0.008)\, t, \qquad r^2 = 0.945, \tag{4.23}$$

$$a_1(Q)^{-1} = (0.038 \pm 0.005) + (0.4967 \pm 0.0004)\, t, \qquad r^2 = 0.99995. \tag{4.24}$$

The shift in $a_0(Q)$ is not very reliable, but the slope in a_1 is quite close to the expected value.

This asymptotics arises from the $a_{d=1}$ contribution in the abc-expansion of the GW invariants in (2.18). Since $a_{d=1} = n_0^{(1)}$ one will always find the resolved-conifold asymptotics multiplied by this factor.

Conifold Leading Degree

The second dominant degree, $d = a_0(Q) + a_1(Q)\, g$, is harder to analyze as everything must now be approached numerically; from the computation of $a_0(Q)$ and $a_1(Q)$ to the asymptotics.

The numerical fit to $1/a_1(Q)$ is shown in the lower-right plot of figure 12. It is obtained from first fitting straight lines $d = \alpha\, g + \beta$ for different (fixed) values of t. Then fitting these results against a linear dependence in t we have obtained

$$a_1(Q)^{-1} = (-0.466 \pm 0.005) + (0.2728 \pm 0.0005)\, t, \qquad r^2 = 0.9998. \tag{4.25}$$

On what concerns $a_0(Q)$, its numerical calculation is shown in the lower-left plot of figure 12, but there is no obvious fit to do here (numerically, the dependence of $1/a_0(Q)$ does not seem to be linear in t, yielding a poor $r^2 = 0.849$, and this will become even more evident in following examples). At this moment we cannot provide an analytical interpretation for these numbers, or even guarantee that the fit to a straight line is justified since the interval in t we have considered might be too small to be significant. Nonetheless, we do report the results.

Because we now lack the precision we had along the Kähler leading degree, we cannot provide a systematic exploration of the GW asymptotics with conifold leading degree. We can, however, identify particular values of t for which the exploration becomes simpler. One such point is found when $a_1(Q) = 1$, or $t \approx 5.6993\ldots$. In this case we explore the growth of $N_{g,g+\Delta}$ for some integer $\Delta \in \mathbb{Z}$ (implicitly associated to $a_0(Q)$). The numerical exploration of this diagonal slice in the GW-table yields the result

$$N^{\mathbb{P}^2}_{g,g+\Delta} \sim \frac{\Gamma\left(2g-\frac{3}{2}\right)}{A_0^{2g-\frac{3}{2}}}\, \mathrm{e}^{\alpha_0+\alpha_1\,\Delta} \left(-1\right)^{\Delta+1}, \tag{4.26}$$

where $A_0 \approx 0.655995\ldots$, and α_0 and α_1 are pure numbers which cannot be computed with much precision. The interesting point is that the value of A_0 can be matched to the saddle-point prediction involving the *conifold* action,

$$A_1(Q)\,\sqrt{Q} = 0.655995043\ldots, \tag{4.27}$$

where the $\sqrt{Q}$ comes from including the factor Q^d that multiplies $N^{\mathbb{P}^2}_{g,g+\Delta}$ in the saddle-point expression. On the other hand, the one-loop coefficient in (4.26) should correspond to

$$\left(\frac{a_2}{\pi a_1 A_1}\right)^{1/2} F_0^{(1)[\mathrm{c}]}, \tag{4.28}$$

but $a_2(Q)$ is directly related to the second derivative at the saddle point and thus it cannot be computed from first principles.

4.2 The Example of Local $\mathbb{P}^1 \times \mathbb{P}^1$

Let us next address another (toric) local surface, the non-compact CY threefold known as local $\mathbb{P}^1 \times \mathbb{P}^1$, which is the total space of the line bundle $\mathcal{O}(-2,-2) \to \mathbb{P}^1 \times \mathbb{P}^1$. Generically, local $\mathbb{P}^1 \times \mathbb{P}^1$ has two complex structure moduli, z_1 and z_2, implying that the mirror map is similarly twofold, $Q_1 = \mathrm{e}^{-t_1} = \mathcal{O}(z_1)$ and $Q_2 = \mathrm{e}^{-t_2} = \mathcal{O}(z_2)$. In order to have reasonable large-order data for the resurgence analysis, in what follows we shall restrict to a slice of this variety where $z_1 = z_2$.

Free Energies and Gromov–Witten Invariants

Instead of working in the full two-dimensional moduli space, we shall restrict to the (simpler) one-dimensional *diagonal slice* where the sizes of both $\mathbb{P}^1$'s in the local $\mathbb{P}^1 \times \mathbb{P}^1$ geometry are set to be *equal*. One is thus left with a single modulus. The resulting such theory is closely related to a rather well-known gauge theory, called ABJM gauge theory [57] (see also [58]), and we shall use this name in the following to denote this diagonal slice of local $\mathbb{P}^1 \times \mathbb{P}^1$.

Of course the general local $\mathbb{P}^1 \times \mathbb{P}^1$ geometry has two Picard–Fuchs operators; annihilating periods. One immediate simplification of the diagonal slice is to reduce this number to just one,

$$\left\{(z\partial_z)^4 - 4z\left(4\,(z\partial_z)^3 + 4\,(z\partial_z)^2 + z\partial_z\right)\right\} f(z) = 0. \tag{4.29}$$

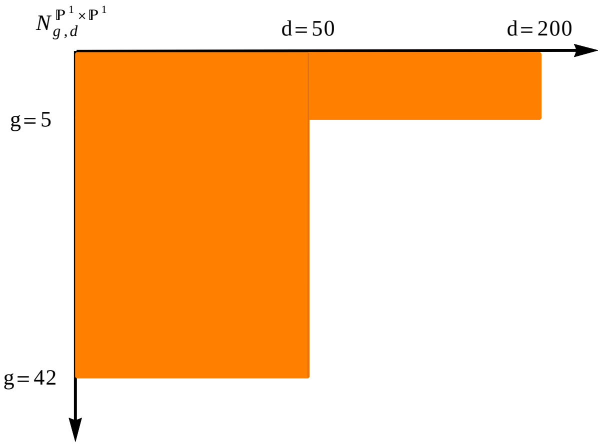

Figure 13: Maximum degree and genus of the GW invariants we computed for ABJM.

From its solutions, we can identify the mirror map and the genus-zero free energy,

$$-t = \log z + 4z + 18z^2 + \frac{400}{3}z^3 + \cdots = \log Q, \tag{4.30}$$

$$F_0^{(0)} = c_3 t^3 + c_2 t^2 + c_1 t - 4Q - \frac{9}{2}Q^2 - \frac{328}{27}Q^3 + \cdots . \tag{4.31}$$

After dealing with the genus-one free energy, $F_1^{(0)}$, one can proceed and use the holomorphic anomaly equations to compute higher-genus free energies[8], from which the GW invariants are eventually read. For example, in the language of modular forms,

$$\begin{aligned} F_2^{(0)} &= \frac{5E_2^3}{5184cd^2} - \frac{E_2^2}{576d^2} + \frac{E_2\left(c^2 - cd + d^2\right)}{864cd^2} + \frac{-16c^3 + 15c^2 d - 21cd^2 + 2d^3}{51840cd^2} = \\ &= -\frac{Q}{60} - \frac{Q^2}{20} - \frac{Q^3}{10} + \cdots , \end{aligned} \tag{4.32}$$

where $E_2(\tau)$ is the second Eisenstein series, $c = \vartheta_3^4(\tau)$ and $d = \vartheta_4^4(\tau)$ are powers of theta functions, and the modular parameter τ is a function of z; see [59] for full details. Also, in this language $F_1^{(0)} = \log \eta(\tau)$ with $\eta(\tau)$ the Dedekind eta-function. In appendix B.2 we list the first few GW invariants, and figure 13 schematically represents the ones we have computed and will work with.

The instanton actions for ABJM were extensively discussed in [26] and are associated to special points in moduli space: large Kähler structure ($z = \infty$) yielding $A_{\rm K} = 2\pi t$, conifold point ($z = z_{\rm c}$) yielding $A_{\rm c}$, and orbifold point ($z = 0$) yielding $A_{\rm o}$. These three actions are actually *linearly dependent* with integer coefficients. This implies that the ABJM transseries (whose construction is still an open problem for future research) might either involve only two of these actions (selected upon some criteria of relevance), or it might involve all three of them (in which case one would obtain a resonant transseries as in, *e.g.*, [37, 27, 28]).

[8]This was done in [53] using the language of propagators, and addressing the full local $\mathbb{P}^1 \times \mathbb{P}^1$ geometry; and in [59] using modular forms, and while restricting to the ABJM diagonal slice.

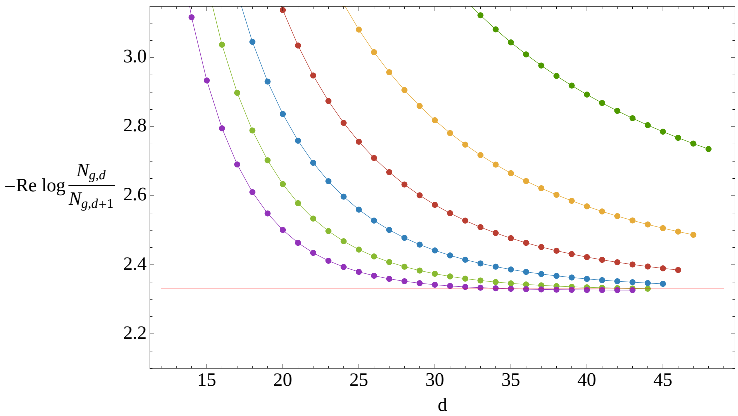

Figure 14: ABJM: The exponent t_c in the growth of $N_{\boldsymbol{g},d}$ is captured from the ratio of two consecutive GW invariants, when the degree is large. We plot that ratio alongside six Richardson extrapolations, which are clearly converging faster towards the expected result (up to a numerical relative error of about 0.3%).

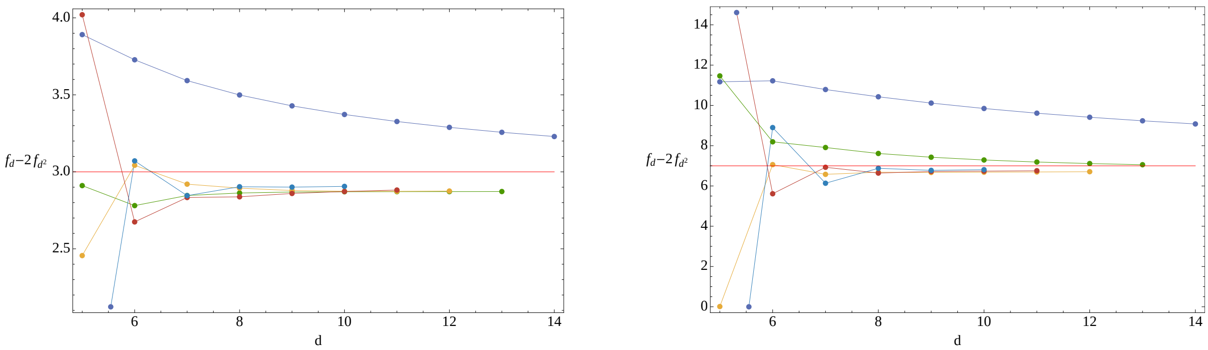

Figure 15: ABJM: The exponent $2\boldsymbol{g}-3$ is the leading large-order term in $f_d - 2f_{d^2}$. We have data up to $d = 200$ so that the horizontal axis can only reach $d = 14$. The plots illustrate the first few Richardson transforms for $g = 3$ (left) and $g = 5$ (right), converging faster towards the expected result (up to numerical relative errors of about 3% in both cases).

Analysis of Large-Degree Growth

The large degree, fixed genus, growth is completely analogous to that of local $\mathbb{P}^2$,

$$N_{\boldsymbol{g},d} \sim c_{\boldsymbol{g}}\, d^{2\boldsymbol{g}-3}\, \mathrm{e}^{dt_c}\, (\log d)^{\delta}\,. \tag{4.33}$$

The value of the Kähler parameter at the conifold point is now $t_c := t(z = 1/16) = 8K/\pi = 2.33248723\ldots$ [59], where $K = \sum_{n=0}^{+\infty}(-1)^n\,(2n+1)^{-2}$ is the Catalan constant. The exponent δ numerically matches to the expected $2\boldsymbol{g}-2$. This g-dependence of the exponents may be tested using the same large-d sequences as for local $\mathbb{P}^2$, *i.e.*, the combinations (4.12) and (4.13). These numerical results are illustrated in figures 14, 15 and 16.

Analysis of Large-Genus Growth

Again, the strategy is essentially the same as for the example of local $\mathbb{P}^2$. As before, the GW invariants can be expanded in terms of *abc*-coefficients according to equation (2.18), but where

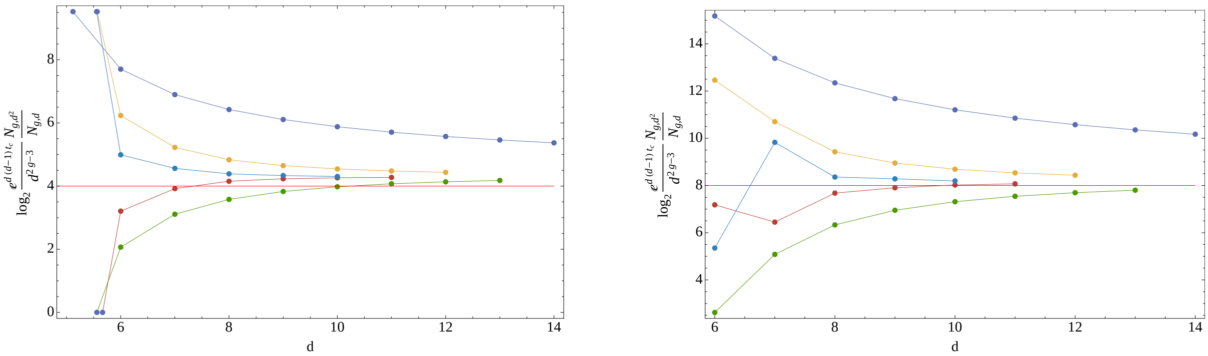

Figure 16: ABJM: The exponent δ of the logarithm $\log d$ is the leading term in the sequence (4.13). Having data up to $d = 200$ implies the horizontal axis only reaches $d = 14$. We plot the first few Richardson transforms for $g = 3$ (left) and $g = 5$ (right), converging faster towards the expected result (up to small numerical relative errors of about 8% and 3%, respectively).

in the present example one explicitly has $G_{\mathrm{ABJM}}(d) = \lfloor d(d-4)/4 \rfloor + 1$. A table with these first few coefficients is shown in appendix B.2.

The first few coefficients seem to answer to the closed-form formula

$$b^{\mathrm{ABJM}}_{d,\left\lfloor \frac{d(d-4)}{4} \right\rfloor - k} = p_{d,-4}(k)\, 4d \left(\left\lfloor \frac{(d+2)^2}{4} \right\rfloor - k \right), \tag{4.34}$$

where

$$p_{d,-4}(k) = \begin{cases} p_{\mathrm{e},-4}(k)/2 & \text{even } d, \\ p_{\mathrm{o},-4}(k) & \text{odd } d, \end{cases} \tag{4.35}$$

and

$$\sum_{k=0}^{+\infty} p_{\mathrm{e},-4}(k)\, q^k \stackrel{?}{=} \left(1 + 2q + 2q^4\right) \prod_{m=1}^{+\infty} \frac{1}{\left(1-q^m\right)^4}, \tag{4.36}$$

$$\sum_{k=0}^{+\infty} p_{\mathrm{o},-4}(k)\, q^k \stackrel{?}{=} \left(1 + q^2 + q^6\right) \prod_{m=1}^{+\infty} \frac{1}{\left(1-q^m\right)^4}. \tag{4.37}$$

But with the (limited) available data we cannot confirm that these formulae are complete.

Combined/Diagonal Large-Growth in Genus and Degree

The combined growth in genus and degree is similar to the one for local $\mathbb{P}^2$. The two leading combinations, again arising from Kähler and conifold instanton actions, will allow us to connect the factorial growth of the perturbative free energies with the factorial growth of GW invariants. This is illustrated in figure 17. As already happened before, the growth associated to the Kähler action, $d = (2g-3)/t$, is well understood since the example of the resolved conifold, whereas the one associated to the conifold action, $d = a_0(Q) + a_1(Q)\, g$, can only be probed numerically.

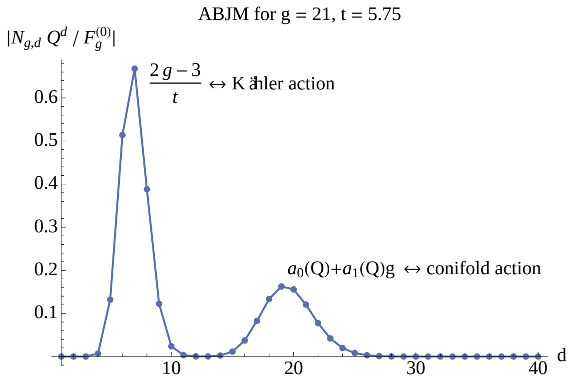

Figure 17: ABJM: Graphical representation of which GW invariants contribute the most to a free energy $F_g^{(0)}(Q)$, for fixed values of g and $Q = \mathrm{e}^{-t}$. As for local $\mathbb{P}^2$ in figure 3, ABJM has saddle points corresponding to both Kähler and conifold actions. The values of g and t in the plot were chosen as to clearly see both saddles in the same figure.

Kähler Leading Degree

This growth is completely determined, at least up to the first exponentially-subleading instanton corrections, by the first GV invariant of ABJM which in this case is $n_0^{(1)} = -4$. Thus we have

$$N_{g,d}^{\mathrm{ABJM}}\, Q^d \Big|_{g=\frac{t}{2}d+q} \sim \sum_{h=0}^{+\infty} \frac{\Gamma\left(2g-\frac{3}{2}-h\right)}{A_{\mathrm{K}}^{2g-\frac{3}{2}-h}} \frac{n_0^{(1)}\, t^{\frac{3}{2}-h}}{2^{2h+1}\, \pi^{h+2}}\, \mathcal{P}_h(q), \tag{4.38}$$

where $A_{\mathrm{K}} = 2\pi t$ and the definition of $\mathcal{P}_h(q)$ is given in (3.14), *i.e.*, they are precisely the same polynomials which have already appeared for resolved conifold and local $\mathbb{P}^2$. Computational tests on the validity of (4.38) are shown in figures 10 and 11, with the exact same discussion as for resolved conifold and local $\mathbb{P}^2$. In fact, all the very same comments we made for local $\mathbb{P}^2$ in section 4.1 also apply now. In particular, the numerical check of $a_0 = -3/t$ and $a_1 = 2/t$ is indeed confirmed as

$$a_0(Q)^{-1} = (0.01 \pm 0.07) + (-0.33 \pm 0.01)\, t, \qquad r^2 = 0.970, \tag{4.39}$$

$$a_1(Q)^{-1} = (-0.003 \pm 0.005) + (0.5000 \pm 0.0009)\, t, \qquad r^2 = 0.99992. \tag{4.40}$$

This check is shown in the upper plots of figure 18.

Conifold Leading Degree

In this case, the analysis can only be carried out numerically, due to lack of theoretical knowledge of where $a_0(Q)$ and $a_1(Q)$ come from. The strategy is essentially the one already started with local $\mathbb{P}^2$, and we find

$$a_1(Q)^{-1} = (-0.595 \pm 0.009) + (0.307 \pm 0.002)\, t, \qquad r^2 = 0.9993. \tag{4.41}$$

This fit is shown in the lower-right plot of figure 18. The lower-left plot of this figure shows the numerical calculation of $a_0(Q)$, again with no obvious fit to do here.

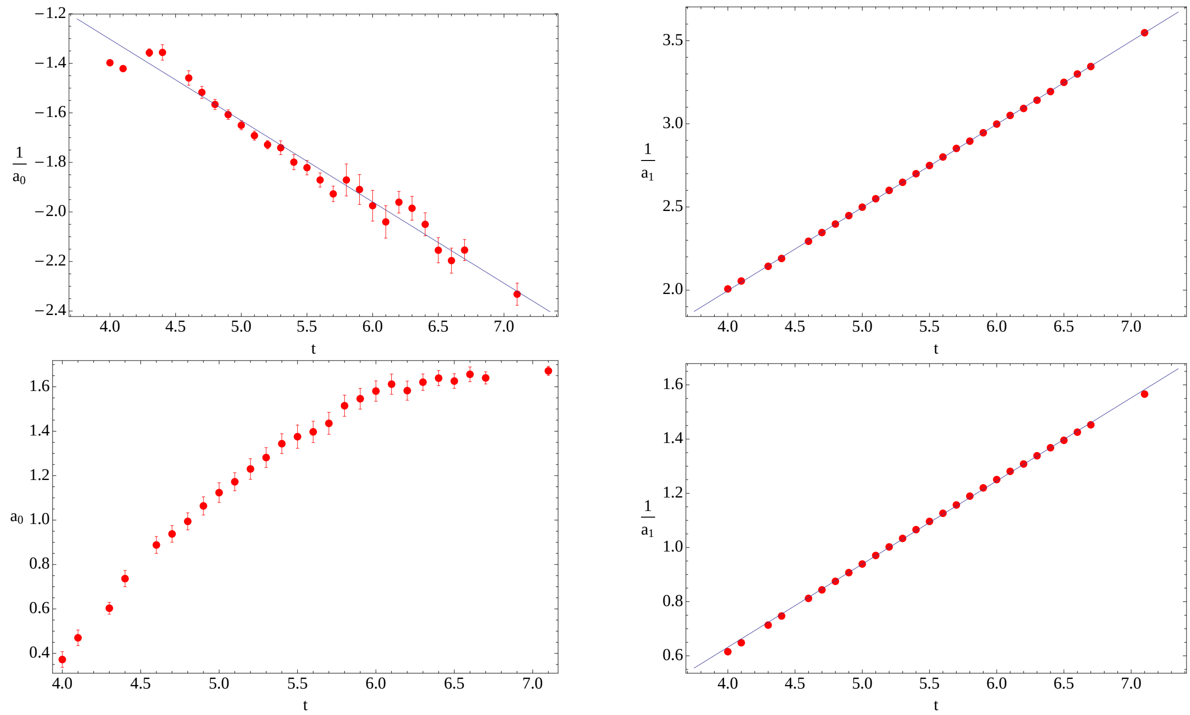

Figure 18: ABJM: Numerical calculation of $a_0(Q)$ and $a_1(Q)$ associated to the Kähler instanton action (the two upper plots) and to the conifold instanton action (the two lower plots). We are showing test for their inverses whenever the dependence seems linear, although we were not able to confirm this analytically in the case of the conifold action.

4.3 The Example of the Local Curve X_p

Our next example deals with local curves. The non-compact CY threefolds to be considered are the total spaces of the rank-two holomorphic vector bundles $X_p \simeq \mathcal{O}(p-2) \oplus \mathcal{O}(-p) \to \mathbb{P}^1$, with p an integer (but due to the invariance $p-2 \leftrightarrow -p$, one may choose $p \in \mathbb{N}$). When $p=1$ one finds the resolved conifold, $\mathcal{O}(-1) \oplus \mathcal{O}(-1) \to \mathbb{P}^1$ (addressed earlier), and when $p=2$ one finds the Dijkgraaf–Vafa geometries $\mathcal{O}(0) \oplus \mathcal{O}(-2) \to \mathbb{P}^1$ relating to hermitian matrix models [60].

By making use of the topological vertex machinery [61] one may actually compute high genus GW invariants for the local curve directly in the A-model. We shall nonetheless begin with some comments pertaining to the B-model free energy, following [42].

Free Energies and Gromov–Witten Invariants

The B-model free energy has the general structure [42]

$$F_g^{X_p}(w) = \frac{1}{(w-w_{\mathrm{c}})^{5(g-1)}} \sum_{n=1}^{5(g-1)} a_{g,n}(p)\,(w-1)^n\,, \tag{4.42}$$

where the coefficients $a_{g,n}$ are of the form

$$a_{g,n} = \frac{b_{g,n}(p)}{(p-1)^k}, \tag{4.43}$$

with k a positive integer and $b_{g,n}(p)$ a polynomial in p. They are not known in general and have to be fixed with GW invariants up to degree $d = 5(g-1)$ (we present some of these coefficients in appendix B.3). The modulus w is related to the Kähler parameter t through the mirror map

$$Q \equiv \mathrm{e}^{-t} = w^{(p-1)^2-1} - w^{(p-1)^2}, \tag{4.44}$$

where the critical point is at

$$w_{\mathrm{c}} = \frac{p(p-2)}{(p-1)^2}, \tag{4.45}$$

which translates to

$$t_{\mathrm{c}} = \log\left((p\,(p-2))^{p(2-p)}\,(p-1)^{2(p-1)^2} \right). \tag{4.46}$$

It is interesting to notice that, unlike the previous geometries, all these formulae are now *exact*. Further notice that the double-scaled theory at the critical point is now in the universality class of 2d gravity (the free energy being related to the Painlevé I equation) which is a distinct universality class from the previous $c = 1$ examples [42].

As mentioned earlier, one can compute the partition function, and thus the free energy, as a sum over integer partitions directly in the A-model using the topological vertex [61]. We shall not get into any details, which may be found in [42], and simply quote the end results. We have computed[9] GW invariants $N_{g,d}^{X_p}$ with fixed $p = 3, 4, 5$ and in appendix B.3 we list a few such invariants. Figure 19 schematically represents all the invariants we did compute and will work with herein. In the rest of this section we will mostly omit the p-dependence of the GW invariants for shortness, but our results for the different types of growth will always be for general p unless explicitly stated otherwise. We should also point out that we are including an extra sign in our GW invariants [48, 49]

$$N_{g,d}^{X_p} \to (-1)^{g-1}\, N_{g,d}^{X_p}. \tag{4.47}$$

This is essentially required in order to produce integer GV invariants.

For $g \leq 9$ we have enough data to completely fix the coefficients in (4.42), which means the GW invariants can then be computed to arbitrarily high degree. It is also worth mentioning that for $g = 0, 1$ there are explicit formulae for the GW invariants [42]

$$N_{0,d}^{X_p}(p) = -\frac{(d\,f-1)!}{d!\,d^2\,\left(d\,(f-1)\right)!}, \tag{4.48}$$

$$N_{1,d}^{X_p}(p) = \frac{1}{24d}\sum_{n=0}^{d-1}\frac{f^{d-n}}{n!}\prod_{k=1}^{n}\left(d\,(f-1)+k-1\right) - \frac{1}{24}\frac{(d\,f-1)!}{d!\,\left(d\,(f-1)\right)!}\,(f+2)\,, \tag{4.49}$$

where we have set $f \equiv (p-1)^2$, and where higher-genus closed-form generalizations are not known. One general thing which is known [42] is that if written for arbitrary p, as $N_{g,d}^{X_p}(p)$, the GW invariants are polynomials of degree $2g+2d-2$ in p, with rational coefficients,

$$N_{g,d}^{X_p}(p) = \sum_{n=0}^{2g+2d-2} N_{g,d,n}\, p^n. \tag{4.50}$$

[9] On a technical aside, let us mention that the main obstacle in such A-model computations is the growth in degree, since it implies considering an exponentially-growing number of partitions and ever larger expressions to put together. The expansion of the free energy in powers of g_s is also time and resource-consuming, but this computation can be improved via some definite numerical procedures.

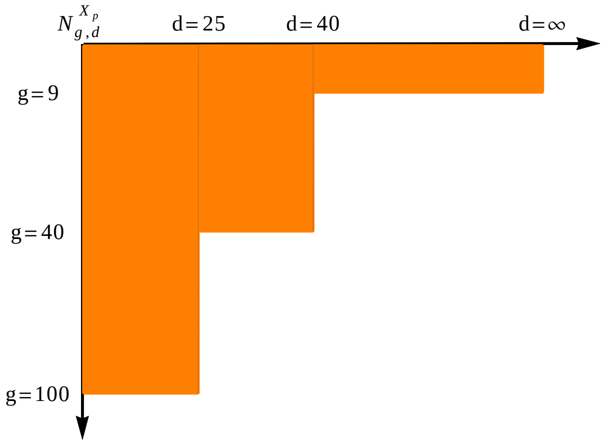

Figure 19: Maximum degree and genus of the GW invariants we computed for the local curves X_p with $p = 3, 4, 5$. For $g \leq 9$ we have all the required data to fix (4.42) and thus can compute GW invariants for any degree.

Analysis of Large-Degree Growth

The analysis of the fixed-genus, large-degree growth of GW invariants in this example is best achieved within the B-model formulation (4.42). The A-model (topological vertex) calculation is only efficient up to about degree $d = 40$ and, as we shall see, the large-degree convergence of the GW invariants is very slow. Using data up to genus $g = 40$ (for $p = 3, 4$) we have fixed the coefficients $a_{g,n}$ up to $g = 9$ and then can compute $N_{g\leq 9,d}$ up to very high degree.

To see how this works, rewrite (4.42) as

$$F_g^{X_p}(t) = \sum_{k=0}^{5(g-1)} \alpha_{g,k} \left(w - w_{\rm c}\right)^{k-5(g-1)} \qquad \text{with} \qquad \alpha_{g,k} = \sum_{n=1}^{5(g-1)} \binom{n}{k} a_{g,n} \left(w_{\rm c} - 1\right)^{n-k}. \quad (4.51)$$

A Lagrange inversion turns (4.51) into a Q-expansion (related to w via the mirror map (4.44)), from where GW invariants are easily extracted. We will skip these details and refer the reader to Appendix A of [42] for the definition of Lagrange inversion as well as instructive examples. In the end, one finds the explicit result

$$N_{\boldsymbol{g},d}^{X_p} = \frac{(-1)^{d-1}}{d} \sum_{k=0}^{5(\boldsymbol{g}-1)} \alpha_{\boldsymbol{g},k} \left(5\left(g-1\right)-k\right) f^{d+5(\boldsymbol{g}-1)-k} P_{d-1}^{(u,v)}\left(\frac{f-2}{f}\right), \quad (4.52)$$

where

$$u = k - d - 5\left(\boldsymbol{g}-1\right), \qquad v = d\left(f-1\right) + 5\left(\boldsymbol{g}-1\right) - k, \quad (4.53)$$

and where the $P_n^{(a,b)}(z)$ are Jacobi polynomials. Finding the large-degree behavior of the GW invariants now reduces to the corresponding large-degree behavior of the Jacobi polynomials. We still had to approach this behavior numerically, essentially because the degree d appears in three different places. Furthermore, the aforementioned slow convergence of the GW invariants will be made clear in the following, as the large-degree expansion turns out to be a power-series expansion in $\sqrt{d}$ for which our standard techniques of Richardson extrapolation are not very useful. However, restricting the study to a grid of perfect squares, *i.e.*, $d = \ell^2$, we then get back the very fast convergence via Richardson transforms, from where one can then comfortably find rational numbers out of decimal expansions.

Consider the following combination

$$P_{d,\boldsymbol{g},k}(f) \equiv f^{d+5(\boldsymbol{g}-1)-k}\, \left(5\left(\boldsymbol{g}-1\right)-k\right)\, P^{(u,v)}_{d-1}\left(\frac{f-2}{f}\right), \tag{4.54}$$

for which we find a large-degree expansion of the form

$$P_{d,\boldsymbol{g},k}(f) = (-1)^{d-1}\, \mathrm{e}^{d t_{\mathrm{c}}}\, d^{\frac{5}{2}(\boldsymbol{g}-1)-\frac{k}{2}} \sum_{n=0}^{+\infty} c^{(n)}_{\boldsymbol{g},k}\, d^{-\frac{n}{2}} \simeq (-1)^{d-1}\, \mathrm{e}^{d t_{\mathrm{c}}}\, d^{\frac{5}{2}(\boldsymbol{g}-1)-\frac{k}{2}} \left(c^{(0)}_{\boldsymbol{g},k} + \frac{c^{(1)}_{\boldsymbol{g},k}}{\sqrt{d}} + \cdots \right). \tag{4.55}$$

Using $\widehat{g} \equiv 5(g-1)$ for shortness, the first coefficients are

$$c^{(0)}_{g,k} = \frac{\mathrm{e}^{\frac{1}{2}(\widehat{g}-k)t_{\mathrm{c}}}\, \mathcal{A}^{k-\widehat{g}}}{\Gamma\left(\frac{1}{2}\left(\widehat{g}-k\right)\right)}, \qquad c^{(1)}_{g,k} = \frac{\sqrt{2}}{3}\, \frac{\mathrm{e}^{\frac{1}{2}(\widehat{g}-k)t_{\mathrm{c}}}\, \mathcal{A}^{k-\widehat{g}}}{\Gamma\left(\frac{1}{2}\left(\widehat{g}-k-1\right)\right)}\, \frac{f-2}{\sqrt{f\left(f-1\right)}} \left(\widehat{g}-k\right), \tag{4.56}$$

where we have defined

$$\mathcal{A} = \sqrt{2}\, \frac{w_{\mathrm{c}}^{1-(p-1)^2/2}}{p-1}. \tag{4.57}$$

In general, they will have the structure

$$c^{(j)}_{g,k} = \frac{\mathrm{e}^{\frac{1}{2}(\widehat{g}-k)t_{\mathrm{c}}}\, \mathcal{A}^{k-\widehat{g}}}{\Gamma\left(\frac{1}{2}\left(\widehat{g}-k-j\right)\right)}\, \frac{1}{\left(f\left(f-1\right)\right)^{\frac{j}{2}}} \sum_{j_0=1}^{j} \widehat{c}^{(j)}_{j_0}(f)\, \left(\widehat{g}-k\right)^{j_0}, \tag{4.58}$$

with $\widehat{c}^{(j)}_{j_0}(f)$ a polynomial in f of degree j. We refer to appendix B.3 for a few such explicit results at the lowest orders. From these results it immediately follows that the leading term in $P_{d,g,0}$ reproduces the known behavior of the GW invariants (2.9) (with $\alpha = \beta = 0$ and $\gamma = -1/2$), and the coefficients can be shown to match the solution of Painlevé I, in the appropriate double-scaling limit. This leading behavior then has corrections, suppressed by powers of $d^{-1/2}$.

The GW invariants for arbitrary p (or f) thus have the following large-degree expansion[10]

$$N_{\boldsymbol{g},d} \sim \mathrm{e}^{d t_{\mathrm{c}}}\, d^{\frac{5}{2}(\boldsymbol{g}-1)-1} \left(c^{(0)}_{\boldsymbol{g},0}\, \alpha_{\boldsymbol{g},0} + \frac{c^{(0)}_{\boldsymbol{g},1}\, \alpha_{\boldsymbol{g},1} + c^{(1)}_{\boldsymbol{g},0}\, \alpha_{\boldsymbol{g},0}}{\sqrt{d}} + \cdots \right) = \tag{4.59}$$

$$= \mathrm{e}^{d t_{\mathrm{c}}}\, d^{\frac{5}{2}(\boldsymbol{g}-1)-1} \sum_{j=0}^{+\infty} \sum_{j'=0}^{\mathrm{Min}(j,5(\boldsymbol{g}-1))} c^{(j-j')}_{\boldsymbol{g},j'}\, \alpha_{\boldsymbol{g},j'}\, d^{-\frac{j}{2}}. \tag{4.60}$$

This result is illustrated and tested in figure 20. On its left plot we consider the ratio $N^{(\mathrm{pred})}_{\boldsymbol{g},d}/N_{\boldsymbol{g},d}$, where the asymptotic prediction in the numerator consists of using the expansion (4.60) up to the subleading correction $j = 0$ (blue), $j = 2$ (green), $j = 4$ (yellow) and $j = 6$ (red), up to degree $d = 100$ and fixed genus $g = 3$. At degree $d = 100$ the leading-order term is of the right order of magnitude, but it is still off by about $\sim 75\%$. Upon inclusion of subleading terms, the ratio then

[10]Note that one interesting feature of this $\gamma = -1/2$ universality class, and as compared to the general structure in (2.9), is that there are no logarithmic contributions to the large-degree asymptotics.

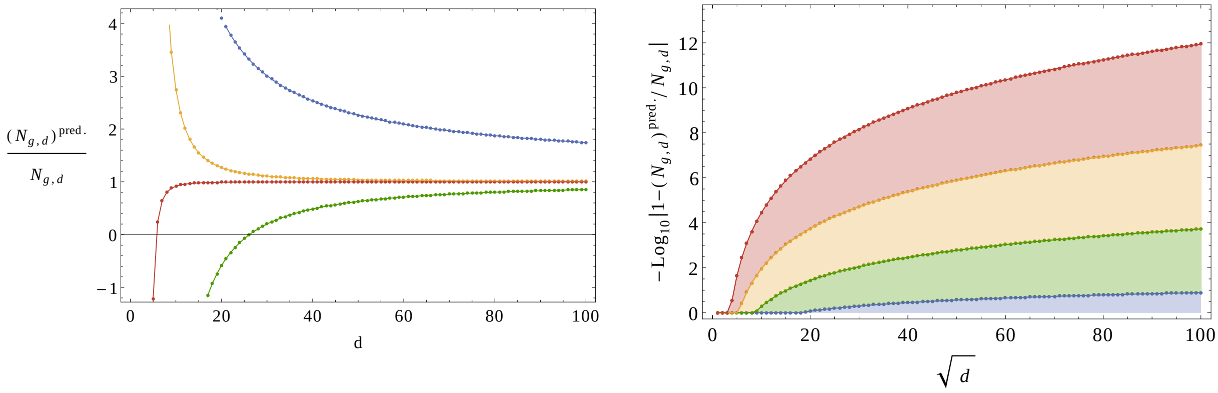

Figure 20: Local curve: Left: Comparison between $p = 3$ GW invariants and their asymptotic prediction in (4.60), at fixed genus $g = 3$ and degree $d \leq 100$, and up to subleading correction $j = 0$ (blue), $j = 2$ (green), $j = 4$ (yellow) and $j = 6$ (red). Right: Number of decimal places of agreement between the analytical $p = 3$ GW invariants and their asymptotic prediction, for fixed genus $g = 6$ (and using the same color code).

starts approaching 1, faster and faster. On the right plot of figure 20 we show the number of decimal places of agreement between the GW invariants and their large-degree expansion, with the same color coding. This time we move only along perfect squares and work with fixed genus $g = 6$. At $d = 10000$ the leading term is still only good enough for the first decimal place, but then the agreement improves significantly once we start adding subleading corrections.

Analysis of Large-Genus Growth

As discussed earlier, the large-genus fixed-degree growth of the GW invariants may be read directly from the *abc*-formula (2.18). In the case of the local curve, it simply reads

$$N_{g,\boldsymbol{d}}^{X_p} = f_g^{\text{CS}} \left\{ \sum_{n|\boldsymbol{d}} a_n^{X_p} \left(\frac{\boldsymbol{d}}{n}\right)^{2g-3} + \frac{2g}{B_{2g}} \frac{1}{\boldsymbol{d}} \left(c_{\boldsymbol{d}}^{X_p}\, \delta_{g,1} + \sum_{n=1}^{G_{X_p}(\boldsymbol{d})-1} b_{\boldsymbol{d},n}^{X_p}\, n^{2g-2} \right) \right\}, \tag{4.61}$$

where now $G_{X_p}(d) = (d-1)\left((p-2)\,d-2\right)/2$. A table with the first few *abc*-coefficients may be found in appendix B.3. To show an example, let us write down the first couple of terms for $p = 3$

$$N_{g,\boldsymbol{d}}^{X_3} \sim \frac{2\,(2g-1)}{\boldsymbol{d}^3} \left(\frac{\boldsymbol{d}}{2\pi}\right)^{2g} \left\{ 1 + (-1)^{\boldsymbol{d}-1}\, 7^{\frac{1+(-1)^{\boldsymbol{d}}}{2}} \frac{1}{2^{2g}} + 55^{(1+2\boldsymbol{d}^2) \bmod 3} \frac{1}{3^{2g}} + \mathcal{O}(4^{-2g}) \right\}. \tag{4.62}$$

This expression is valid for any degree, unlike in previous examples.

Combined/Diagonal Large-Growth in Genus and Degree

The combined "diagonal" growth will turn out to be similar to the previous local-surface examples (and in fact will lead to some sort of *large-order universality* for topological strings in different double-scaled universality classes). In fact, also in the local-curve case we cannot (analytically) pinpoint the nonperturbative structure of the GW invariants in a general situation where $d = a_0(Q) + a_1(Q)\, g$. As usual, the one exception happens at large-radius $t \to +\infty$, where the contribution of the GW invariants to the free energy is strongly peaked around $d = (2g-3)/t$. These Kähler and critical-point peaks are illustrated in figure 21.

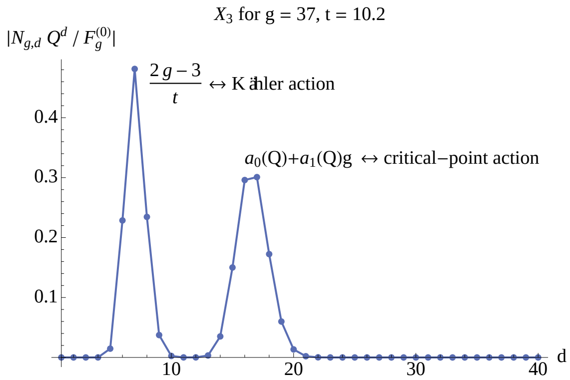

Figure 21: Local curve: Graphical representation of which GW invariants contribute the most to a free energy $F_g^{(0)}(Q)$, for fixed values of g and $Q = \mathrm{e}^{-t}$, and with $p = 3$. As for the earlier examples of local $\mathbb{P}^2$ in figure 3 and ABJM in figure 17, also the local curve has saddle points corresponding to both Kähler and critical-point actions. The values of g and t in the plot were chosen as to clearly see both saddles in the same figure.

The nonperturbative structure of the local-curve free-energy was addressed in [42, 20, 21], where instantons associated to spectral-curve B-cycles were found to control the large-order behavior of the free energy. But, as we shall see, as one moves towards larger and larger values of t this picture changes. Let us first address this question within the free energy itself, before translating to the GW invariants. For the remainder of this section we work with an approximated free energy

$$F_g^{X_p}(t) \approx (F^{X_p})_g^{\star}(t) := \sum_{d=1}^{d_{\max}(g)} N_{g,d}^{X_p}\, \mathrm{e}^{-dt}, \tag{4.63}$$

where $d_{\max}(g)$ is the highest degree for which we have computed $N_{g,d}^{X_p}$ (our data is represented in figure 19). We should stress that, with the leading contributions arising from near $d = \frac{2g-3}{t}$, we can always be sure that no significant contributions were left unaccounted for, and, in the end, the high accuracy of the large-order predictions will confirm that there are no issues with our approximation (4.63). What we find at large-order resembles the resolved conifold (3.4), in that the leading factorial growth is governed by a Gaussian-like action $A = 2\pi t$ with a one-instanton sector that truncates at two-loops[11]. In addition, there is a tower of other contributions that amounts to replacing the Kähler modulus t with $t_n = t + 2\pi\mathrm{i}\, n$, $n \in \mathbb{Z}_{\neq 0}$, or, equivalently, with shifted instanton actions $A_n = A + 4\pi^2\mathrm{i}\, n$. The result is

$$\begin{aligned} F_g^{X_p}(t) \sim{}& \frac{\Gamma(2g-1)}{\pi\,(2\pi t)^{2g-1}} \left(t + \frac{t}{2g-2} \right) + \\ &+ \sum_{m=1}^{+\infty} \frac{\Gamma(2g-1)}{\pi\,|A_m|^{2g-1}} \left\{ 2\,|t_m| \cos\left((2g-2)\,\theta_m\right) + \frac{2\,|t_m|}{2g-2} \cos\left((2g-2)\,\theta_m\right) \right\}, \end{aligned} \tag{4.64}$$

where we have also defined $\theta_m := \arg A_m = \arctan \frac{2\pi n}{t}$. It may be instructive to rewrite the above large-order relation in a more standard resurgence language, similar to (2.3). The difference is that now we have infinitely-many instanton actions A_m, where expansions around each sector

[11] This is also true for all higher instanton sectors.

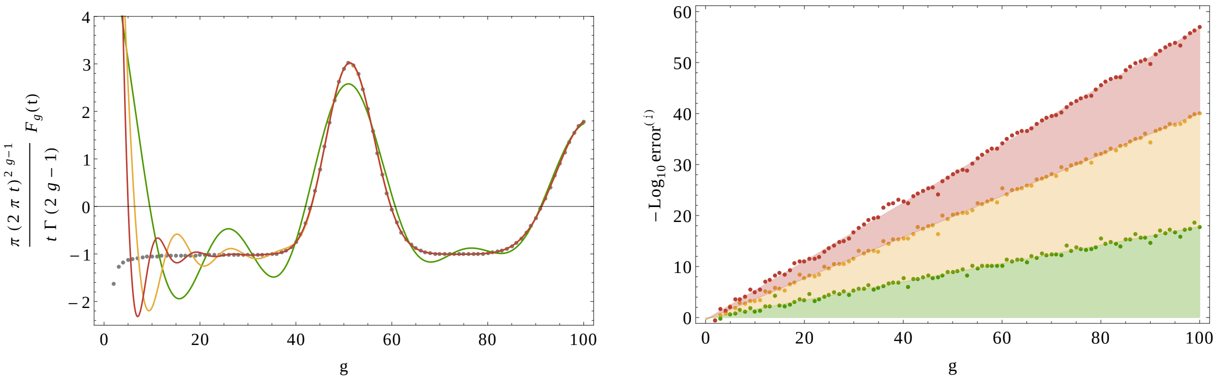

Figure 22: Local curve: Left: Comparison between the $p = 3$ free energy, with an appropriate pre-factor (the gray dots), and the predictions coming from (4.64) up to $m = 2$ (green), $m = 4$ (yellow) and $m = 6$ (red); showing a quicker convergence the more terms are included. Right: Logarithm of the error in the predictions (with the same colors), this time against the normalized free energy. For $m = 6$, at genus $g = 100$, the error is roughly of the order of one part in 10^{60}.

truncate at two loops. In this way we rewrite (4.64) as

$$F_g^{X_p,(0)}(t) \sim \frac{S_1}{2\pi \mathrm{i}} \sum_{m\in\mathbb{Z}} \frac{\Gamma(2g-1)}{A_m^{2g-1}} \left\{ F_{m,1}^{X_p,(1)}(t_m) + \frac{F_{m,2}^{X_p,(1)}(t_m)\, A_m}{2g-2} \right\} + \text{2-instanton corrections.} \tag{4.65}$$

One immediately identifies the Stokes constant $S_1 = 2\mathrm{i}$, and the one-instanton, one- and two-loop coefficients

$$F_{m,1}^{X_p,(1)}(t_m) = t_m, \qquad F_{m,2}^{X_p,(1)}(t_m) = \frac{1}{2\pi}. \tag{4.66}$$

Tests of the large-order prediction (4.64) are shown in figure 22, where it proves convenient to normalize the local-curve free energy against the Gaussian contribution, *i.e.*, we use $\mathcal{F}_g \equiv F_g - F_g^{\mathrm{G}}$. The large-order growth of this normalized free-energy then corresponds to the second line in (4.64). In the left plot we show the normalized free energies for $t = 100$ (multiplied by an appropriate factor to make all numbers of $\mathcal{O}(1)$; the gray dots), alongside the sum in (4.64) up to $m = 2$ (green), $m = 4$ (yellow) and $m = 6$ (red). One can clearly see that the agreement with the data gets better and better by including more terms in the tower of corrections in (4.64). In the right plot we further illustrate this by showing how small the error is for $t = 24$. We use the normalized free-energy and define the error as $\left|1 - \mathcal{F}_g^{\mathrm{pred},m} / \mathcal{F}_g^{(0)}\right|$, where $\mathcal{F}_g^{\mathrm{pred},m}$ just corresponds to taking the second line of (4.64) up to a given maximum (the colors are the same as the ones used on the left). We see that for $m = 6$, at $g = 100$, the error is of the order $10^{-60}\%$.

Let us comment on the relation to the large-order behavior found in [20, 21]. There should be a value of the Kähler parameter for which there is an effective competition between the B-cycle action found in [20, 21] and the Gaussian-like tower described above. Unfortunately, our data does not allow us to directly look at this interplay, for as one moves towards smaller t the contribution to the free energies is no longer dominated just by the invariants close to $d = \frac{2g-3}{t}$. There will also be other relevant contributions at higher degree, which we do not have enough data to account for. Nonetheless, do notice that an exchange in large-order dominance should be precisely related to this emergence of relevant contributions beyond the large-radius "peak".

Given the above large-order behavior of the free energy, we may next deduce its consequences towards the "diagonal" growth of GW invariants. After accounting for the appropriate Gaussian correction, it turns out that the GW large-order is of the exact same type as in earlier examples (in this case, $n_0^{(1)} = (-1)^{p-1}$),

$$N_{g,d}^{X_p}\, Q^d \Big|_{g=\frac{t}{2}d+q} \sim \sum_{h=0}^{+\infty} \frac{\Gamma\left(2g-\frac{3}{2}-h\right)}{(2\pi t)^{2g-\frac{3}{2}-h}}\, \frac{n_0^{(1)}\, t^{\frac{3}{2}-h}}{2^{2h+1}\,\pi^{h+2}}\, \mathcal{P}_h(q), \tag{4.67}$$

where the $\mathcal{P}_h(q)$ are precisely the polynomials which were introduced in (3.9), and which also appeared in the similar large-order results for local $\mathbb{P}^2$ and local $\mathbb{P}^1\times\mathbb{P}^1$. Computational tests on the validity of this expression are shown in figures 10 and 11, with their details and discussion being the same as before. One thus finds that even for theories in different (critical) universality classes, there is some sort of *universal large-order behavior* taking place at large radius[12]. This is also very clear in the plots in figures 10 and 11. Furthermore, in the case of the local curve X_p, this large-order behavior turns out to be *independent* of p (up to a sign).

4.4 The Example of Hurwitz Theory

Let us now address a slightly more algebraic example, that of Hurwitz theory. Generically, it addresses branched covers of algebraic curves, but herein we restrict to so-called *simple* Hurwitz numbers, denoted by $H_{g,d}^{\mathbb{P}^1}\left(1^d\right)$, which count the number of degree-d disconnected coverings of $\mathbb{P}^1$ by a genus-g Riemann surface. These numbers have a combinatorial definition in terms of Young tableaux, but—in line with what we have been doing—they also have a string-theoretic origin. Indeed, Hurwitz theory may be thought of as a topological string theory, as it can be obtained by a particular limit of the A-model on the local curve X_p [42]. This limit consists in taking

$$p \to +\infty, \qquad t \to +\infty, \qquad g_{\mathrm{s}} \to 0, \tag{4.68}$$

while the combinations

$$g_{\mathrm{H}} \equiv p\, g_{\mathrm{s}}, \qquad \mathrm{e}^{-t_{\mathrm{H}}} \equiv (-1)^p\, p^2 \mathrm{e}^{-t}, \tag{4.69}$$

are held fixed. A number of results can then be straightforwardly obtained by applying this limit to our results in the previous section.

Free Energies and Gromov–Witten Invariants

The Hurwitz free-energy was shown to satisfy a Toda-like equation in [63],

$$\exp\left\{F^{\mathrm{H}}(t_{\mathrm{H}}-g_{\mathrm{H}}) + F^{\mathrm{H}}(t_{\mathrm{H}}) + F^{\mathrm{H}}(t_{\mathrm{H}}+g_{\mathrm{H}})\right\} = g_{\mathrm{H}}^2\, \mathrm{e}^{t_{\mathrm{H}}}\, \partial_{t_{\mathrm{H}}}^2 F^{\mathrm{H}}(t_{\mathrm{H}}). \tag{4.70}$$

However, regarding Hurwitz theory as a limiting local-curve in the sense explained above, implies one may compute the genus-g free energy directly in the B-model as

$$F_g^{\mathrm{H}} = \frac{1}{(1-\chi)^{5(g-1)}} \sum_{n=1}^{3g-3} a_{g,n}^{\mathrm{H}}\, \chi^n. \tag{4.71}$$

Here, the new variable χ is related to the local-curve B-model modulus w as

$$w - 1 = -\frac{\chi}{p^2}, \tag{4.72}$$

[12] It would be interesting to compare this to the B-model large-radius universality recently uncovered in [62, 34].

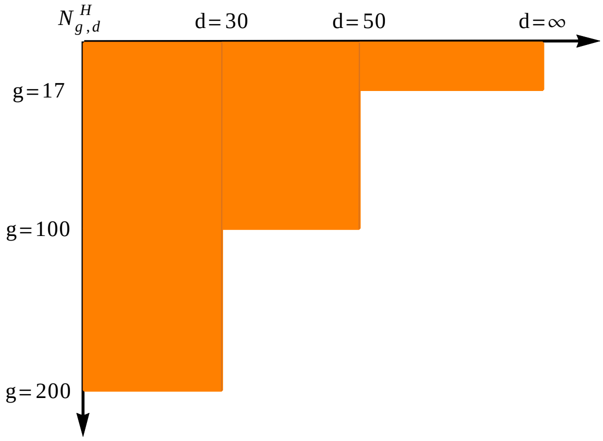

Figure 23: Maximum degree and genus of the GW invariants we computed for Hurwitz theory. These are related to simple Hurwitz numbers via (4.75). For $g \leq 17$ we have all the required data to fix (4.71) and thus can compute GW invariants for any degree.

and in the Hurwitz limit the mirror map becomes

$$\mathrm{e}^{-t_{\mathrm{H}}} = \chi\, \mathrm{e}^{-\chi}. \tag{4.73}$$

In (4.71) one needs to use the appropriate limit of the $a_{g,n}(p)$ coefficients from (4.42), defined as

$$a^{\mathrm{H}}_{g,n} = \lim_{p\to+\infty} p^{8(g-1)-2n} \left(-1\right)^n a_{g,n}. \tag{4.74}$$

From explicit results in appendix B.3 one can see that only some of the coefficients contribute in the limit. The coefficients $a^{\mathrm{H}}_{g,n}$ also turn out to be related to the perturbative free energies of 2d gravity as, under the appropriate double-scaling limit, the difference equation (4.70) reduces to the Painlevé I equation. A large-order analysis of the Hurwitz free energy was performed in [21] finding that large-order effects were, as expected, governed by the $p \to +\infty$ limit of the B-cycle instanton-action that controlled the large-order effects of the local curve.

In the A-model formulation, GW invariants are defined as usual. Furthermore, without surprise, they may also be obtained from the limit

$$N^{\mathrm{H}}_{g,d} = \frac{H^{\mathbb{P}^1}_{g,d}\left(1^d\right)^{\bullet}}{(2g+2d-2)!} = \lim_{p\to+\infty} p^{2-2g-2d}\, N^{X_p}_{g,d}. \tag{4.75}$$

Here we have written the GW invariants in terms of *connected*, simple Hurwitz numbers $H^{\mathbb{P}^1}_{g,d}\left(1^d\right)^{\bullet}$. In practice, we computed the $N^{\mathrm{H}}_{g,d}$ along the same lines as we computed the $N^{X_p}_{g,d}$, *i.e.*, starting from the partition function, then computing the free energy at fixed degree, and finally expanding in powers of g_{H}. We have computed (4.75) up to the totals schematically shown in figure 23 (also see appendix B.4). For $g \leq 17$, data up to $d = 50$ is enough to fix all the coefficients in (4.71), and we may thus compute GW invariants for any degree. This data will not be crucial in the following, since several results just follow from the "finite p" case addressed before. Nonetheless, the ability to generate more data also allows us to make predictions to higher orders.

Analysis of Large-Degree Growth

The asymptotic[13] growth of Hurwitz numbers at large degree d, with fixed genus, may be extracted from what we found earlier for the local curve. In particular, one can apply the limit (4.75) directly to (4.60), so that after introducing[14]

$$\widehat{c}^{(j)}_{g,k} = \frac{2^{\frac{1}{2}(k-5(g-1))}}{\Gamma\left(\frac{1}{2}\left(5\left(g-1\right)-k-j\right)\right)} \sum_{j_0=1}^{j} \widehat{c}^{\mathrm{H},(j)}_{j_0} \left(5\left(g-1\right)-k\right)^{j_0}, \quad \widehat{c}^{\mathrm{H},(j)}_{j_0} = \lim_{f\to+\infty} \frac{\widehat{c}^{(j)}_{j_0}(f)}{\left(f\left(f-1\right)\right)^{\frac{j}{2}}},$$

$$\alpha^{\mathrm{H}}_{g,k} = \lim_{f\to+\infty} f^{4(g-1)-k}\,\alpha_{g,k}(f), \tag{4.76}$$

we immediately arrive at

$$N^{\mathrm{H}}_{\boldsymbol{g},d} \sim \mathrm{e}^{d}\, d^{\frac{5}{2}(\boldsymbol{g}-1)-1} \sum_{j=0}^{+\infty} \sum_{j'=0}^{\mathrm{Min}(j,3(\boldsymbol{g}-1))} \widehat{c}^{(j-j')}_{\boldsymbol{g},j'}\, \alpha^{\mathrm{H}}_{\boldsymbol{g},j'}\, d^{-\frac{j}{2}}. \tag{4.77}$$

Another route to this result would be to directly write GW invariants for Hurwitz theory, as we did in (4.52) for the local curve (one would now have to use the Hurwitz mirror map (4.73)). In this case, one obtains the GW invariants as[15]

$$N^{\mathrm{H}}_{\boldsymbol{g},d} = \frac{(-1)^{d}}{d} \sum_{k=0}^{3\boldsymbol{g}-3} \alpha^{\mathrm{H}}_{\boldsymbol{g},k} \left(5\left(\boldsymbol{g}-1\right)-k\right) L^{k-d-5(\boldsymbol{g}-1)}_{d-1}(d), \tag{4.78}$$

where the $L^{a}_{m}(z)$ are the associated Laguerre polynomials. Since the sum in (4.78) now runs over fewer values, it becomes easier to fix the necessary coefficients and generate GW invariants to arbitrarily large degree. Associated to the fact that the coefficients $\widehat{c}^{(j)}_{g,k}$ no longer depend on an extra parameter, we can find the large-degree expansion (4.77) to very high order with little effort. We present some of these results in appendix B.4.

Analysis of Large-Genus Growth

Hurwitz theory does not have an *abc*-formula, because the would-be GV invariants are no longer integers. Nonetheless, one can proceed empirically, using numerics and Richardson extrapolation, in order to find the growth of Hurwitz numbers for large genus, while at fixed degree. At low degree, the large-genus expansions actually *truncate*. For instance, for $d = 2,3,4$ we find

$$H^{\mathbb{P}^1}_{g,2}\left(1^{d}\right)^{\bullet} = \frac{1}{2}, \tag{4.79}$$

$$H^{\mathbb{P}^1}_{g,3}\left(1^{d}\right)^{\bullet} = \frac{3^{2g-2}}{2}, \tag{4.80}$$

$$H^{\mathbb{P}^1}_{g,4}\left(1^{d}\right)^{\bullet} = \frac{1}{2}\left(2^{2g+2}-1\right)\left(3^{2g+4}-1\right). \tag{4.81}$$

[13]Reference [64] also studies asymptotics of Hurwitz numbers $H_{g,\mu}$, with μ a partition with ℓ parts $\mu_1,\ldots,\mu_\ell$. However, the asymptotics considered in [64] are in the limit $\lim_{N\to+\infty} H_{g,N\mu}$. This is conceptually different from our large-degree expansion of simple Hurwitz numbers: our case corresponds to a partition $(1,\ldots,1)$ with d entries (the number which is growing), while in the results of [64] the length of the partition is always kept fixed.

[14]In this limit we can equally take $f \sim p^2 \to +\infty$.

[15]We use the $\alpha^{\mathrm{H}}_{g,k}$ coefficients for convenience; they are related to the $a^{\mathrm{H}}_{g,i}$ in (4.74) via $(-1)^k \alpha^{\mathrm{H}}_{g,k} = \sum_{i=1}^{3g-3} \binom{i}{k} a^{\mathrm{H}}_{g,i}$. They could just as well be fixed by using the mirror map and the Toda equation (4.70).

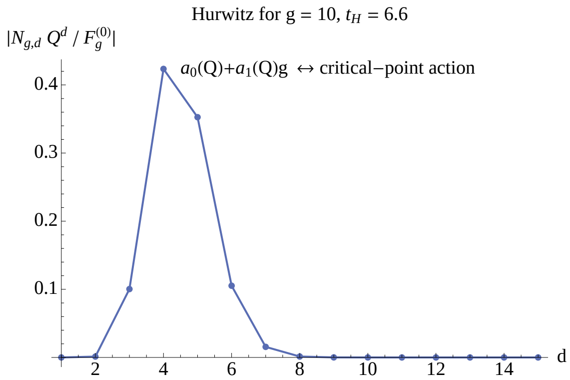

Figure 24: Hurwitz: Graphical representation of which GW invariants contribute the most to a free energy $F_g^{(0)}(Q)$, for fixed values of g and $Q = \mathrm{e}^{-t_{\mathrm{H}}}$. This time around we find a single saddle-point seemingly corresponding to the critical-point action.

That is no longer the case for degree $d \geq 5$, where we now find

$$H_{g,\boldsymbol{d}}^{\mathbb{P}^1}\left(1^d\right)^{\bullet} = \frac{2}{(\boldsymbol{d}!)^2}\left(\frac{\boldsymbol{d}\,(\boldsymbol{d}-1)}{2}\right)^{2\boldsymbol{d}+2g-2} - \frac{2}{((\boldsymbol{d}-1)!)^2}\left(\frac{(\boldsymbol{d}-1)\,(\boldsymbol{d}-2)}{2}\right)^{2\boldsymbol{d}+2g-2} + \\ + \frac{2}{\boldsymbol{d}^2\,((\boldsymbol{d}-2)!)^2}\left(\frac{\boldsymbol{d}\,(\boldsymbol{d}-3)}{2}\right)^{2\boldsymbol{d}+2g-2} - \frac{1}{2\,((\boldsymbol{d}-2)!)^2}\left(\frac{\left(\boldsymbol{d}^2-5d+8\right)}{2}\right)^{2\boldsymbol{d}+2g-2} + \cdots . \tag{4.82}$$

These results can also be easily derived by computing the free energy directly for low degree. For the purpose of illustration, let us show how the agreement between the exact $H_{g,d}^{\mathbb{P}^1}\left(1^d\right)^{\bullet}$ (for $d = 6$ and $g = 100$) and its prediction from (4.82) improves, as we include more terms. Note that this is an integer number with 241 digits, but we only display the first 82. One has:

$$H_{100,6}^{\mathbb{P}^1}\left(1^d\right)^{\bullet} = 3677302902113658612010882234808693441789186153144735319701111906118487881570479530 2\ldots$$

$$\text{1-term} = 36773029021136586120108822348086934556780750396609834115336352765962460171085765176\ldots$$

$$\text{2-terms} = 36773029021136586120108822348086934417891861507720945226447463877073571282196876287\ldots$$

$$\text{3-terms} = 36773029021136586120108822348086934417891861531447353197011119061187444102489809778\ldots$$

$$\text{4-terms} = 36773029021136586120108822348086934417891861531447353197011119061184878815704795232\ldots$$

Combined/Diagonal Large-Growth in Genus and Degree

Uncovering the combined growth in genus and degree for Hurwitz theory is a harder problem than in previous examples. The main reason being that in this example the "large-radius peak", where GW invariants near $d = (2g-3)/t$ give the main contribution to the free energy, no longer seems to exist. We did still numerically find another "critical-point peak", as shown in figure 24, but with the data we have available we were not able to find a linear relation, nor to uncover what the large-order behavior should be, analytically.

4.5 The Example of the Compact Quintic

For our final example, we shall consider a compact geometry, in comparison to the non-compact local geometries we have been addressing up to now. This is actually the first example in which mirror symmetry was explicitly worked out and GW invariants systematically computed [4], the quintic CY threefold. The mirror of the quintic is described by the equation

$$\sum_{i=1}^{5} x_i^5 - \frac{1}{z} \prod_{i=1}^{5} x_i = 0, \tag{4.83}$$

where z captures the complex structure of the CY manifold. We will follow the notation in [65].

Free Energies and Gromov–Witten Invariants

As there is a single modulus, there is also a single Picard–Fuchs equation for the periods of this geometry, namely

$$\left\{ (z\partial_z)^4 - 5z\,(5z\partial_z + 1)\,(5z\partial_z + 2)\,(5z\partial_z + 3)\,(5z\partial_z + 4) \right\} f(z) = 0. \tag{4.84}$$

From its solutions, we find the mirror map and the genus-zero free energy,

$$-t = \log z + 770z + 717825z^2 + \frac{3225308000}{3} z^3 + \cdots \equiv \log Q, \tag{4.85}$$

$$F_0^{(0)} = c_3 t^3 + c_2 t^2 + c_1 t + 2875Q + \frac{4876875}{8} Q^2 + \frac{8564575000}{27} Q^3 + \cdots . \tag{4.86}$$

Akin to what happened for the local geometries, here the higher-genus free energies can also be described in compact form in terms of a few generators (or propagators). Each of them has a holomorphic expansion around the large-radius point ($Q = 0$), from which one can read the GW invariants. For example,

$$F_2^{(0)} = \frac{575}{48} Q + \frac{5125}{2} Q^2 + \frac{7930375}{6} Q^3 + \cdots . \tag{4.87}$$

In this work we use the free energies which were computed in [65], and which are available online[16]. In appendix B.5 we list a sample of the first GW invariants, and figure 25 schematically represents the ones we used in our upcoming analysis. Note that we now have significantly less data than for the earlier non-compact examples, implying we will not have as many results.

Another important point is that there are essentially no studies of nonperturbative sectors for the quintic, mainly due to a lack of data to drive the analysis. However, it is not too difficult to check that there is an instanton action associated to the conifold point (located at $z = 5^{-5}$), $A_{\rm c} = 2\pi T_{\rm c}$, which is proportional to the flat coordinate $T_{\rm c}$ vanishing at the conifold point. A test of this instanton action is shown in figure 26. We should also expect a Kähler instanton action, but we do not have enough free energies available to report definite results.

Analysis of Large-Degree Growth

The large-degree growth at fixed genus was already considered in [6], being in the same universality class as local $\mathbb{P}^2$ or local $\mathbb{P}^1 \times \mathbb{P}^1$. In this case, the familiar asymptotic formula holds,

$$N_{\boldsymbol{g},d}^{\text{quint}} \sim c_{\boldsymbol{g}}\, d^{2\boldsymbol{g}-3}\, \mathrm{e}^{d t_{\rm c}}\, (\log d)^{2\boldsymbol{g}-2}\,, \tag{4.88}$$

where now $t_{\rm c} := t(z = 5^{-5}) = 7.58995\ldots$. One can numerically check the value of this critical exponent, $t_{\rm c}$, as well as the powers in $d^{2\boldsymbol{g}-3}$ and $(\log d)^{2\boldsymbol{g}-2}$, using the same asymptotic techniques described for local $\mathbb{P}^2$ and ABJM. We show these numerical results in figures 27 and 28.

[16] http://uw.physics.wisc.edu/∼strings/aklemm/highergenusdata/

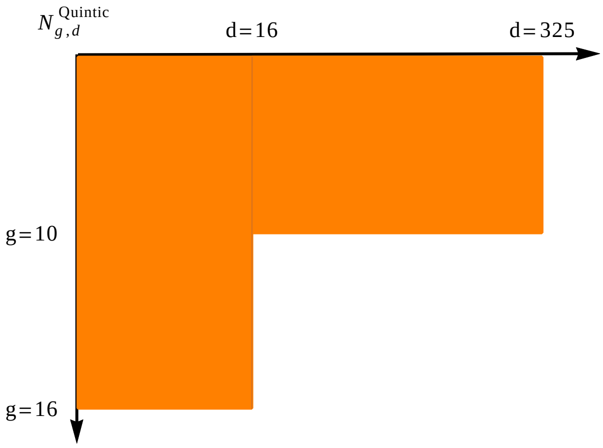

Figure 25: Maximum degree and genus of the GW invariants computed for the quintic.

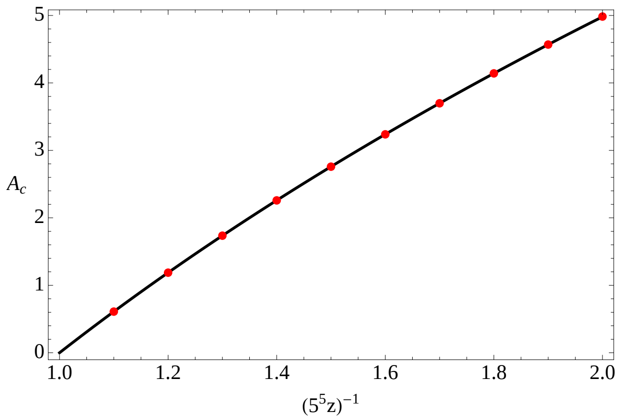

Figure 26: Quintic: Near the conifold point, the instanton action $A_{\rm c} = 2\pi T_{\rm c}$ controls the factorial growth of the free energies. In the figure we plot the analytic dependence of $A_{\rm c}$ against its numerical values computed from the large-genus growth of $F_g^{(0)}$, with a very clean match.

Analysis of Large-Genus Growth

The fixed-degree, large-genus expansion of the GW invariants determines the *abc*-coefficients for the quintic in the same way it did for other geometries. We already showed an example for degree $d = 4$ earlier, in equation (2.17). In appendix B.5 we present a sample of other such coefficients. Unfortunately, the scarce data available limits the analysis of the b-coefficients, and we have no other large-genus results to present for this example.

Combined/Diagonal Large-Growth in Genus and Degree

As in previous examples, also for the quintic we find two saddle-points which are illustrated in figure 29. They are associated to the Kähler instanton action, located at $d = (2g-3)/t$, and to the conifold instanton action, located at $d = a_0(Q) + a_1(Q)\, g$, just like before.

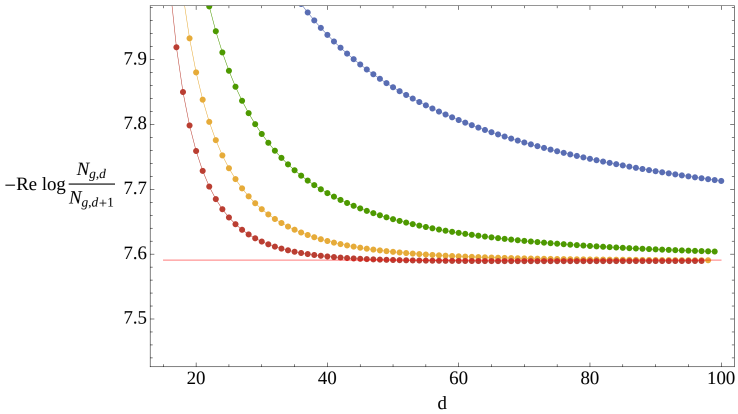

Figure 27: Quintic: The exponent t_c in the growth of $N_{\boldsymbol{g},d}$ is captured from the ratio of two consecutive GW invariants, when the degree is large. We plot that ratio alongside three Richardson extrapolations, which are clearly converging faster towards the expected result (up to a numerical relative error of about 0.2%).

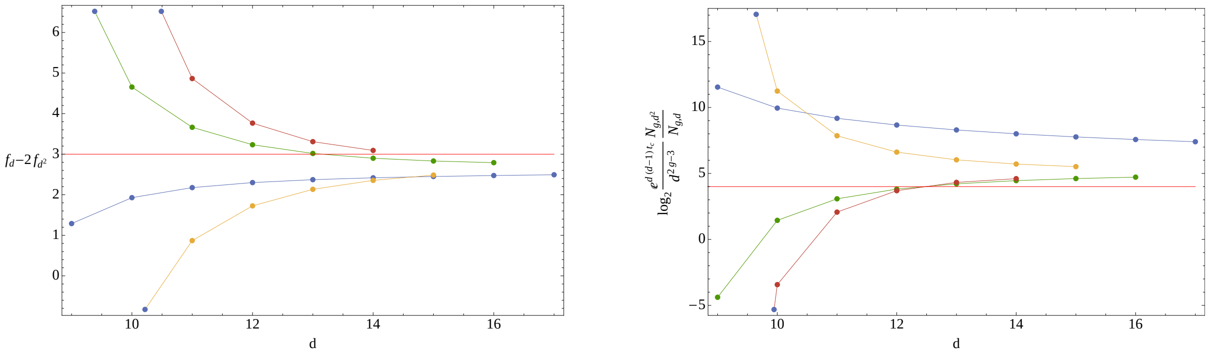

Figure 28: Quintic: On the left we address the exponent $2\boldsymbol{g}-3$, which is the leading large-order term in $f_d - 2f_{d^2}$. We have data up to $d = 325$ so that the horizontal axis can only reach $d = 17$. The plot illustrates the first few Richardson transforms for $g = 3$, converging faster towards the expected result (up to a numerical relative error of about 3%). On the right we address the exponent $2\boldsymbol{g}-2$ of the logarithm $\log d$, which is the leading term in the sequence (4.13). We plot the first few Richardson transforms for $g = 3$, converging faster towards the expected result (up to a numerical relative error of about 15%).

Kähler Leading Degree

The scarce amount of available data does not let us check that the leading degree is $d = (2g-3)/t$ in the same way as we did for local $\mathbb{P}^2$ or ABJM. Nevertheless, we can assume that this indeed holds, and then explore the asymptotics of $N^{\text{quint}}_{g,d}\, Q^d\Big|_{g=\frac{t}{2}d+q}$, just as we did in (4.22). We find that the same formula applies, but with the appropriate GV invariant $n_0^{(1)} = 2875$. Computational tests on the validity of such expression are shown in figures 10 and 11, with their details and discussion being the exact same as before.

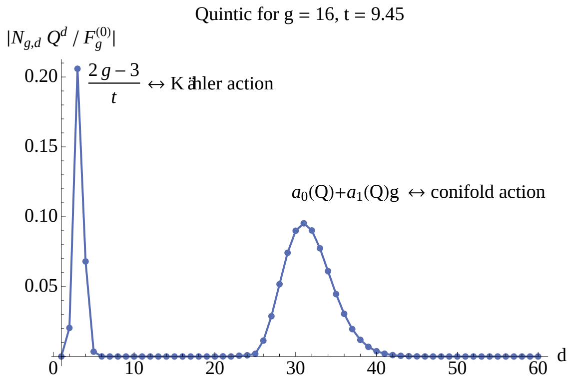

Figure 29: Quintic: Graphical representation of which GW invariants contribute the most to a free energy $F_g^{(0)}(Q)$, for fixed values of g and $Q = \mathrm{e}^{-t}$. The values of g and t are carefully chosen so that both saddles are clearly visible in the same plot.

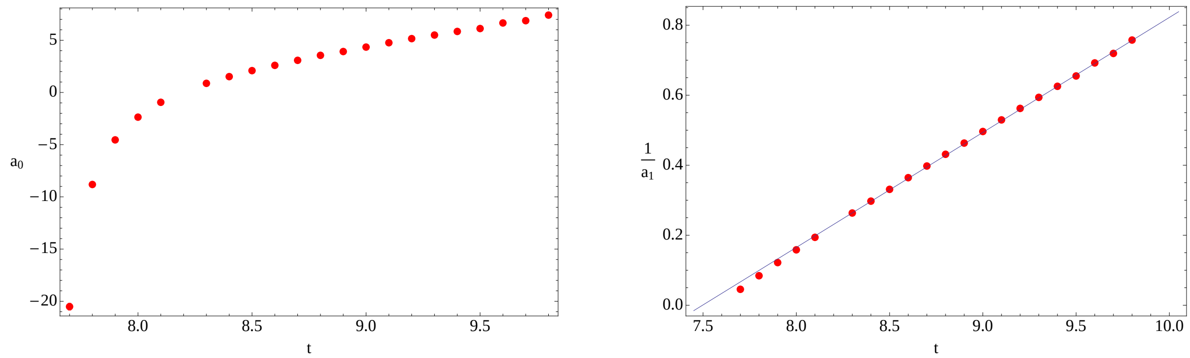

Figure 30: Quintic: Numerical calculation of $a_0(Q)$ and $a_1(Q)$ associated to the conifold instanton action. We show the inverse of a_1 because the dependence seems linear, although we are not able to confirm this analytically. The plot for a_0 does not seem to lead to any linear dependence.

Conifold Leading Degree

For the conifold leading degree we can do better. Figure 30 shows the dependence of a_0 and a_1 upon the modulus t. The inverse of the slope, a_1^{-1}, resembles a straight line

$$a_1(Q)^{-1} = (-2.46 \pm 0.01) + (0.328 \pm 0.002)\, t, \qquad r^2 = 0.9995. \tag{4.89}$$

Acknowledgments

We would like to thank Aleksey Zinger for discussions, and Marcos Mariño, José Mourão and João Pimentel Nunes for useful comments on the draft. RS would further like to thank the University of Geneva for extended hospitality, where a part of this work was conducted. RV would further like to thank the DESY Theory Group for support and hospitality. This research was partially supported by the FCT-Portugal grants EXCL/MAT-GEO/0222/2012, UID/MAT/04459/2013 and PTDC/MAT-GEO/3319/2014. The research of RS was partially supported by the Swiss-NSF grant NCCR 51NF40-141869 "The Mathematics of Physics" (SwissMAP).

A Analysis of the abc-Coefficients

When the GW invariants, $N_{g,d}$, may be written in terms of GV invariants, $n_g^{(d)}$, then there is a third representation in terms of some other integers we denoted by a_d, $b_{d,n}$, c_d. They appear naturally when considering the large-genus expansion of $N_{g,d}$.

PROPOSITION A.1. *The relation between GW and GV invariants, and abc-coefficients is*

$$N_{g,d} = f_g^{CS} \left\{ \sum_{m|d} a_m \left(\frac{d}{m}\right)^{2g-3} + \frac{2g}{B_{2g}} \frac{1}{d} \left(c_d\, \delta_{g,1} + \sum_{m=1}^{G(d)-1} b_{d,m}\, m^{2g-2} \right) \right\}, \tag{A.1}$$

$$a_d = n_0^{(d)}, \tag{A.2}$$

$$b_{d,m} = \sum_{k|d,m} (-1)^{\frac{m}{k}} \frac{2d}{k} \sum_{h=\frac{m}{k}+1}^{G(\frac{d}{k})} n_h^{(\frac{d}{k})} \binom{2h-2}{h-1+\frac{m}{k}}, \tag{A.3}$$

$$c_d = \sum_{m|d} m \left\{ n_1^{(m)} + 2 \sum_{h=2}^{G(m)} \frac{n_h^{(m)}}{h} \binom{2h-3}{h-2} \right\}. \tag{A.4}$$

Here $f_0^{CS} = 1$*,* $f_g^{CS} = (-1)^{g-1} \frac{B_{2g}}{2g(2g-2)!}$ *for* $g \geq 1$*, and* B_{2g} *are the Bernoulli numbers.* $G(d)$ *satisfies* $n_g^{(d)} = 0$ *for* $g > G(d)$*. Since the GV invariants are integers, so are the abc-coefficients.*

Proof. We start from the definition of GV invariants,

$$N_{g,d} = \sum_{h=0}^{g} c_{h,g} \sum_{m|d} n_h^{(m)} \left(\frac{d}{m}\right)^{2g-3} = \sum_{m|d} \sum_{h=0}^{G(m)} c_{h,g}\, n_h^{(m)} \left(\frac{d}{m}\right)^{2g-3}, \tag{A.5}$$

where in the second equality we have noticed that $n_h^{(m)} = 0$ for $h > G(m)$. The coefficients $c_{h,g}$ generate $\left(2 \sin \frac{x}{2}\right)^{2h-2} = \sum_{h=g}^{+\infty} c_{h,g}\, x^{2g-2}$, and they are explicitly given by

$$c_{0,g} = f_g^{\rm CS}, \qquad c_{1,g} = \delta_{g,1}, \qquad c_{h,g} = (-1)^{g-1} \frac{2}{(2g-2)!} \sum_{k=1}^{h-1} \binom{2h-2}{h-1+k} (-1)^k\, k^{2g-2}. \tag{A.6}$$

Next, we organize the terms in (A.5) from more to less important as g grows, using (A.6). In order to do this, we split the h-sum in (A.5) into $h = 0$, $h = 1$, and $h \geq 2$. For $h \geq 2$ we can assume that also $g \geq 2$ and manipulate to arrive at (A.1). The steps are straightforward once one knows the goal, and they simply require the exchange of double sums, such as, *e.g.*, $\sum_{h=2}^{G(m)} \sum_{k=1}^{h-1} = \sum_{k=1}^{G(m)-1} \sum_{h=k+1}^{G(m)}$; or relabelings, such as, *e.g.*, $\sum_{m|d} f(m) = \sum_{m|d} f(d/m)$. The end result, after four of these manipulations, is

$$N_{g,d} = f_g^{\rm CS} \left\{ \sum_{m|d} n_0^{(m)} \left(\frac{d}{m}\right)^{2g-3} + \frac{2g}{B_{2g}} \frac{1}{d} \left(\delta_{g,1} \sum_{m|d} n_1^{(m)}\, m + \right.\right.$$
$$\left.\left. + \delta_{g\geq 2} \sum_{m=1}^{G(d)-1} \sum_{k|d,m} \sum_{h=\frac{m}{k}+1}^{G(\frac{d}{k})} n_h^{(\frac{d}{k})} \frac{2d}{k} \binom{2h-2}{h-1+\frac{m}{k}} (-1)^{\frac{m}{k}}\, m^{2g-2} \right) \right\}, \tag{A.7}$$

from where one immediately can read the abc-coefficients. □

We finish this appendix with a short note on how the GV and GW invariants, and the *abc*-coefficients, may be laid out in Dirichlet series for each genus g, in contrast to the usual Taylor-series expansion in the form of free energies. If we define the generating functions

$$\mathcal{GV}_g(s) := \sum_{d=1}^{+\infty} \frac{n_g^{(d)}}{d^s}, \qquad \mathcal{GW}_g(s) := \sum_{d=1}^{+\infty} \frac{N_{g,d}}{d^s}, \qquad \widetilde{\mathcal{GW}}_g(s) := \frac{\mathcal{GW}_g(s)}{\zeta\left(s-(2g-3)\right)}, \tag{A.8}$$

then it follows from (A.5) the linear transformations

$$\widetilde{\mathcal{GW}}_g(s) = \sum_{h=0}^{g} c_{h,g}\, \mathcal{GV}_h(s) \qquad \text{and} \qquad \mathcal{GV}_g(s) = \sum_{h=0}^{g} \alpha_{g,h}\, \widetilde{\mathcal{GW}}_h(s). \tag{A.9}$$

Here, the α-coefficients arise from the generating function defined in [66],

$$\left(\frac{\arcsin(\sqrt{r}/2)}{\sqrt{r}/2}\right)^{2g-2} =: \sum_{h=0}^{+\infty} \alpha_{g+h,g}\, r^h. \tag{A.10}$$

We can also define Dirichlet series for the *abc*-coefficients, as

$$\mathcal{A}(s) := \sum_{d=1}^{+\infty} \frac{a_d}{d^s}, \qquad \widehat{\mathcal{B}}_{2g-2}(s) := \frac{(-1)^{g-1}}{(2g-2)!}\, \frac{1}{\zeta\left(s-(2g-3)\right)} \sum_{d=1}^{+\infty} \frac{\mathrm{b}_{2g-2}(d)}{d^s}, \tag{A.11}$$

where

$$\mathrm{b}_{2g-2}(d) := \frac{1}{d}\left(c_d\, \delta_{g,1} + \sum_{n=1}^{G(d)-1} b_{d,n}\, n^{2g-2}\right). \tag{A.12}$$

They are linearly related to the previous Dirichlet series as

$$\widetilde{\mathcal{GW}}_g(s) = f_g^{\mathrm{CS}}\, \mathcal{A}(s) + \widehat{\mathcal{B}}_{2g-2}(s), \qquad \mathcal{GV}_0(s) = \mathcal{A}(s), \qquad \mathcal{GV}_g(s) = \sum_{h=1}^{g} \alpha_{g,h}\, \widehat{\mathcal{B}}_{2h-2}(s). \tag{A.13}$$

The last expression can be inverted to define $\widehat{\mathcal{B}}_{2g-2}(s) = \sum_{h=1}^{g} c_{h,g}\, \mathcal{GV}_h(s)$.

B Large-Order Enumerative Data

B.1 Local $\mathbb{P}^2$

GW Invariants

$g\backslash d$	1	2	3	4	5
0	3	$-\frac{45}{8}$	$\frac{244}{9}$	$-\frac{12333}{64}$	$\frac{211878}{125}$
1	$\frac{1}{4}$	$-\frac{3}{8}$	$-\frac{23}{3}$	$\frac{3437}{16}$	$-\frac{43107}{10}$
2	$\frac{1}{80}$	0	$\frac{3}{20}$	$-\frac{514}{5}$	$\frac{43497}{8}$
3	$\frac{1}{2016}$	$\frac{1}{336}$	$\frac{1}{56}$	$\frac{1480}{63}$	$-\frac{1385717}{336}$
4	$\frac{1}{57600}$	$\frac{1}{1920}$	$\frac{7}{1600}$	$-\frac{2491}{900}$	$\frac{3865243}{1920}$
5	$\frac{1}{1774080}$	$\frac{1}{14080}$	$\frac{61}{49280}$	$\frac{4471}{22176}$	$-\frac{65308319}{98560}$
6	$\frac{691}{39626496000}$	$\frac{11747}{1320883200}$	$\frac{377977}{1100736000}$	$-\frac{4874687}{1238328000}$	$\frac{202790371913}{1320883200}$
7	$\frac{1}{1916006400}$	$\frac{31}{29030400}$	$\frac{703}{7603200}$	$\frac{11705}{4790016}$	$-\frac{8293308997}{319334400}$
8	$\frac{3617}{237124952064000}$	$\frac{3617}{28952985600}$	$\frac{160186079}{6586804224000}$	$\frac{3770876653}{3705077376000}$	$\frac{8819809463417}{2634721689600}$
9	$\frac{43867}{100178317983744000}$	$\frac{2395577687}{16696386330624000}$	$\frac{17484552727}{2782731055104000}$	$\frac{588854611393}{1252228974796800}$	$-\frac{531409226640767 9}{16696386330624000}$
10	$\frac{174611}{14085222152601600000}$	$\frac{44875027}{27618082652160000}$	$\frac{89481327671}{55893738700800000}$	$\frac{93741595374923}{440163192268800000}$	$\frac{16804318069652153}{469507405086720000}$
11	$\frac{77683}{2238269847522508800000}$	$\frac{5670859}{31164993699840000}$	$\frac{2507998840003}{6217416243118080000}$	$\frac{266915773471339}{2797837309403136000}$	$\frac{20387731289881801}{4144944162078720000}$
12	$\frac{236364091}{24548175894662951731200000}$	$\frac{300418759661}{148776823604017889280000}$	$\frac{68679218847036397}{681893774851748659200000}$	$\frac{4060700279791909811}{95891312088527155200000}$	$\frac{383134958212924668527 3}{81827252982209839104000 0}$
13	$\frac{657931}{24817936069329577574400000}$	$\frac{39993651697}{17984011644441722880000}$	$\frac{35113217570719}{1406912475585576960000}$	$\frac{34042475874467141}{1824848240391880704000}$	$\frac{1305499938936005786273}{4136322678221596262400000}$
14	$\frac{3392780147}{467818094906862537277440000000000}$	$\frac{817660015427}{3360038029927907328000000}$	$\frac{79851777025777281929}{12994947080746181591040000000}$	$\frac{119372831992394692724021}{14619315465839454289920000000}$	$\frac{1123556115201711190774230 7}{5197978832298472636416000000}$
15	$\frac{1723168255201}{87332217430579318202050805760000000}$	$\frac{38546620788077648821}{14555369571763219700341800960000000}$	$\frac{365005208696824752679561}{242589492862720328339030016000000}$	$\frac{388022989819002868290113941}{1091652717882241477525635072000000}$	$\frac{21397598170831649091330142404 43}{14555369571763219700341800960000000}$
16	$\frac{7709321041217}{1442975557378319358981518131200000000}$	$\frac{4757368049287722181}{1658592594687723401128181760000000}$	$\frac{110504096133213204298403}{301373341139999866119782400000000}$	$\frac{34719695239163450665340522203}{22546493084036239984086220800000000}$	$\frac{478657719223430557454615233435 31}{480991852459439786327172710400000 00}$

$g\backslash d$	6	7	8	9
0	$-\frac{102365}{6}$	$\frac{64639725}{343}$	$-\frac{1140830253}{512}$	$\frac{6742982701}{243}$
1	79522	$-\frac{39826681}{28}$	$\frac{803703117}{32}$	$-\frac{15878598203}{36}$
2	$-\frac{1552743}{8}$	$\frac{92569957}{16}$	$-\frac{776658618}{5}$	$\frac{311565686229}{80}$
3	$\frac{34386105}{112}$	$-\frac{4563656185}{288}$	$\frac{27816690931}{42}$	$-\frac{771022095237}{32}$
4	$-\frac{217225227}{640}$	$\frac{364416184789}{11520}$	$-\frac{316806697367}{150}$	$\frac{726200060335821}{6400}$
5	$\frac{5383395285}{19712}$	$-\frac{17012987874515}{354816}$	$\frac{64688948714407}{12320}$	$-\frac{11945278310269797}{28160}$
6	$-\frac{24163714857019}{146764800}$	$\frac{64139775474690313}{1132185600}$	$-\frac{431003499904037995 3}{412776000}$	$\frac{991900415691784747}{768000}$
7	$\frac{540810103943}{7096320}$	$-\frac{20390495664732131}{383201280}$	$\frac{675146333220270311}{39916800}$	$-\frac{7710530504497344961 1}{23654400}$
8	$-\frac{2431338026245535 3}{878240563200}$	$\frac{1741466801411501222 71}{4311362764800}$	$-\frac{931925090539277177671 1}{411675264000}$	$\frac{28901988252740100498438 59}{418209792000}$
9	$\frac{229746711843473009}{28540831334400}$	$-\frac{71968023889934347066967}{2862237656678400}$	$\frac{528752014379148901144752 67}{208704829132800 0}$	$-\frac{2198077616037166910710794671}{176681336832000}$
10	$-\frac{994544782717679582 99}{52167489454080000}$	$\frac{7327413761814208985386483}{56340888610406400 0}$	$-\frac{351563397698815428247365484 3}{146721064089600000}$	$\frac{3337167001575229075850450161439}{17389163151360000 0}$
11	$\frac{30997881964033427587 7}{82898883241574400 0}$	$-\frac{1332859697395708004527165 1}{2356073523707904000}$	$\frac{1001813296434398195310909261 7}{518118020259840000}$	$-\frac{100952237872222674774049307921 99}{39475658686464000 0}$
12	$-\frac{2930891797753721359716 01}{478521947264385024000 0}$	$\frac{1467383987133527878069931695921}{7013764541332271923200 00}$	$-\frac{4292705511982985443590265175261 81}{3196377069617571840000 0}$	$\frac{987623989916571095263236845356903 09}{3330372526748467200000}$
13	$\frac{8084238020477841645415 7}{9191828173825769472000}$	$-\frac{2997997652543647916154322561 9}{4512352012605377740800 0}$	$\frac{181956303001255901436463972048 57}{2248001455555215360000}$	$-\frac{92309507389254031690279328664032668 1}{3063942724608589824000 0}$
14	$-\frac{142728776986168158244625612 3}{17326596107661575454720000 00}$	$\frac{1710697905914403226126573514710790 3}{935636189813725074554880000 00}$	$-\frac{6927527005787031979868370050723275607}{16243683850932726988800000 00}$	$\frac{22263736991301596394490090922075629687049}{825076005126741688320000000}$
15	$\frac{153803338770860319406845530599}{49761947253891349402877952000 0}$	$-\frac{21927613660522606018612458566133101 77}{4990412424604532468688617472000 0}$	$\frac{3598896597319399294130225815187642461058 71}{1819421196470402462542725120000 00}$	$-\frac{106480974409527581871979972109650680232750 43}{4968550801079781430394880000 00}$
16	$\frac{999967541303011049654487279265447}{534435391621599762585747456000000 00}$	$\frac{2688927552566365493409683974771147699637}{28859511147566387179630362624000000 0}$	$-\frac{6108244374311877666529467820160309173334243}{751549769467874666136207360000000 00}$	$\frac{2703407492297994032881552152254344023290794754 93}{17814513054053325419524915200000000 0}$

abc-Coefficients

d	$a_d^{\mathbb{P}^2}$	$c_d^{\mathbb{P}^2}$
1	3	0
2	−6	0
3	27	−30
4	−192	468
5	1 695	−7 560
6	−17 064	123 054
7	188 454	−2 014 488
8	−2 228 160	33 210 684
9	27 748 899	−551 883 810
10	−360 012 150	9 239 062 680
11	4 827 935 937	−155 687 687 496
12	−66 537 713 520	2 638 717 494 534
13	938 273 463 465	−44 952 069 548 178
14	−13 491 638 200 194	769 253 530 779 972
15	197 287 568 723 655	−13 217 019 911 660 760
16	−2 927 443 754 647 296	227 905 457 523 361 164

$[b_{d,n}^{\mathbb{P}^2}]$ $n\backslash d$	4	5	6	7	8	9	10	11	12
1	336	−8 220	158 112	−2 852 178	50 177 472	−872 820 522	15 111 672 960	−261 287 923 314	4 519 291 217 184
2	120	−3 960	95 364	−1 949 220	37 023 696	−678 641 328	12 204 852 900	−217 166 980 668	3 840 996 869 640
3	0	−1 710	54 672	−1 285 452	26 679 744	−518 992 740	9 736 728 480	−178 799 167 602	3 240 289 008 192
4	0	−600	29 052	−819 000	18 795 144	−390 496 464	7 674 526 800	−145 852 020 072	2 713 595 908 644
5	0	−210	14 688	−502 698	12 935 232	−289 170 162	5 978 222 760	−117 901 473 690	2 256 269 192 064
6	0	0	6 600	−297 360	8 704 224	−210 776 976	4 603 163 850	−94 464 959 688	1 862 891 778 168
7	0	0	2 808	−168 420	5 716 608	−151 246 602	3 504 280 200	−75 031 171 842	1 527 561 613 296
8	0	0	972	−91 644	3 667 920	−106 820 532	2 637 683 220	−59 087 632 428	1 244 182 530 852
9	0	0	336	−46 872	2 290 176	−74 248 344	1 963 227 240	−46 140 388 866	1 006 686 336 672
10	0	0	0	−22 848	1 394 016	−50 759 784	1 444 755 510	−35 729 687 796	809 231 436 144
11	0	0	0	−10 164	821 952	−34 124 490	1 051 214 760	−27 438 015 792	646 325 964 576
12	0	0	0	−4 284	471 024	−22 534 812	756 025 920	−20 895 548 256	512 927 324 016
13	0	0	0	−1 470	259 104	−14 613 048	537 393 120	−15 780 170 406	404 480 624 544
14	0	0	0	−504	137 904	−9 288 756	377 354 040	−11 816 821 368	316 945 489 680
15	0	0	0	0	69 120	−5 786 568	261 725 400	−8 773 420 590	246 780 346 080
16	0	0	0	0	33 456	−3 522 204	179 174 760	−6 457 541 244	190 927 009 332
17	0	0	0	0	14 784	−2 095 956	121 053 360	−4 710 998 490	146 768 446 368
18	0	0	0	0	6 192	−1 212 624	80 627 580	−3 405 917 196	112 094 549 136
19	0	0	0	0	2 112	−682 830	52 935 600	−2 439 572 652	85 052 045 088
20	0	0	0	0	720	−370 656	34 205 400	−1 730 850 132	64 106 083 800
21	0	0	0	0	0	−194 922	21 753 000	−1 215 940 374	47 992 597 344
22	0	0	0	0	0	−97 200	13 584 180	−845 593 716	35 683 209 288
23	0	0	0	0	0	−46 818	8 332 680	−581 826 564	26 344 946 736
24	0	0	0	0	0	−20 592	5 000 940	−395 979 804	19 311 539 496
25	0	0	0	0	0	−8 586	2 940 480	−266 385 570	14 051 779 776
26	0	0	0	0	0	−2 916	1 682 760	−177 075 888	10 147 793 400
27	0	0	0	0	0	−990	939 600	−116 199 666	7 271 460 336
28	0	0	0	0	0	0	506 220	−75 250 296	5 168 924 064
29	0	0	0	0	0	0	265 200	−48 026 484	3 643 846 992
30	0	0	0	0	0	0	131 760	−30 198 564	2 546 877 264
31	0	0	0	0	0	0	63 240	−18 669 882	1 764 218 448
32	0	0	0	0	0	0	27 720	−11 347 512	1 210 848 048
33	0	0	0	0	0	0	11 520	−6 757 344	822 942 432
34	0	0	0	0	0	0	3 900	−3 945 084	553 704 336
35	0	0	0	0	0	0	1 320	−2 245 122	368 537 904
36	0	0	0	0	0	0	0	−1 247 400	242 587 920
37	0	0	0	0	0	0	0	−670 098	157 750 848
38	0	0	0	0	0	0	0	−350 064	101 321 496
39	0	0	0	0	0	0	0	−173 448	64 177 008
40	0	0	0	0	0	0	0	−83 028	40 082 040
41	0	0	0	0	0	0	0	−36 300	24 627 888
42	0	0	0	0	0	0	0	−15 048	14 889 864
43	0	0	0	0	0	0	0	−5 082	8 824 464
44	0	0	0	0	0	0	0	−1 716	5 132 160
45	0	0	0	0	0	0	0	0	2 910 672
46	0	0	0	0	0	0	0	0	1 613 520
47	0	0	0	0	0	0	0	0	864 864
48	0	0	0	0	0	0	0	0	450 840
49	0	0	0	0	0	0	0	0	222 912
50	0	0	0	0	0	0	0	0	106 488
51	0	0	0	0	0	0	0	0	46 464
52	0	0	0	0	0	0	0	0	19 224
53	0	0	0	0	0	0	0	0	6 480
54	0	0	0	0	0	0	0	0	2 184

B.2 Local $\mathbb{P}^1 \times \mathbb{P}^1$

GW Invariants

$g \backslash d$	1	2	3	4	5
0	-4	$-\frac{9}{2}$	$-\frac{328}{27}$	$-\frac{777}{16}$	$-\frac{30004}{125}$
1	$-\frac{1}{3}$	$-\frac{1}{2}$	$-\frac{10}{9}$	$\frac{19}{4}$	$\frac{1739}{15}$
2	$-\frac{1}{60}$	$-\frac{1}{20}$	$-\frac{1}{10}$	$-\frac{3}{10}$	$-\frac{301}{12}$
3	$-\frac{1}{1512}$	$-\frac{1}{168}$	$-\frac{5}{252}$	$-\frac{1}{18}$	$\frac{2839}{1512}$
4	$-\frac{1}{43200}$	$-\frac{11}{14400}$	$-\frac{41}{7200}$	$-\frac{89}{3600}$	$-\frac{1213}{8640}$
5	$-\frac{1}{1330560}$	$-\frac{43}{443520}$	$-\frac{73}{44352}$	$-\frac{153}{12320}$	$-\frac{10943}{190080}$
6	$-\frac{691}{29719872000}$	$-\frac{13129}{1100736000}$	$-\frac{2267171}{4953312000}$	$-\frac{2160757}{353808000}$	$-\frac{20769907}{457228800}$
7	$-\frac{1}{1437004800}$	$-\frac{683}{479001600}$	$-\frac{1181}{9580032}$	$-\frac{349697}{119750400}$	$-\frac{48828041}{1437004800}$
8	$-\frac{3617}{177843714048000}$	$-\frac{9878027}{59281238016000}$	$-\frac{961112857}{29640619008000}$	$-\frac{6743400971}{4940103168000}$	$-\frac{126150957659}{5081248972800}$
9	$-\frac{43867}{75133738487808000}$	$-\frac{14519977}{758926651392000}$	$-\frac{20981454499}{2504457949593600}$	$-\frac{560753220877}{894449267712000}$	$-\frac{1338714602069027}{75133738487808000}$
10	$-\frac{174611}{10563916614451200000}$	$-\frac{7628929201}{352130553815040000}$	$-\frac{3758215587571}{1760652769075200000}$	$-\frac{249984752232979}{880326384537600000}$	$-\frac{2664352417203304 7}{2112783322890240000}$
11	$-\frac{77683}{167870238564188160000}$	$-\frac{13576114129}{55956746188062720000}$	$-\frac{3009598592467}{5595674618806272000}$	$-\frac{593149477064657}{466306218233856000}$	$-\frac{1245113981875959 7}{1410674273648640000}$
12	$-\frac{236364091}{1841113192099721379840000}$	$-\frac{55076851392547}{2045681324555245977600000}$	$-\frac{412075312845854291}{30685219868328689664000000}$	$-\frac{12375485255560486957}{219180141916633497600000}$	$-\frac{346791327549904666511}{566496366799914270720000}$
13	$-\frac{657931}{18613452051997183180800000}$	$-\frac{1839708635993}{6204484017332394393600000}$	$-\frac{2064657193026691}{620448401733239439360000}$	$-\frac{226949920317097051}{9124241201959403520000}$	$-\frac{784314870834354533509 1}{18613452051997183180800000}$
14	$-\frac{3392780147}{350863571180146902958080000000}$	$-\frac{3449782246249747}{10632229429701421301760000000}$	$-\frac{28182980126545347731}{3439838933138695127040000000}$	$-\frac{35369731160070885253787}{3248736770186545397760000000}$	$-\frac{41270501114884209670059 59}{143209620889855878758400000 0}$
15	$-\frac{1723168255201}{654991630729344886515381043200000000}$	$-\frac{150279226704334411}{42559560151354443568250880000000}$	$-\frac{438006250435845069564433}{218330543576448295505127014400000}$	$-\frac{369545712849515646148157911}{779751941344458198232596480000000}$	$-\frac{67571599828608726744462924257 9}{3447324372259709929028321280000 00}$
16	$-\frac{7709321041217}{10822316680337395192361385598400000000}$	$-\frac{1379636742002760473707}{3607438893445798397453795328000000000}$	$-\frac{88182268714296427709084377}{180371944672289919872689766400000000}$	$-\frac{185171708976932688218478318913}{901859723361449599363448832000000000}$	$-\frac{28719458882573992023182459667439 7}{21644633360674790384722771968000000 00}$

$g \backslash d$	6	7	8	9
0	$-\frac{4073}{3}$	$-\frac{2890808}{343}$	$-\frac{7168777}{128}$	$-\frac{285797488}{729}$
1	$\frac{4507}{3}$	$\frac{354010}{21}$	$\frac{4291121}{24}$	$\frac{49841828}{27}$
2	$-\frac{8179}{10}$	$-\frac{521257}{30}$	$-\frac{4535909}{15}$	$-\frac{23452729}{5}$
3	$\frac{63823}{252}$	$\frac{1204781}{108}$	$\frac{8995490}{27}$	$\frac{335218687}{42}$
4	$-\frac{39561}{800}$	$-\frac{104182657}{21600}$	$-\frac{699162611}{2700}$	$-\frac{35503100669}{3600}$
5	$\frac{1364423}{221760}$	$\frac{973064867}{665280}$	$\frac{32043241}{216}$	$\frac{1024830677081}{110880}$
6	$-\frac{3994795379}{4953312000}$	$-\frac{684528541741}{2122848000}$	$-\frac{17140336370063}{265356000}$	$-\frac{5580297058509073}{825552000}$
7	$-\frac{17208259}{79833600}$	$\frac{3348832897}{65318400}$	$\frac{56187418523}{2566080}$	$\frac{471670912480501}{119750400}$
8	$-\frac{7927439452913}{29640619008000}$	$-\frac{761823908002769}{88921857024000}$	$-\frac{9396307073631421}{1587890304000}$	$-\frac{275605355413655801 33}{14820309504000}$
9	$-\frac{3436874923482659}{12522289747968000}$	$-\frac{11397824941288873}{5366695606272000}$	$\frac{34062699801911821}{26833478031360}$	$\frac{5018812333652931839 23}{695682763776000}$
10	$-\frac{164201337998690833}{586884256358400000}$	$-\frac{2057927401444571242 7}{528195830722560000 0}$	$-\frac{230721132644322713 3}{857460764160000 0}$	$-\frac{2053679554520139335871 79}{880326384537600000}$
11	$-\frac{788949589692678609 1}{279783730940313600 00}$	$-\frac{402250283211161659 49}{763046538928128000 0}$	$-\frac{956525732060946535 9}{299768283150336000}$	$\frac{877398611009851093200503}{1398918654701568000 0}$
12	$-\frac{864184981304145550432139}{306852198683286896640000 00}$	$-\frac{857294791161678772345031}{119552804681800089600000}$	$-\frac{20189747571711395089269023}{1643851064374751232000000}$	$-\frac{8209878060327926372943757013}{511420331138811494400000}$
13	$-\frac{962200106135242679164 3}{344693556518466355200 00}$	$-\frac{900336637173581902740022 3}{930672602599859159040000}$	$-\frac{691937769345222335067871}{332383072357092556800 0}$	$-\frac{3471261518274708433859810 9}{155112100433309859840000}$
14	$-\frac{16076286612752251861306780403}{58477261863357817159680000000}$	$-\frac{22749755467330881884420779435 79}{17543178559007345147904000000 0}$	$-\frac{163509269273170929755804145433}{447530065280799621120000000}$	$-\frac{21760503667650107342123869364624 3}{29238630931678908579840000000}$
15	$-\frac{2939410211065193059560472155999 77}{10916527178822414775256350720000 00}$	$-\frac{80881040524722692826677012778708 19}{46785116480667491893955788800000 0}$	$-\frac{676354133533279533634914799323599}{1063298101833352088498995200000}$	$-\frac{27697040345840037413979280614710568 73}{18194211964704024625427251200000 0}$
16	$-\frac{15780831705018554592522936743857691}{601239815574299732908965888000000000}$	$-\frac{59385854531893992032195734428800641}{2589070976157271577119948800000000 0}$	$-\frac{1065142795758158496348139116595466598 1}{96627827503012457074655232000000000}$	$-\frac{302688719433999098300108612993961712885 3}{901859723361449599363448832000000000}$

abc-Coefficients

d	a_d^{ABJM}	c_d^{ABJM}
1	−4	0
2	−4	0
3	−12	0
4	−48	36
5	−240	440
6	−1 356	4 728
7	−8 428	46 144
8	−56 000	444 236
9	−392 040	4 247 208
10	−2 859 120	40 641 800
11	−21 554 940	389 829 264
12	−167 010 960	3 751 216 056
13	−1 324 106 888	36 216 220 352
14	−10 705 217 964	350 781 045 720
15	−88 021 082 760	3 407 942 473 760

$[b_{d,n}^{\mathrm{ABJM}}]$ $n \backslash d$	5	6	7	8	9	10	11	12	13	14
1	240	3 696	46 480	516 608	5 458 896	56 047 920	566 614 752	5 676 814 656	56 583 881 744	562 375 292 640
2	0	1 080	20 048	276 320	3 314 736	37 133 120	399 615 744	4 197 108 768	43 398 021 680	444 144 819 608
3	0	192	7 560	135 552	1 906 632	23 655 120	273 738 872	3 033 716 736	32 692 599 888	345 696 739 584
4	0	0	2 128	60 272	1 032 048	14 484 240	182 145 920	2 144 755 608	24 199 605 872	265 271 553 568
5	0	0	560	23 936	526 896	8 517 680	117 770 400	1 483 520 832	17 608 053 216	200 749 949 008
6	0	0	0	8 096	248 832	4 796 320	73 908 032	1 003 948 416	12 596 117 248	149 866 011 064
7	0	0	0	2 304	109 584	2 579 920	45 003 288	664 568 064	8 859 926 192	110 385 406 208
8	0	0	0	400	42 768	1 317 840	26 517 568	430 050 624	6 126 652 064	80 225 632 704
9	0	0	0	0	15 120	635 440	15 107 840	271 850 880	4 164 242 368	57 530 966 192
10	0	0	0	0	4 176	286 600	8 284 672	167 686 224	2 780 750 960	40 703 206 040
11	0	0	0	0	1 080	119 680	4 368 320	100 802 304	1 823 545 568	28 406 120 960
12	0	0	0	0	0	44 880	2 194 896	58 948 344	1 173 389 568	19 549 240 592
13	0	0	0	0	0	14 960	1 052 304	33 475 392	740 408 448	13 262 762 576
14	0	0	0	0	0	4 200	472 208	18 409 920	457 577 744	8 866 106 984
15	0	0	0	0	0	720	198 968	9 775 488	276 724 344	5 837 236 384
16	0	0	0	0	0	0	75 504	4 991 760	163 466 992	3 782 616 656
17	0	0	0	0	0	0	26 400	2 440 128	94 223 168	2 410 952 656
18	0	0	0	0	0	0	7 216	1 133 328	52 839 904	1 510 198 592
19	0	0	0	0	0	0	1 848	496 320	28 797 600	928 817 232
20	0	0	0	0	0	0	0	201 960	15 179 424	560 254 240
21	0	0	0	0	0	0	0	75 072	7 729 904	331 025 408
22	0	0	0	0	0	0	0	24 816	3 771 664	191 292 248
23	0	0	0	0	0	0	0	6 912	1 762 904	107 927 680
24	0	0	0	0	0	0	0	1 176	774 384	59 321 360
25	0	0	0	0	0	0	0	0	321 776	31 689 280
26	0	0	0	0	0	0	0	0	121 264	16 398 200
27	0	0	0	0	0	0	0	0	42 120	8 188 992
28	0	0	0	0	0	0	0	0	11 440	3 926 384
29	0	0	0	0	0	0	0	0	2 912	1 796 144
30	0	0	0	0	0	0	0	0	0	776 440
31	0	0	0	0	0	0	0	0	0	314 160
32	0	0	0	0	0	0	0	0	0	116 144
33	0	0	0	0	0	0	0	0	0	38 192
34	0	0	0	0	0	0	0	0	0	10 584
35	0	0	0	0	0	0	0	0	0	1 792

B.3 Local Curve X_p

GW Invariants ($p = 3$)

$g\backslash d$	1	2	3	4	5
0	-1	$-\frac{7}{8}$	$-\frac{55}{27}$	$-\frac{455}{64}$	$-\frac{3876}{125}$
1	$-\frac{1}{12}$	$-\frac{1}{24}$	$\frac{29}{36}$	$\frac{499}{48}$	$\frac{517}{5}$
2	$-\frac{1}{240}$	$\frac{1}{240}$	$-\frac{1}{48}$	$-\frac{289}{48}$	$-\frac{3223}{20}$
3	$-\frac{1}{6048}$	$\frac{1}{864}$	$-\frac{29}{6048}$	$\frac{1303}{864}$	$\frac{72269}{504}$
4	$-\frac{1}{172800}$	$\frac{31}{172800}$	$-\frac{49}{34560}$	$-\frac{6139}{34560}$	$-\frac{1125103}{14400}$
5	$-\frac{1}{5322240}$	$\frac{127}{5322240}$	$-\frac{199}{483840}$	$\frac{84361}{5322240}$	$\frac{12249269}{443520}$
6	$-\frac{691}{118879488000}$	$\frac{50443}{16982784000}$	$-\frac{2720467}{23775897600}$	$\frac{249581}{261273600}$	$-\frac{66551283493}{9906624000}$
7	$-\frac{1}{5748019200}$	$\frac{2047}{5748019200}$	$-\frac{25307}{821145600}$	$\frac{612943}{821145600}$	$\frac{7230097}{6220800}$
8	$-\frac{3617}{711374856192000}$	$\frac{29626847}{711374856192000}$	$-\frac{230666941}{28454994247680}$	$\frac{48487137157}{142274971238400}$	$-\frac{554800764943}{3487131648000}$
9	$-\frac{43867}{300534953951232000}$	$\frac{205341427}{42933564850176000}$	$-\frac{629443591103}{300534953951232000}$	$\frac{961270972003}{6133366407168000}$	$\frac{14464052721917}{1318135762944000}$
10	$-\frac{174611}{42255666457804800000}$	$\frac{22886438381}{42255666457804800000}$	$-\frac{58569593119}{109754977812480000}$	$\frac{720232362527}{10145418117120000}$	$-\frac{2207278848840899}{5030436483072000000}$
11	$-\frac{77683}{671480954256752640000}$	$\frac{40728187021}{671480954256752640000}$	$-\frac{90287957696327}{671480954256752640000}$	$\frac{21353300295137323}{671480954256752640000}$	$-\frac{118984943834529673}{5595674618806272000}$
12	$-\frac{236364091}{73644527683988855193600000}$	$\frac{10116146730709}{1502949544571201126400000}$	$-\frac{494490375367752331}{14728905536797771038720000}$	$\frac{22847027901760786661}{1618561047999755059200000}$	$-\frac{8562442142897866938823}{55791308851506708480000}$
13	$-\frac{657931}{7445380820798873272320000}$	$\frac{5519124592117}{7445380820798873272320000}$	$-\frac{8848530827163257}{1063625831542696181760000}$	$\frac{6613967529546778693}{1063625831542696181760000}$	$-\frac{93353626811600760223}{8863548596189134848000000}$
14	$-\frac{3392780147}{1403454284720587611832320000000}$	$\frac{113842807340681357}{1403454284720587611832320000000}$	$-\frac{574932794580846537683}{2806908569441175223664640000000}$	$\frac{7639861475203005199911167}{2806908569441175223664640000000}$	$-\frac{842614759417851975912303341}{116954523726715634319360000000}$
15	$-\frac{1723168255201}{26199665229173795460615241728000000}$	$\frac{330399609216620221161}{37428093184533993515164631040000000}$	$-\frac{1194562501188511719879799}{23817877481067086782377492480000000}$	$\frac{443454848811426733157645182 3}{37428093184533993515164631040000000}$	$-\frac{106988312835123898773224056893 1}{218330543576448295505127014400000000}$
16	$-\frac{7709321041217}{432892667213495807694455439360000000000}$	$\frac{41389102105896393386 87}{432892667213495807694455439360000000000}$	$-\frac{151169603510220244838 13287}{123683619203855945055558696960000000}$	$\frac{6348744284129633258570817381 1}{123683619203855945055558696960000000}$	$-\frac{5915195973811026338724392701 7}{178321250293909955385753600000000}$

$g\backslash d$	6	7	8	9
0	$-\frac{33649}{216}$	$-\frac{296010}{343}$	$-\frac{2629575}{512}$	$-\frac{23535820}{729}$
1	$\frac{69233}{72}$	$\frac{122277}{14}$	$\frac{2516457}{32}$	$\frac{19063805}{27}$
2	$-\frac{709589}{240}$	$-\frac{364485}{8}$	$-\frac{10145271}{16}$	$-\frac{99036127}{12}$
3	$\frac{4881895}{864}$	$\frac{51792793}{336}$	$\frac{2287161665}{672}$	$\frac{14119735147}{216}$
4	$-\frac{1256227439}{172800}$	$-\frac{706373407}{1920}$	$-\frac{50901674059}{3840}$	$-\frac{661637288195}{1728}$
5	$\frac{637217167}{96768}$	$\frac{17408293523}{26880}$	$\frac{4634510561477}{118272}$	$\frac{209946174158039}{120960}$
6	$-\frac{73821506344907}{16982784000}$	$-\frac{88004085998713}{101606400}$	$-\frac{18385328817719477}{203212800}$	$-\frac{531930200348345869 9}{849139200}$
7	$\frac{2478531287861}{1149603840}$	$\frac{26149263474683}{29030400}$	$\frac{21279414022674341}{127733760}$	$\frac{2639073564503740762 9}{1437004800}$
8	$-\frac{587136595535395663}{711374856192000}$	$-\frac{587446211107586767}{7904165068800}$	$-\frac{393287543823357493057 1}{15808330137600}$	$-\frac{929255303311169539094 71}{2092278988800}$
9	$\frac{4517456050821971}{18077290463232}$	$\frac{636124878003504206407}{1284337410048000}$	$\frac{816690643828304347133 11}{267142181289984}$	$\frac{963177139647587423956053049}{10733391212544000}$
10	$-\frac{234163100058529196039}{3841424223436800000}$	$-\frac{115634124065723893523 83}{42682491371520000}$	$-\frac{588071219111565550330423 33}{18780296203468800 0}$	$-\frac{2262875181856074764275564963}{147747085516800000}$
11	$\frac{719363160261321256 09}{583896481962393600 0}$	$\frac{200124600732817756395293}{16219346721177600 00}$	$\frac{40359889817546681496887302 07}{149217989834833920 00}$	$\frac{3743528683384700075455037734 2007}{1678702385641881600 00}$
12	$-\frac{2084826944072748470875990 7}{105206468119984078848000 00}$	$-\frac{542458961039665984689795 67}{114443710464629145600 0}$	$-\frac{250674689246604296157370851842 69}{125888081511092060160000}$	$-\frac{14701494739057001383114370103493437 1}{52603234059992039424000 0}$
13	$\frac{536962392969347759739863}{1489076164159774654464000}$	$\frac{642430330665486062044961308 3}{41363226782215962624000 0}$	$\frac{20873028848545072148500913735543}{16545290712886385049600 0}$	$\frac{5657826780768321067134334033636759 99}{1861345205199718318080000}$
14	$\frac{469427567993730416648375884 67}{1403454284720587611832320000000}$	$-\frac{684796258461593081090177787853 49}{155939364968954179092480000 00}$	$-\frac{7462493477470737932968854254407011 7}{1075443896337615028224000000}$	$-\frac{1398937503358243444174018442021115115 49}{4839497533519267627008000 00}$
15	$\frac{690406435105374593304540653263}{972158264533350480913367040 0000}$	$\frac{64305904521791265263089278688306 3}{598740007065537626505216000000}$	$\frac{627300489634350114607078614960050061787}{187811220280815738068926464 00000}$	$\frac{664153687461513236935239989999557287715967}{2743995101505424744513536000000}$
16	$\frac{282586758312127263790301478456126737}{432892667213495807694455439360000000000}$	$-\frac{114547992305059506786973894725587454 23}{480991852459439786327172710400000000}$	$-\frac{1363302927302988570563017772391725997446507}{961983704918879572654345420800000000}$	$-\frac{92568231275189731784281287465046027982207 29}{515471144574298413544243200000000}$

GW Invariants ($p = 4$)

$g\backslash d$	1	2	3	4	5
0	-1	$-\frac{17}{8}$	$-\frac{325}{27}$	$-\frac{6545}{64}$	$-\frac{135751}{125}$
1	$-\frac{1}{12}$	$\frac{19}{24}$	$\frac{899}{36}$	$\frac{27259}{48}$	$\frac{733289}{60}$
2	$-\frac{1}{240}$	$-\frac{1}{60}$	$-\frac{353}{16}$	$-\frac{36971}{24}$	$-\frac{16982771}{240}$
3	$-\frac{1}{6048}$	$-\frac{5}{3024}$	$\frac{19811}{2016}$	$\frac{1098707}{432}$	$\frac{229596091}{864}$
4	$-\frac{1}{172800}$	$-\frac{17}{86400}$	$-\frac{27601}{11520}$	$-\frac{47879159}{17280}$	$-\frac{121765461971}{172800}$
5	$-\frac{1}{5322240}$	$-\frac{13}{532224}$	$\frac{207377}{591360}$	$\frac{505917799}{241920}$	$\frac{668133202007}{483840}$
6	$-\frac{691}{118879488000}$	$-\frac{177587}{59439744000}$	$-\frac{20600063}{609638400}$	$-\frac{1929770759171}{1698278400}$	$-\frac{35019291429971663}{16982784000}$
7	$-\frac{1}{5748019200}$	$-\frac{41}{114960384}$	$\frac{608293}{273715200}$	$\frac{120088412839}{261273600}$	$\frac{13811792690497117}{5748019200}$
8	$-\frac{3617}{711374856192000}$	$-\frac{871697}{20922789888000}$	$-\frac{170423473}{1437120921600}$	$-\frac{119287599186139}{836911595520}$	$-\frac{121990130503445492479}{54721142784000}$
9	$-\frac{43867}{300534953951232000}$	$-\frac{143752159}{300534953951232000}$	$\frac{203655917057}{100178317983744000}$	$\frac{10660374319331812 7}{3066683203584000}$	$\frac{719498012093262711 74617}{42933564850176000}$
10	$-\frac{174611}{42255666457804800000}$	$-\frac{11443481107}{2112783322890240000 0}$	$-\frac{52705078513}{80486983729152000}$	$-\frac{2618254475872522943}{384142422343680000}$	$-\frac{362071558894720352989201}{349220383948800000}$
11	$-\frac{77683}{671480954256752640000}$	$-\frac{313295539}{516523810966732800 0}$	$-\frac{11019091639}{83736245698560000}$	$\frac{3675558043563876018 47}{335740477128376320000}$	$\frac{359451266407055496776098951}{671480954256752640000}$
12	$-\frac{236364091}{736445276839888551936 00000}$	$-\frac{14579173496971}{2166015520117319270400000}$	$-\frac{12700334115371351}{3776642445332761804 80000}$	$-\frac{140054283613121937 33313}{956422437454400716 80000}$	$-\frac{351012043943353781465473193969}{150294954457120112640 0000}$
13	$-\frac{657931}{7445380820798873272320000}$	$-\frac{551912656591}{7445380820798873272320000}$	$-\frac{268107951006667}{322310858043241267200 00}$	$\frac{615347215598470826527 19}{372269041039943663616 0000}$	$\frac{6482406744174784747692 07065247}{744538082079887327232 0000}$
14	$-\frac{3392780147}{140345428472058761183232 0000000}$	$-\frac{5692140875951089 9}{701727142360293805916160000000}$	$-\frac{638818147835218018 09}{311878729937908358184960 00000}$	$-\frac{224406516723380312704493653}{1403454284720587611832320 00000}$	$-\frac{302420578908216130543590201370 2349}{1079580219015836624486400 00000}$

$g\backslash d$	6	7	8	9
0	$-\frac{2869685}{216}$	$-\frac{61474519}{343}$	$-\frac{1329890705}{512}$	$-\frac{28987537150}{729}$
1	$\frac{18717967}{72}$	$\frac{464455025}{84}$	$\frac{11327475403}{96}$	$\frac{136565667553}{54}$
2	$-\frac{5381731}{2}$	$-\frac{22036018993}{240}$	$-\frac{70086064021}{24}$	$-\frac{707327090361}{8}$
3	$\frac{2688414323}{144}$	$\frac{6308773621271}{6048}$	$\frac{151643915710429}{3024}$	$\frac{2184401515751299}{1008}$
4	$-\frac{545578025851}{5760}$	$-\frac{1530116785712353}{172800}$	$-\frac{11284216876808383}{17280}$	$-\frac{234534838338474617}{5760}$
5	$\frac{108738017888147}{295680}$	$\frac{312909069492089831}{5322240}$	$\frac{16333562642052580 79}{241920}$	$\frac{550256607647923824 1}{8960}$
6	$-\frac{6997202403239429}{6220800}$	$-\frac{373459687377415063844 83}{118879488000}$	$-\frac{104278002692442663481 73}{182891520}$	$-\frac{233139375686656098171 3991}{304819200}$
7	$\frac{2651293137143277721}{958003200}$	$\frac{79215507891637037743 91}{5748019200}$	$\frac{11526119491909502319 95509}{2874009600}$	$\frac{76826764091311025736 271619}{958003200}$
8	$-\frac{5178967803514175937 17}{92990177280}$	$-\frac{325912990316246426502766531}{64670441472000}$	$-\frac{997663269331170441794 8283407}{4184557977600}$	$-\frac{567588007641954801270 4775106611}{7904165068800}$
9	$\frac{950239809754938635545 2083}{1022227734528000}$	$\frac{246004534540232771934 108679343}{15817629155328000}$	$\frac{182093267541335190916 6906143414583}{150267476975616000}$	$\frac{112602372369298265375 2255982772919}{202790117376000}$
10	$-\frac{183476429898082882952 95488977}{1408522215260160000}$	$-\frac{172954149362602217123 3685662747363}{42255666457804800000}$	$-\frac{204228108170951368714 04457956586919}{384142422343680000}$	$-\frac{191636254283998146568 815957058268537}{5121898964582400}$
11	$\frac{596415661464136693137 697889}{38497933393920000}$	$\frac{366167372426241124013 6707345083589}{39498879662161920000}$	$\frac{296307047232743424527 94756202872857 69}{14597412049059840000}$	$\frac{825818671710641274443 1011836619764670579}{373044974587084800 00}$
12	$-\frac{608556587018883505678 85282731037}{385371678095179776 0000}$	$-\frac{706116574023660789895 84379196986745 2377}{387602777284151869 44000000}$	$-\frac{384833322503573928285 33062907248055828 7417}{566496366799914270 720000}$	$-\frac{218609764325534592885 07518622246195950849 3487}{188832122266380902 40000}$
13	$\frac{172718922656717877487 39267492483891}{124089680346647887 87200000}$	$\frac{211802117547239628439 8170384220718251 91}{676852801890806661 120000}$	$\frac{746621767362683352925 30939751893019329 22599}{372269041039943663 6160000}$	$\frac{667918121646959624696 3267913436459760860 651169}{124089680346647887 8720000}$
14	$-\frac{166775802669013751255 12130491894189 8939}{155939364968954179 09248000000}$	$-\frac{134652560084048937312 86085495999559056 06287}{284676325501133389 8240000000}$	$-\frac{737401029394296883088 31602187480948488 0887508621}{140345428472058761 183232000000}$	$-\frac{387518836866852010921 022121162874752228 08455450817}{173265961076615754 5472000000}$

GW Invariants ($p = 5$)

$g\backslash d$	1	2	3	4	5
0	-1	$-\frac{31}{8}$	$-\frac{1081}{27}$	$-\frac{39711}{64}$	$-\frac{1502501}{125}$
1	$-\frac{1}{12}$	$\frac{89}{24}$	$\frac{6359}{36}$	$\frac{111683}{16}$	$\frac{16070779}{60}$
2	$-\frac{1}{240}$	$-\frac{121}{120}$	$-\frac{85963}{240}$	$-\frac{197668}{5}$	$-\frac{150052997}{48}$
3	$-\frac{1}{6048}$	$\frac{127}{1512}$	$\frac{2496749}{6048}$	$\frac{10213679}{72}$	$\frac{20912845673}{864}$
4	$-\frac{1}{172800}$	$-\frac{113}{43200}$	$-\frac{51292123}{172800}$	$-\frac{5063796817}{14400}$	$-\frac{4689771445013}{34560}$
5	$-\frac{1}{5322240}$	$\frac{97}{1330560}$	$\frac{754719389}{5322240}$	$\frac{280683071213}{443520}$	$\frac{279300567109261}{483840}$
6	$-\frac{691}{118879488000}$	$\frac{71377}{29719872000}$	$-\frac{5624857012753}{118879488000}$	$-\frac{1212079708651081}{1415232000}$	$-\frac{100403802229172521}{52254720}$
7	$-\frac{1}{5748019200}$	$\frac{47}{130636800}$	$\frac{66103930829}{5748019200}$	$\frac{429195149945273}{479001600}$	$\frac{29429674459681876031}{5748019200}$
8	$-\frac{3617}{711374856192000}$	$\frac{7399919}{177843714048000}$	$-\frac{1500817402061531}{711374856192000}$	$-\frac{43952516821221902969}{59281238016000}$	$-\frac{1582604803187531884596949}{142274971238400}$
9	$-\frac{43867}{300534953951232000}$	$\frac{359321779}{75133738487808000}$	$\frac{90440635274083823}{300534953951232000}$	$\frac{17701559417259800542 73}{3577797070848000}$	$\frac{6458698618481869384775687}{322808758272000}$
10	$-\frac{174611}{42255666457804800000}$	$\frac{5721475337}{10563916614451200000}$	$-\frac{1445908672390511633}{42255666457804800000}$	$-\frac{953524716525652016577047}{35213055381504000000}$	$-\frac{21084950486690513579949 25399}{69844076789760000}$
11	$-\frac{77683}{671480954256752640000}$	$\frac{10181988631}{167870238564188160000}$	$\frac{8404935672120899}{2654074918010880000}$	$\frac{690294090841914518802 2819}{5595674618806272000 0}$	$\frac{25953769584845771578899872122733}{671480954256752640000}$
12	$-\frac{236364091}{73644527683988855193600000}$	$\frac{11265692740487}{16737392655452012544000000}$	$-\frac{17886595467415886757433}{73644527683988855193600000}$	$-\frac{24441725617869296300243543 33}{51571798098031411200000}$	$-\frac{686630261286237073041659578 0196981}{161856104799975505920000}$
13	$-\frac{657931}{744538082079887327232 0000}$	$\frac{1379780654587}{18613452051997183180800000}$	$\frac{116554080140664203519}{7445380820798873272320000}$	$\frac{963758442519422467913212 9343}{620448401733239439360000}$	$\frac{29989296635457879842516554508 0384741}{7445380820798873272320000}$
14	$-\frac{3392780147}{14034542847205876118323200000000}$	$\frac{28460699290583489}{35086357118014690295808000000}$	$-\frac{121102281067403496894 5681}{14034542847205876118323200000000}$	$-\frac{22313460524752532991662797177513}{50849792924658971443200000000}$	$-\frac{93629642772235838781088435030216 48488031}{28069085694411752236646400000 0}$

$g\backslash d$	6	7	8
0	$-\frac{57940519}{216}$	$-\frac{2264243157}{343}$	$-\frac{89356415775}{512}$
1	$\frac{738336881}{72}$	$\frac{11040903561}{28}$	$\frac{488061295075}{32}$
2	$-\frac{25198631807}{120}$	$-\frac{1024183157553}{80}$	$-\frac{2927984828945}{4}$
3	$\frac{632343482237}{216}$	$\frac{193386110471989}{672}$	$\frac{12405342237661025}{504}$
4	$-\frac{1311340311427561}{43200}$	$-\frac{31333617914393097}{6400}$	$-\frac{365286253160191729}{576}$
5	$\frac{3262323187822313 69}{1330560}$	$\frac{1183060100223700213}{17920}$	$\frac{105733749188511284195}{8064}$
6	$-\frac{518805783921016551781}{326592000}$	$-\frac{959215799383554370832 0321}{13208832000}$	$-\frac{886941430250428862276 62879}{396264960}$
7	$\frac{12113890568753891583629}{1437004800}$	$\frac{1415269422454494282621223}{212889600}$	$\frac{56037550810020398761 81291}{1741824}$
8	$-\frac{6622576662655838885035653017}{177843714048000}$	$-\frac{1354777125672365591084827118569}{26347216896000}$	$-\frac{936850741428206710441614494 27033}{2371249520640}$
9	$\frac{783794001111843493142790 27311}{564915326976000}$	$\frac{1135768803910926080409920613 8370103}{33392772661248000}$	$\frac{420057563767285497425637392683064039}{1001783179837440}$
10	$-\frac{465792151540378161817211663 0040431}{10563916614451200000}$	$-\frac{2764925885442252889459591298 62043137}{142274971238400000}$	$-\frac{4970952776185433051089334470 8080217349}{128047474114560 00}$
11	$\frac{8808231882730776101769349618945129}{72987060245299200 00}$	$\frac{72907754520508376028294872310463177 33}{75362621128704000 0}$	$\frac{7073643279686842530970341917187547 9549571}{22382698475225088 00}$
12	$-\frac{5804934477642370219907847577165166714 41}{2023201309999693824 00000}$	$-\frac{182068788900609351943651857539304079 29163139}{4306697525379465216 00000}$	$-\frac{508303577890288398045502452170839969 8108133169}{2231652354060268339 2000}$
13	$\frac{111136180569751035818081142802471508 54579}{1861345205199718318 080000}$	$\frac{150064859580750048564707087544613881 29213551}{9191828173825769472 0000}$	$\frac{157771262377778266621124705417775678 8422958137}{1079040698666503372 800}$
14	$-\frac{384219929651072270879331036412862037 3034050167}{35086357118014690295808 0000000}$	$-\frac{291352586375670453754583404739639702 92006196070059}{5197978832298472636416 0000000}$	$-\frac{393219011646522757394488811701978470 91438402109296463}{4678180949068625372774 400000}$

abc-Coefficients $(p = 3, 4, 5)$

d	$a_d^{X_3}$	$c_d^{X_3}$
1	1	0
2	−1	0
3	2	−3
4	−7	20
5	31	−160
6	−156	1 299
7	863	−10 752
8	−5 135	89 748
9	32 285	−757 038
10	−211 919	6 449 360
11	1 440 522	−55 402 743
12	−10 079 340	479 334 719

d	$a_d^{X_4}$	$c_d^{X_4}$
1	−1	0
2	−2	2
3	−12	30
4	−102	546
5	−1 086	10 190
6	−13 284	196 760
7	−179 226	3 879 960

d	$a_d^{X_5}$	$c_d^{X_5}$
1	1	0
2	−4	4
3	40	−144
4	−620	4 676
5	12 020	−158 440
6	−268 248	5 543 968

$[b_{d,n}^{X_3}]$ $n\backslash d$	4	5	6	7	8	9	10	11	12
1	16	−190	1 788	−16 002	141 360	−1 241 928	10 895 500	−95 708 426	842 761 224
2	8	−100	1 152	−11 606	109 536	−1 005 840	9 117 690	−82 098 544	736 906 908
3	0	−50	732	−8 162	83 168	−804 582	7 561 760	−69 937 406	640 885 648
4	0	−20	420	−5 600	62 168	−635 364	6 212 920	−59 169 440	554 415 000
5	0	−10	240	−3 710	45 472	−495 594	5 059 640	−49 716 590	477 058 704
6	0	0	120	−2 394	32 752	−381 600	4 082 030	−41 491 164	408 345 116
7	0	0	60	−1 484	23 040	−290 178	3 264 580	−34 391 874	347 692 560
8	0	0	24	−896	15 968	−217 710	2 586 240	−28 316 200	294 520 212
9	0	0	12	−504	10 752	−161 298	2 030 940	−23 156 254	248 183 184
10	0	0	0	−280	7 136	−117 756	1 579 430	−18 809 780	208 067 064
11	0	0	0	−140	4 576	−84 852	1 217 400	−15 175 006	173 532 528
12	0	0	0	−70	2 896	−60 174	928 780	−12 159 730	143 992 200
13	0	0	0	−28	1 744	−42 066	702 140	−9 675 754	118 858 968
14	0	0	0	−14	1 040	−28 872	525 000	−7 645 946	97 609 596
15	0	0	0	0	576	−19 530	388 820	−5 998 388	79 736 400
16	0	0	0	0	320	−12 906	284 520	−4 672 250	64 796 976
17	0	0	0	0	160	−8 406	206 140	−3 611 828	52 372 440
18	0	0	0	0	80	−5 328	147 340	−2 771 274	42 105 228
19	0	0	0	0	32	−3 312	104 220	−2 109 316	33 662 016
20	0	0	0	0	16	−1 980	72 580	−1 592 910	26 764 632
21	0	0	0	0	0	−1 170	49 980	−1 192 576	21 157 176
22	0	0	0	0	0	−648	33 800	−885 478	16 629 624
23	0	0	0	0	0	−360	22 600	−651 310	12 991 464
24	0	0	0	0	0	−180	14 760	−474 826	10 089 336
25	0	0	0	0	0	−90	9 540	−342 584	7 785 000
26	0	0	0	0	0	−36	5 980	−244 838	5 969 832
27	0	0	0	0	0	−18	3 700	−172 920	4 546 464
28	0	0	0	0	0	0	2 200	−120 890	3 439 848
29	0	0	0	0	0	0	1 300	−83 380	2 583 360
30	0	0	0	0	0	0	720	−56 870	1 926 792
31	0	0	0	0	0	0	400	−38 170	1 425 432
32	0	0	0	0	0	0	200	−25 322	1 046 832
33	0	0	0	0	0	0	100	−16 456	761 952
34	0	0	0	0	0	0	40	−10 560	550 224
35	0	0	0	0	0	0	20	−6 600	393 360
36	0	0	0	0	0	0	0	−4 070	278 880
37	0	0	0	0	0	0	0	−2 420	195 432
38	0	0	0	0	0	0	0	−1 430	135 744
39	0	0	0	0	0	0	0	−792	93 024
40	0	0	0	0	0	0	0	−440	63 120
41	0	0	0	0	0	0	0	−220	42 144
42	0	0	0	0	0	0	0	−110	27 864
43	0	0	0	0	0	0	0	−44	18 024
44	0	0	0	0	0	0	0	−22	11 544
45	0	0	0	0	0	0	0	0	7 200
46	0	0	0	0	0	0	0	0	4 440
47	0	0	0	0	0	0	0	0	2 640
48	0	0	0	0	0	0	0	0	1 560
49	0	0	0	0	0	0	0	0	864
50	0	0	0	0	0	0	0	0	480
51	0	0	0	0	0	0	0	0	240
52	0	0	0	0	0	0	0	0	120
53	0	0	0	0	0	0	0	0	48

$[b_{d,n}^{X_4}]$ $n\backslash d$	3	4	5	6	7
1	30	720	15 430	318 912	6 572 342
2	12	464	11 380	255 102	5 516 812
3	6	272	8 200	200 952	4 589 830
4	0	160	5 740	156 240	3 784 480
5	0	80	3 930	119 568	3 093 020
6	0	40	2 600	90 366	2 505 328
7	0	16	1 680	67 128	2 011 576
8	0	8	1 040	49 248	1 600 592
9	0	0	630	35 472	1 262 366
10	0	0	360	25 212	986 440
11	0	0	200	17 544	763 896
12	0	0	100	12 060	585 844
13	0	0	50	8 064	445 116
14	0	0	20	5 328	334 712
15	0	0	10	3 408	249 214
16	0	0	0	2 148	183 484
17	0	0	0	1 296	133 686
18	0	0	0	780	96 180
19	0	0	0	432	68 432
20	0	0	0	240	47 992
21	0	0	0	120	33 250
22	0	0	0	60	22 652
23	0	0	0	24	15 232
24	0	0	0	12	10 024
25	0	0	0	0	6 510
26	0	0	0	0	4 116
27	0	0	0	0	2 562
28	0	0	0	0	1 540
29	0	0	0	0	910
30	0	0	0	0	504
31	0	0	0	0	280
32	0	0	0	0	140
33	0	0	0	0	70
34	0	0	0	0	28
35	0	0	0	0	14

$[b_{d,n}^{X_5}]$ $n\backslash d$	2	3	4	5	6
1	4	−180	7 056	−260 540	9 556 212
2	0	−108	5 236	−211 520	8 175 516
3	0	−60	3 744	−169 620	6 945 208
4	0	−30	2 640	−134 270	5 856 240
5	0	−12	1 784	−104 980	4 903 560
6	0	−6	1 192	−80 980	4 075 344
7	0	0	752	−61 690	3 363 468
8	0	0	472	−46 330	2 755 086
9	0	0	272	−34 340	2 241 132
10	0	0	160	−25 060	1 808 952
11	0	0	80	−18 030	1 449 900
12	0	0	40	−12 740	1 152 810
13	0	0	16	−8 870	909 984
14	0	0	8	−6 040	712 212
15	0	0	0	−4 050	553 308
16	0	0	0	−2 640	425 880
17	0	0	0	−1 690	325 272
18	0	0	0	−1 040	245 940
19	0	0	0	−630	184 416
20	0	0	0	−360	136 728
21	0	0	0	−200	100 512
22	0	0	0	−100	72 912
23	0	0	0	−50	52 416
24	0	0	0	−20	37 116
25	0	0	0	−10	26 016
26	0	0	0	0	17 904
27	0	0	0	0	12 204
28	0	0	0	0	8 112
29	0	0	0	0	5 340
30	0	0	0	0	3 408
31	0	0	0	0	2 148
32	0	0	0	0	1 296
33	0	0	0	0	780
34	0	0	0	0	432
35	0	0	0	0	240

Large-Degree Expansion Coefficients $\widehat{c}^{(j)}_{j_0}$

$j \backslash j_0$	1	2	3	4
1	$\frac{\sqrt{2}}{3}(f-2)$			
2	$\frac{f^2+5f+5}{18}$	$(f-2)^2$		
3	$-\frac{\sqrt{2}(f-2)\left(f^2+23f-23\right)}{810}$	$\frac{\sqrt{2}\left(f^2+5f-5\right)(f-2)}{54}$	$\frac{\sqrt{2}(f-2)^3}{81}$	
4	$\frac{-7f^4+2f^3-33f^2+62f-31}{1620}$	$\frac{7f^4-2f^3+1113f^2-2222f+1111}{9720}$	$\frac{(f-2)^2\left(f^2+5f-5\right)}{162}$	$\frac{(f-2)^4}{486}$

Free Energy Coefficients $a_{g,i}(p)$

i	$a_{2,i}(p)$
1	$-\frac{1}{240f^5}$
2	$-\frac{-2f^3+25f^2+f+12}{2880f^5}$
3	$\frac{-12f^3+9f^2-35f+2}{2880f^4}$
4	$-\frac{7f+5}{2880f^2}$
5	$\frac{f-1}{2880f}$

i	$a_{3,i}(p)$
1	$\frac{1}{6048f^{10}}$
2	$\frac{3f^4-70f^3+497f^2-630f+280}{241920f^{10}}$
3	$\frac{-137f^5+1278f^4-3045f^3+3187f^2-1883f+360}{181440f^{10}}$
4	$\frac{1741f^6-8517f^5+17136f^4-21039f^3+13013f^2-4734f+360}{362880f^{10}}$
5	$-\frac{636f^6-3031f^5+7693f^4-9638f^3+7735f^2-3031f+636}{120960f^9}$
6	$\frac{360f^6-4734f^5+13118f^4-21039f^3+17031f^2-8517f+1741}{362880f^8}$
7	$\frac{360f^5-1853f^4+3187f^3-3075f^2+1278f-137}{181440f^7}$
8	$\frac{295f^4-630f^3+482f^2-70f+3}{241920f^6}$
9	$\frac{f^2+12f-1}{72576f^3}$
10	$\frac{f^2-1}{725760f^2}$

If we define the following quantity (recall that $f \equiv (p-1)^2$)

$$\bar{a}_{g,i}(f) = C_g\, f^{6(g-1)}\, a_{g,i}(f) + \binom{5(g-1)}{i} \left(f^i - f^{i+g-1}\right), \tag{B.1}$$

we find that it has the following "reflection" property

$$\bar{a}_{g,i}(f) = f^{6(g-1)}\, \bar{a}_{g,5(g-1)-i} \left(\frac{1}{f}\right). \tag{B.2}$$

This would, in general, reduce the number of GW invariants needed to completely fix (4.42), from $5(g-1)$ down to $\lceil \frac{5(g-1)}{2} \rceil$. The available amount of data is unfortunately not enough to completely pinpoint a general expression for the constant C_g.

i	$a_{4,i}(p)$
1	$-\frac{1}{172800f^{15}}$
2	$\frac{2f^5-75f^4+994f^3-5350f^2+8461f-2604}{14515200f^{15}}$
3	$-\frac{2582f^6-42087f^5+243480f^4-584534f^3+616185f^2-314250f+45360}{43545600f^{15}}$
4	$\frac{88290f^7-910787f^6+3434955f^5-6337605f^4+6666425f^3-3968880f^2+1197450f-98280}{43545600f^{15}}$
5	$-\frac{1403015f^8-10868010f^7+34735692f^6-63129674f^5+70900605f^4-49330860f^3+20133240f^2-3982608f+181440}{87091200f^{15}}$
6	$\frac{3509560f^9-25035695f^8+83179010f^7-163178700f^6+202937816f^5-163942655f^4+83098100f^3-24287100f^2+3040776f-60480}{87091200f^{15}}$
7	$\frac{-1527084f^9+13390590f^8-52041408f^7+115753075f^6-164355872f^5+152803338f^4-92842411f^3+34605080f^2-6972948f+437688}{43545600f^{14}}$
8	$\frac{218844f^9-3486474f^8+17302540f^7-46417988f^6+76401669f^5-82177936f^4+57873320f^3-26020704f^2+6695295f-763542}{21772800f^{13}}$
9	$\frac{-60480f^9+3040776f^8-24287100f^7+83108110f^6-163942655f^5+202937816f^4-163188710f^3+83179010f^2-25035695f+3509560}{87091200f^{12}}$
10	$\frac{-181440f^{15}+3982608f^{14}-20127234f^{13}+49330860f^{12}-70900605f^{11}+63123668f^{10}-34735692f^9+10868010f^8-1403015f^7}{87091200f^{18}}$
11	$-\frac{98280f^{15}-1198815f^{14}+3968880f^{13}-6666425f^{12}+6338970f^{11}-3434955f^{10}+910787f^9-88290f^8}{43545600f^{18}}$
12	$-\frac{44905f^{15}-314250f^{14}+616185f^{13}-584079f^{12}+243480f^{11}-42087f^{10}+2582f^9}{43545600f^{18}}$
13	$\frac{35f^{16}-2604f^{15}+8461f^{14}-5385f^{13}+994f^{12}-75f^{11}+2f^{10}}{14515200f^{18}}$
14	$\frac{5f^{17}-84f^{15}-5f^{14}}{14515200f^{18}}$
15	$\frac{f^{18}-f^{15}}{43545600f^{18}}$

B.4 Hurwitz Theory

GW Invariants

$g\backslash d$	1	2	3	4	5
0	1	$\frac{1}{4}$	$\frac{1}{6}$	$\frac{1}{6}$	$\frac{5}{24}$
1	0	$\frac{1}{48}$	$\frac{1}{18}$	$\frac{13}{96}$	$\frac{59}{180}$
2	0	$\frac{1}{1440}$	$\frac{13}{1440}$	$\frac{41}{720}$	$\frac{475}{1728}$
3	0	$\frac{1}{80640}$	$\frac{41}{45360}$	$\frac{11407}{725760}$	$\frac{28361}{181440}$
4	0	$\frac{1}{7257600}$	$\frac{671}{10886400}$	$\frac{2263}{725760}$	$\frac{382777}{5806080}$
5	0	$\frac{1}{958003200}$	$\frac{73}{23950080}$	$\frac{597871}{1277337600}$	$\frac{15547991}{718502400}$
6	0	$\frac{1}{174356582400}$	$\frac{597871}{5230697472000}$	$\frac{43212893}{784604620800}$	$\frac{1022880049}{179338199040}$
7	0	$\frac{1}{41845579776000}$	$\frac{7913}{2353813862400}$	$\frac{7198313}{1379524608000}$	$\frac{12922577953}{10461394944000}$
8	0	$\frac{1}{12804747411456000}$	$\frac{28009}{351778775040000}$	$\frac{5258993}{12934088294400}$	$\frac{382138274807}{1707299654860800}$
9	0	$\frac{1}{4865804016353280000}$	$\frac{72041}{46446311065190400}$	$\frac{216768080227}{8174550747473510400}$	$\frac{125674143249703}{3649353012264960000}$
10	0	$\frac{1}{2248001455555215360000}$	$\frac{170549237}{6744004366665646080000}$	$\frac{1179123917171}{802857662698291200000}$	$\frac{18432707543100 8963}{404640261999938764800000}$
11	0	$\frac{1}{1240896803466478878720000}$	$\frac{19397633}{553971787261820928000000}$	$\frac{76573708078381}{1094908944235128422400000}$	$\frac{19235772250685904 91}{36737076418415493120000000}$
12	0	$\frac{1}{806582922253211271168000000}$	$\frac{317733228541}{7622208615292846512537600000 0}$	$\frac{220579817634963263}{76222086152928465125376000000}$	$\frac{33439900288759913609}{6335342225697950348083200000}$
13	0	$\frac{1}{609776689223427721003008000000}$	$\frac{9860686403}{228666258458785395376128000000}$	$\frac{4652751075086 3}{443030924873982541824000000}$	$\frac{102450805079122730939}{217777389008367043215360000000}$
14	0	$\frac{1}{530505719624382117272616960000000}$	$\frac{75397891}{192718452320182405693440000000}$	$\frac{851248180689373 3}{252621771249705770129817600000 0}$	$\frac{950743906311597291987913}{254642745419703416290856140800000 0}$
15	0	$\frac{1}{526261673867387060334436024320000000}$	$\frac{170314355593}{542707351175742905969887150080000 00}$	$\frac{351117401827649127278 89}{364699339990099232811764164853760000000}$	$\frac{26606061289477016408183279}{100192126370906382640594550784000000 0}$
16	0	$\frac{1}{590465598079208281695237219287040000000}$	$\frac{2084647712458321}{929983316974753043669998620377088000000 00}$	$\frac{16794886120398053567 3}{681306459322163401956042945331200000 00}$	$\frac{402047172242853466275197431}{236186239231683312678094887714816000000}$

$g\backslash d$	6	7	8	9
0	$\frac{3}{10}$	$\frac{343}{720}$	$\frac{256}{315}$	$\frac{6561}{4480}$
1	$\frac{115}{144}$	$\frac{9893}{5040}$	$\frac{42037}{8640}$	$\frac{367439}{30240}$
2	$\frac{1661}{1440}$	$\frac{767417}{172800}$	$\frac{261361}{16200}$	$\frac{15108833}{268800}$
3	$\frac{55753}{48384}$	$\frac{2738647}{388800}$	$\frac{412284571}{10886400}$	$\frac{3140437471}{16934400}$
4	$\frac{9481571}{10886400}$	$\frac{7462983907}{870912000}$	$\frac{2811659419}{40824000}$	$\frac{465909559267}{975421440}$
5	$\frac{28579051}{54743040}$	$\frac{34396604159}{4105728000}$	$\frac{77904394307}{766402560}$	$\frac{14991936313159}{14902272000}$
6	$\frac{1337241862799}{5230697472000}$	$\frac{2025328823951}{298896998400}$	$\frac{819214623006433}{6538371840000}$	$\frac{261079725106644953}{146459529216000}$
7	$\frac{3973994287}{38041436160}$	$\frac{9307987032467}{2011806720000}$	$\frac{3715721690609 6621}{282457663488000}$	$\frac{178582160207019 41329}{6590678814720000}$
8	$\frac{18394776850969}{508124897280000}$	$\frac{297199380624273277}{10975497781248000 0}$	$\frac{895735471786522771}{75027816864000000}$	$\frac{1038404336159857103861}{289723577794560000}$
9	$\frac{4005380438852029}{371570488521523200}$	$\frac{90318559404494842518 1}{656883542207692800000}$	$\frac{633628965971751842352 29}{668826879338741760000}$	$\frac{2841782237406240238759 93}{681212562289459200000}$
10	$\frac{1410401144643066084823}{505800327499923456000000}$	$\frac{4500992260015424569092 89}{735709567272615936000000}$	$\frac{35957949077439493707853 19}{541928922321346560000000}$	$\frac{146532357171216340857023 6000261}{339897820079948562432000000}$
11	$\frac{61160969148062980271}{96693257412972380160000}$	$\frac{48956631672052094321207}{2034998402186280960000000}$	$\frac{692539665012309892590084 42389}{1675210684679746486272000000}$	$\frac{266289802794163330934736586907}{668175201866565550080000000}$
12	$\frac{1819819968550228975273}{14346336561816010752000000}$	$\frac{44019262592850826413236771 7149}{522665733620080903716864000000 0}$	$\frac{1014459497773757084741668831073}{43974280472843345264640000000}$	$\frac{5393369974004766186340527506300 4691}{16260711712624739226746880000000}$
13	$\frac{33150508387853935434687511}{1463464054136226530407219200000}$	$\frac{5719533508427635618134027037}{216488765404767238225920000000}$	$\frac{36374009263094720801024419 6600427}{313599440172048542230118400000 00}$	$\frac{11636645222506936507074326065047 9031}{465647653588799350584115200000 00}$
14	$\frac{45203940962276495770417 7}{124700175030706262507520000000}$	$\frac{4851900632792476488461396857583}{649598840356386266048102400000000}$	$\frac{12737191540420446923050567445935 21}{241138963465628235123916800000000}$	$\frac{7067955032501615775396462138653 0269}{412615559707852757878702080000 00}$
15	$\frac{5674983424598547994256973725 3}{108541470235148581193977430016000000}$	$\frac{58984681814977066905075902243113}{30835644953167210566470860800000000 0}$	$\frac{665297926386465207437849789595846 2641}{303916116658416027343136804044800000 0}$	$\frac{15527368861275339329217854493976114 92653}{144721960313531441591969906688000000 00}$
16	$\frac{6417398491489066157883893404174 3}{939377087853285902696968303411200000000}$	$\frac{737163020340016779028391114168047 1177}{165330367462178318874666421400371200000 00}$	$\frac{2458906901034026863240997818639887 8953}{296550802606745230762116907008000000 00}$	$\frac{349466875115327350223330738796748675 23408151}{566846974156039950427427730515558400000 00}$

Large-Degree Expansion Coefficients $\widehat{c}_{j_0}^{\mathbf{H},(j)}$

$j \backslash j_0$	1	2	3	4	5	6	7
1	$\frac{\sqrt{2}}{3}$						
2	$\frac{1}{18}$	$\frac{1}{9}$					
3	$-\frac{1}{405\sqrt{2}}$	$\frac{1}{27\sqrt{2}}$	$\frac{\sqrt{2}}{81}$				
4	$-\frac{7}{1620}$	$-\frac{7}{1620}$	$\frac{1}{162}$	$\frac{1}{486}$			
5	$-\frac{5}{2268\sqrt{2}}$	$-\frac{11}{3645\sqrt{2}}$	$\frac{11}{14580\sqrt{2}}$	$\frac{1}{729\sqrt{2}}$	$\frac{1}{3645\sqrt{2}}$		
6	$-\frac{88}{382725}$	$-\frac{8941}{9185400}$	$-\frac{29}{58320}$	$\frac{37}{262440}$	$\frac{1}{8748}$	$\frac{1}{65610}$	
7	$\frac{101}{1020600\sqrt{2}}$	$-\frac{487}{1837080\sqrt{2}}$	$-\frac{11237}{27556200\sqrt{2}}$	$-\frac{1}{9720\sqrt{2}}$	$\frac{13}{393660\sqrt{2}}$	$\frac{1}{65610\sqrt{2}}$	$\frac{1}{688905\sqrt{2}}$

B.5 Quintic

GW Invariants

$g\backslash d$	1	2	3	4	5
0	2875	$\frac{4876875}{8}$	$\frac{8564575000}{27}$	$\frac{15517926796875}{64}$	229305888887648
1	$\frac{2875}{12}$	$\frac{407125}{8}$	$\frac{243388750}{9}$	$\frac{382833353125}{16}$	$\frac{93716201322650}{3}$
2	$\frac{575}{48}$	$\frac{5125}{2}$	$\frac{7930375}{6}$	1010821250	$\frac{3092760574975}{3}$
3	$\frac{2875}{6048}$	$\frac{35125}{336}$	$\frac{9915125}{189}$	$\frac{5046984125}{126}$	$\frac{23896218123175}{756}$
4	$\frac{115}{6912}$	$\frac{4675}{1152}$	$\frac{1589525}{864}$	$\frac{67360625}{48}$	$\frac{41561787260}{27}$
5	$\frac{575}{1064448}$	$\frac{32575}{177408}$	$\frac{4043675}{66528}$	$\frac{63287825}{1386}$	$\frac{5206947677885}{133056}$
6	$\frac{15893}{951035904}$	$\frac{639175}{52835328}$	$\frac{258292345}{118879488}$	$\frac{27956669575}{19813248}$	$\frac{82287406196995}{59439744}$
7	$\frac{115}{229920768}$	$\frac{43315}{38320128}$	$\frac{73795}{513216}$	$\frac{11880005}{266112}$	$\frac{161290779061}{4105728}$
8	$\frac{83191}{5690998849536}$	$\frac{6854215}{55794106368}$	$\frac{1611500095}{64670441472}$	$\frac{265102863775}{118562476032}$	$\frac{211932577236553}{177843714048}$
9	$\frac{1008941}{2404279631609856}$	$\frac{56018159}{4047608807424}$	$\frac{911782482119}{150267476975616}$	$\frac{6122752938019}{12522289747968}$	$\frac{69543046068666559}{1502674769756160}$
10	$\frac{4016053}{338045331662438400}$	$\frac{17574771761}{11268177722081280}$	$\frac{52967024573}{34494421598208}$	$\frac{19290354391705}{93901481017344}$	$\frac{30200588834334623}{3018261889843200}$
11	$\frac{77683}{233558592784957440}$	$\frac{156188119189}{895307939009003520}$	$\frac{64900629868273}{167870238564188160}$	$\frac{5119542339342577}{55956746188062720}$	$\frac{21388698772090845541}{3357404771283763200}$
12	$\frac{5436374093}{589156221471910841548800}$	$\frac{7452323425139}{385069425798634536960}$	$\frac{1421674824149766503}{14728905536797771038720}$	$\frac{19926917133167733049}{490963517893259034624}$	$\frac{40510994157447195164851}{9205565960498606899200}$
13	$\frac{657931}{2589697676799608094720}$	$\frac{21157181251133}{9927174427731831029760}$	$\frac{1156343451901201}{48346628706486190080}$	$\frac{40190107021710619}{224800145555215360}$	$\frac{16106569144712053656541}{5318129157713480908800}$
14	$\frac{3392780147}{488158012076726125854720000}$	$\frac{793454904024257 9}{340231341750445481656320 00}$	$\frac{86996421034648969423}{14773202997058816966656000}$	$\frac{861362461119313322203}{110074845860438244065280}$	$\frac{1453495883702125499362581359}{701727142360293805916160000}$
15	$\frac{1723168255201}{911292703623436363847486668800 0}$	$\frac{2955245637079183959 01}{1164429565741057576027344076800 0}$	$\frac{2361127477917295666944709}{1637479076823362216288452608000}$	$\frac{7437119192767990801108760429}{2183305435764482955051270144000}$	$\frac{184554933760580158769376315287227}{130998326145868977303076208640000}$
16	$\frac{7709321041217}{150571362509042020067636674560 0000}$	$\frac{373313618023948406 39}{1358094642238418220217899417600 0}$	$\frac{43461261079056933322382719}{123683619203855945055558696960000}$	$\frac{4732167756522311723821600679}{3206612349729598575514484736000}$	$\frac{29488730117121598565680453543721}{30920904800963986263889674240000}$

$g\backslash d$	6	7	8	9
0	248249742157695375	$\frac{1012162303458000611256 25}{343}$	$\frac{1923236664000035389443968 75}{512}$	$\frac{367299732093982242625847031250}{729}$
1	$\frac{103669556513320375}{2}$	$\frac{807822345991790360462 5}{84}$	$\frac{178841492957852718965993 75}{96}$	$\frac{197667633696315312223682 28125}{54}$
2	$\frac{45745969626745975}{24}$	$\frac{30792041283179807787 5}{48}$	$\frac{72245925201042275772125}{3}$	$\frac{200554217392584812052111812 5}{24}$
3	$-\frac{86000485655933125}{3024}$	$-\frac{1644218013195575653625}{6048}$	$-\frac{9654693261533922416087 5}{189}$	$\frac{852095807025263579609103162 5}{3024}$
4	$\frac{11489258828963795}{3456}$	$-\frac{1535093970278226402 5}{6912}$	$-\frac{5486660043323943011502 5}{432}$	$-\frac{2938538604365587386358654375}{3456}$
5	$\frac{23811272612797375}{532224}$	$\frac{1201020644801878815275}{1064448}$	$\frac{13478229333060084220975}{1512}$	$-\frac{1183218751141238848441165 25}{76032}$
6	$-\frac{33120827692032011}{475517952}$	$-\frac{4782837934194551255297 5}{951035904}$	$\frac{59980738079669199773205 5}{59439744}$	$\frac{29038649104798678004129906305 75}{475517952}$
7	$\frac{12561251143284275}{114960384}$	$\frac{3018630217601224242 55}{229920768}$	$-\frac{20912896955220542314748 5}{7185024}$	$-\frac{62817497649983608095425165 05}{16422912}$
8	$-\frac{19903799891708726 17}{2845499424768}$	$-\frac{2067108615789624840096 5}{5690998849536}$	$\frac{69995817294851182477408565 5}{355687428096}$	$-\frac{308787889696347475437672978925}{406499917824}$
9	$\frac{940161019171727325 5}{109285437800448}$	$-\frac{23993492213713454134963 03}{2404279631609856}$	$-\frac{1368329061802529347210560821}{18783434621952}$	$\frac{1411998531268889887214919978990 67}{92472293523456}$
10	$\frac{153669694584854459 09}{169022665831219200}$	$\frac{42046581109132794838649 57}{67609066332487680}$	$\frac{11507645930497686080354579 3}{76828484468736}$	$-\frac{113131121646811710089857113995455}{965843804749824}$
11	$\frac{13722135846153244974 5}{5371847634054021 12}$	$-\frac{125597330885299893175663 27}{53718476340540211 20}$	$\frac{124062564694412228442513929}{15260930778562560}$	$\frac{1963701873209869230283957567274977}{38370340243243008 0}$
12	$\frac{59727440646063622544355949}{29457811073595542077440 0}$	$\frac{970443598499590468337434477 3}{11783124429438216830976 0}$	$-\frac{177965536310923136518503685350 83}{73644527683988855193 60}$	$-\frac{157938013805975074469702558203257760 1}{11783124429438216830976}$
13	$\frac{119527759444154422698037 7}{59563046566390986178 56}$	$\frac{28953252999691646320916800 1}{59563046566390986178560}$	$\frac{13352904572725174140749652338 9}{930672602599859159040}$	$\frac{2847801618819756977179354387182 07}{6077861894529692467 20}$
14	$\frac{10084297453221379018142609734 3}{510347012625668222484480000}$	$\frac{2104663017170849991032866626329 3}{22455268555529401789317120 00}$	$-\frac{8517292571303831599316814157436 77}{1403454284720587611832320 00}$	$\frac{23270975106335380999584607425410423 3}{1283158203173108673675264}$
15	$\frac{2134943701656814990839874168502 81}{1103143799123107177289062809600}$	$\frac{26041491986177339927251637556370050 11}{2095973218333903636849219338240 00}$	$\frac{41656182991514222539634505804815675 3}{5954469370266771695594373120 00}$	$-\frac{8408993047710021222656933190193509924683}{62011041962541527717432524800 0}$
16	$\frac{32666334552790628482516023736519771 43}{17315706688539832307778217574400000}$	$\frac{228374503456850461389375240992823456 19}{13852565350831865846222574059520 00}$	$\frac{3084927625027630229938357011952606965 7}{393538788375905279722232217600 00}$	$\frac{73146112118989487140533874622718898577963}{98946895363084756044446957568000}$

abc-Coefficients

d	a_d^5	c_d^5
1	2 875	0
2	609 250	0
3	317 206 375	1 827 750
4	242 467 530 000	14 890 211 500
5	229 305 888 887 625	61 403 873 790 100
6	248 249 742 118 022 000	197 457 023 273 862 750
7	295 091 050 570 845 659 250	578 360 442 201 309 855 500
8	375 632 160 937 476 603 550 000	1 666 868 041 217 485 673 146 500
9	503 840 510 416 985 243 645 106 250	4 995 138 385 753 041 868 290 918 750

$[b_{d,n}^5]$ $n\backslash d$	4	5	6	7	8	9
1	−4 554 000	−754 171 353 500	−10 610 649 655 650 000	−78 888 786 091 018 902 250	−449 855 569 414 532 050 688 000	−2 299 603 226 120 509 586 274 688 500
2	69 000	−153 362 500	37 334 157 802 500	1 580 435 438 359 291 500	23 325 093 871 769 297 460 000	231 499 051 445 295 186 766 218 000
3	0	−585 000	90 666 207 000	−3 222 704 374 813 000	−413 911 345 941 053 996 000	−10 643 964 723 285 251 445 555 750
4	0	12 000	−41 089 500	−26 665 146 130 000	672 649 397 140 099 000	190 464 200 785 075 251 838 500
5	0	−100	414 000	−19 032 205 500	6 999 864 814 448 000	−529 758 825 795 272 232 000
6	0	0	0	68 236 000	45 635 424 050 000	−1 972 500 133 520 016 000
7	0	0	0	0	28 286 032 000	−31 261 607 284 151 250
8	0	0	0	0	−97 480 000	−223 145 746 636 500
9	0	0	0	0	0	−339 972 660 000
10	0	0	0	0	0	122 958 000
11	0	0	0	0	0	−1 086 750

References

[1] W. Lerche, C. Vafa and N.P. Warner, *Chiral Rings in $\mathcal{N}=2$ Superconformal Theories*, Nucl. Phys. **B324** (1989) 427.

[2] B.R. Greene and M.R. Plesser, *Duality in Calabi–Yau Moduli Space*, Nucl. Phys. **B338** (1990) 15.

[3] P. Candelas, M. Lynker and R. Schimmrigk, *Calabi–Yau Manifolds in Weighted* $\mathbb{P}^4$, Nucl. Phys. **B341** (1990) 383.

[4] P. Candelas, X.C. De La Ossa, P.S. Green and L. Parkes, *A Pair of Calabi–Yau Manifolds as an Exactly Soluble Superconformal Theory*, Nucl. Phys. **B359** (1991) 21.

[5] E. Witten, *Phases of $\mathcal{N}=2$ Theories in Two-Dimensions*, Nucl. Phys. **B403** (1993) 159, `arXiv:hep-th/9301042`.

[6] M. Bershadsky, S. Cecotti, H. Ooguri and C. Vafa, *Kodaira–Spencer Theory of Gravity and Exact Results for Quantum String Amplitudes*, Commun. Math. Phys. **165** (1994) 311, `arXiv:hep-th/9309140`.

[7] M. Kontsevich, *Enumeration of Rational Curves via Torus Actions*, Progr. Math. **129** (1995) 335, `arXiv:hep-th/9405035`.

[8] D. Ghoshal and C. Vafa, *$c=1$ String as the Topological Theory of the Conifold*, Nucl. Phys. **B453** (1995) 121, `arXiv:hep-th/9506122`.

[9] A. Strominger, S.-T. Yau and E. Zaslow, *Mirror Symmetry is T-Duality*, Nucl. Phys. **B479** (1996) 243, `arXiv:hep-th/9606040`.

[10] K. Hori and C. Vafa, *Mirror Symmetry*, `arXiv:hep-th/0002222`.

[11] E. Witten, *Mirror Manifolds and Topological Field Theory*, `arXiv:hep-th/9112056`.

[12] S. Hosono, A. Klemm and S. Theisen, *Lectures on Mirror Symmetry*, Lect. Notes Phys. **436** (1994) 235, `arXiv:hep-th/9403096`.

[13] B.R. Greene, *String Theory on Calabi–Yau Manifolds*, `arXiv:hep-th/9702155`.

[14] M. Mariño, *Chern–Simons Theory and Topological Strings*, Rev. Mod. Phys. **77** (2005) 675, `arXiv:hep-th/0406005`.

[15] M. Alim, *Lectures on Mirror Symmetry and Topological String Theory*, `arXiv:1207.0496[hep-th]`.

[16] J. Koplik, A. Neveu and S. Nussinov, *Some Aspects of the Planar Perturbation Series*, Nucl. Phys. **B123** (1977) 109.

[17] D.J. Gross and V. Periwal, *String Perturbation Theory Diverges*, Phys. Rev. Lett. **60** (1988) 2105.

[18] J. Écalle, *Les Fonctions Résurgentes*, Prépub. Math. Université Paris-Sud **81-05** (1981), **81-06** (1981), **85-05** (1985).

[19] I. Aniceto, G. Başar and R. Schiappa, *A Primer on Resurgent Transseries and Their Asymptotics*, to appear (2016).

[20] M. Mariño, *Open String Amplitudes and Large-Order Behavior in Topological String Theory*, JHEP **0803** (2008) 060, `arXiv:hep-th/0612127`.

[21] M. Mariño, R. Schiappa and M. Weiss, *Nonperturbative Effects and the Large-Order Behavior of Matrix Models and Topological Strings*, Commun. Number Theor. Phys. **2** (2008) 349, `arXiv:0711.1954[hep-th]`.

[22] M. Mariño, *Nonperturbative Effects and Nonperturbative Definitions in Matrix Models and Topological Strings*, JHEP **0812** (2008) 114, `arXiv:0805.3033[hep-th]`.

[23] S. Pasquetti and R. Schiappa, *Borel and Stokes Nonperturbative Phenomena in Topological String Theory and $c=1$ Matrix Models*, Ann. Henri Poincaré **11** (2010) 351, `arXiv:0907.4082[hep-th]`.

[24] R. Schiappa and N. Wyllard, *An A_r Threesome: Matrix Models, 2d CFTs and 4d $\mathcal{N} = 2$ Gauge Theories*, J. Math. Phys. **51** (2010) 082304, arXiv:0911.5337[hep-th].

[25] A. Klemm, M. Mariño and M. Rauch, *Direct Integration and Non-Perturbative Effects in Matrix Models*, JHEP **1010** (2010) 004, arXiv:1002.3846[hep-th].

[26] N. Drukker, M. Mariño and P. Putrov, *Nonperturbative Aspects of ABJM Theory*, JHEP **1111** (2011) 141, arXiv:1103.4844[hep-th].

[27] I. Aniceto, R. Schiappa and M. Vonk, *The Resurgence of Instantons in String Theory*, Commun. Number Theor. Phys. **6** (2012) 339, arXiv:1106.5922[hep-th].

[28] R. Schiappa and R. Vaz, *The Resurgence of Instantons: Multi-Cut Stokes Phases and the Painlevé II Equation*, Commun. Math. Phys. **330** (2014) 655, arXiv:1302.5138[hep-th].

[29] R. Couso-Santamaría, J.D. Edelstein, R. Schiappa and M. Vonk, *Resurgent Transseries and the Holomorphic Anomaly*, Ann. Henri Poincaré **17** (2016) 331, arXiv:1308.1695[hep-th].

[30] A. Grassi, M. Mariño, S. Zakany, *Resumming the String Perturbation Series*, JHEP **1505** (2015) 038, arXiv:1405.4214[hep-th].

[31] R. Couso-Santamaría, J.D. Edelstein, R. Schiappa and M. Vonk, *Resurgent Transseries and the Holomorphic Anomaly: Nonperturbative Closed Strings in Local* $\mathbb{CP}^2$, Commun. Math. Phys. **338** (2015) 285, arXiv:1407.4821[hep-th].

[32] I. Aniceto, J.G. Russo and R. Schiappa, *Resurgent Analysis of Localizable Observables in Supersymmetric Gauge Theories*, JHEP **1503** (2015) 172, arXiv:1410.5834[hep-th].

[33] M. Vonk, *Resurgence and Topological Strings*, arXiv:1502.05711[hep-th].

[34] R. Couso-Santamaría, *Universality of the Topological String at Large Radius and NS-Brane Resurgence*, arXiv:1507.04013[hep-th].

[35] M. Mariño, R. Schiappa and M. Weiss, *Multi-Instantons and Multi-Cuts*, J. Math. Phys. **50** (2009) 052301, arXiv:0809.2619[hep-th].

[36] S. Garoufalidis and M. Mariño, *Universality and Asymptotics of Graph Counting Problems in Nonorientable Surfaces*, arXiv:0812.1195[math.CO].

[37] S. Garoufalidis, A. Its, A. Kapaev and M. Mariño, *Asymptotics of the Instantons of Painlevé I*, Int. Math. Res. Notices **2012** (2012) 561, arXiv:1002.3634[math.CA].

[38] S.H. Katz, A. Klemm and C. Vafa, *M-Theory, Topological Strings and Spinning Black Holes*, Adv. Theor. Math. Phys. **3** (1999) 1445, arXiv:hep-th/9910181.

[39] M.-x. Huang, A. Klemm, M. Mariño and A. Tavanfar, *Black Holes and Large Order Quantum Geometry*, Phys. Rev. **D79** (2009) 066001, arXiv:0704.2440[hep-th].

[40] A. Klemm and E. Zaslow, *Local Mirror Symmetry at Higher Genus*, arXiv:hep-th/9906046.

[41] Y. Konishi, *Integrality of Gopakumar–Vafa Invariants of Toric Calabi–Yau Threefolds*, Publ. RIMS **42** (2006) 605, arXiv:math/0504188[math.AG].

[42] N. Caporaso, L. Griguolo, M. Mariño, S. Pasquetti and D. Seminara, *Phase Transitions, Double-Scaling Limit, and Topological Strings*, Phys. Rev. **D75** (2007) 046004, arXiv:hep-th/0606120.

[43] P. Zograf, *On the Large Genus Asymptotics of Weil–Petersson Volumes*, arXiv:0812.0544[math.AG].

[44] M. Mirzakhani and P. Zograf, *Towards Large Genus Asymptotics of Intersection Numbers on Moduli Spaces of Curves*, Geom. Funct. Anal. **25** (2015) 1258, arXiv:1112.1151[math.AG].

[45] Yu.I. Manin and P. Zograf, *Invertible Cohomological Field Theories and Weil–Petersson Volumes*, Annales Inst. Fourier **50** (2000) 519, arXiv:math/9902051[math.AG].

[46] S. Garoufalidis, T.T.Q. Le and M. Mariño, *Analyticity of the Free Energy of a Closed 3-Manifold*, SIGMA **4** (2008) 080, arXiv:0809.2572[math.GT].

[47] M. Mariño, *Les Houches Lectures on Matrix Models and Topological Strings*, arXiv:hep-th/0410165.

[48] R. Gopakumar and C. Vafa, *M-Theory and Topological Strings 1*, arXiv:hep-th/9809187.

[49] R. Gopakumar and C. Vafa, *M-Theory and Topological Strings 2*, arXiv:hep-th/9812127.

[50] C. Faber and R. Pandharipande, *Hodge Integrals and Gromov–Witten Theory*, Invent. Math. **139** (2000) 173, arXiv:math/9810173[math.AG].

[51] M. Mariño and G.W. Moore, *Counting Higher Genus Curves in a Calabi–Yau Manifold*, Nucl. Phys. **B543** (1999) 592, arXiv:hep-th/9808131.

[52] T.M. Chiang, A. Klemm, S.-T. Yau and E. Zaslow, *Local Mirror Symmetry: Calculations and Interpretations*, Adv. Theor. Math. Phys. **3** (1999) 495, arXiv:hep-th/9903053.

[53] B. Haghighat, A. Klemm and M. Rauch, *Integrability of the Holomorphic Anomaly Equations*, JHEP **0810** (2008) 097, arXiv:0809.1674[hep-th].

[54] M. Bershadsky, S. Cecotti, H. Ooguri and C. Vafa, *Holomorphic Anomalies in Topological Field Theories*, Nucl. Phys. **B405** (1993) 279, arXiv:hep-th/9302103.

[55] S. Yamaguchi and S.-T. Yau, *Topological String Partition Functions as Polynomials*, JHEP **0407** (2004) 047, arXiv:hep-th/0406078.

[56] P.S. Aspinwall, B.R. Greene and D.R. Morrison, *Measuring Small Distances in $\mathcal{N} = 2$ Sigma Models*, Nucl. Phys. **B420** (1994) 184, arXiv:hep-th/9311042.

[57] O. Aharony, O. Bergman, D.L. Jafferis and J. Maldacena, *$\mathcal{N} = 6$ Superconformal Chern–Simons-Matter Theories, M2-Branes and their Gravity Duals*, JHEP **0810** (2008) 091, arXiv:0806.1218[hep-th].

[58] M. Mariño and P. Putrov, *Exact Results in ABJM Theory from Topological Strings*, JHEP **1006** (2010) 011, arXiv:0912.3074[hep-th].

[59] N. Drukker, M. Mariño and P. Putrov, *From Weak to Strong Coupling in ABJM Theory*, Commun. Math. Phys. **306** (2011) 511, arXiv:1007.3837[hep-th].

[60] R. Dijkgraaf and C. Vafa, *Matrix Models, Topological Strings, and Supersymmetric Gauge Theories*, Nucl. Phys. **B644** (2002) 3, arXiv:hep-th/0206255.

[61] M. Aganagic, A. Klemm, M. Mariño and C. Vafa, *The Topological Vertex*, Commun. Math. Phys. **254** (2005) 425, arXiv:hep-th/0305132.

[62] M. Alim, S.-T. Yau and J. Zhou, *Airy Equation for the Topological String Partition Function in a Scaling Limit*, arXiv:1506.01375[hep-th].

[63] R. Pandharipande, *The Toda Equations and the Gromov–Witten Theory of the Riemann Sphere*, Lett. Math. Phys. **53** (2000) 59, arXiv:math/9912166[math.AG].

[64] A. Okounkov and R. Pandharipande, *Gromov–Witten Theory, Hurwitz Numbers, and Matrix Models*, arXiv:math/0101147[math.AG].

[65] M.-x. Huang, A. Klemm and S. Quackenbush, *Topological String Theory on Compact Calabi–Yau: Modularity and Boundary Conditions*, Lect. Notes Phys. **757** (2009) 45, arXiv:hep-th/0612125.

[66] J. Bryan and R. Pandharipande, *BPS States of Curves in Calabi–Yau Threefolds*, Geom. Topol. **5** (2001) 287, arXiv:math/0009025[math.AG].